Inaugural dissertation

for

obtaining the doctoral degree

of the

Combined Faculty of Mathematics, Engineering and Natural Sciences

of the

Ruprecht - Karls - University

Heidelberg

Presented by

Lic. Guillermo Martín Gomez

born in Rosario, Argentina,

the land of Lionel Messi, Angel Di Maria and Giovani Lo Celso

Date of oral examination: 10.05.2024

Mechanisms of chloroquine resistance

in *Plasmodium falciparum*

Referees:

Prof. Dr. Michael Lanzer

Prof. Dr. Marcel Deponte

Ich erkläre hiermit, dass ich die vorliegende Doktorarbeit selbstständig unter Anleitung verfasst und keine anderen als die angegebenen Quellen und Hilfsmittel benutzt habe. Ich erkläre hiermit, dass ich an keiner anderen Stelle ein Prüfungsverfahren beantragt bzw. die Dissertation in dieser oder anderer Form bereits anderweitig als Prüfungsarbeit verwendet oder einer anderen Fakultät als Dissertation vorgelegt habe. Die vorliegende Arbeit wurde am Zentrum für Infektiologie, Abteilung Parasitologie des Universitätsklinikums Heidelberg in der Zeit von Januar 2020 bis Februar 2024 unter der Leitung von Prof. Dr. Michael Lanzer ausgeführt.

…… ……

Datum Guillermo Martín Gomez

Acknowledgements

I would like to start by thanking Prof. Dr. Michael Lanzer. You made me feel your interest in me from the day that you interviewed me, and I have felt your trust throughout my PhD, which has been really comforting. I thank you of course for opening the doors of your lab to me, for the guidance and support you provided, and for all the discussions we had these years, where you taught me a lot in scientific and academic matters.

Thanks also to the members of my TAC and of my defence committee for taking the time to read and evaluate my doctoral work, and for taking part in this special moment of my life and career.

My work and the work of many would simply not be possible without the help that we get time and again from Miriam and Sandra. I cannot express how thankful I have felt whenever you showed so much interest and love in trying to help me, specially when I had to deal with the scary bureaucracy and/or the Ausländerbehörde. I also want to thank the staff in our lab Marina, Jessica, Mohammad and Petra, as well as present and past members of the Lanzer lab. Having worked these years alongside you, having had so many lunches together in Mensa, having spent so many times at Neckarwiese, at a bar, or in a trip, have helped me view the world with more open eyes. In different ways, you all helped me become the person that I am today.

In particular, I would like to thank Fi, my mentor and friend. Thank you for introducing me to everything related to the frogs and oocytes (and the patience you had with me in the surgeries), thank you for teaching me about the German culture, thank you for so many delicious pastries, and, above all, for our lasting friendship. Thanks also to Nicole for always being so encouraging with me, for always trying to boost my self-esteem, and for always trying to offer a hand. Gracias también a Carlín. Conocerte ha sido de las mejores cosas que me han pasado en estos años acá, agradezco mucho tenerte a mi lado, amigo. I cannot finish this paragraph without speaking about Kim, my bestie. Thank you, from the bottom of my heart, for the incredible friendship that we built in such short time, and for all the support you gave me in my personal and professional choices. Let the “coffee?” unite everyone the way it united us.

Gracias también a Nico por estos años de amistad. Nos “conocimos” en Argentina, pero nos conocimos acá. Agradezco que nuestra relación haya crecido tanto, aunque espero que no haga falta que me mude de nuevo para que me vengas a visitar para jugar Digimon jajaja. A special thanks goes to Emi, for being there at times when nobody else was, and for always seeing the good things in me.

Another special mention goes to the people who took the time to proof-read this work. I know how busy the lives of academic people are, so I deeply appreciate that you selflessly devoted some of your time to help me to improve this thesis. So thank you Soria, Susi, Carlín, Jakob, Toni, Kim, and Fiona. I also want here to thank Lea. Your independence, professionalism, and ambition to learn and be a better scientist were truly key for me having the time to write this thesis.

Toni, my love, I cannot express in words how thankful I am of having met you. Your company, your support, your love, your sweetness and kindness have filled my life with the light every life should have. I thank you for believing in me, probably more than I believe in myself, and for encouraging me to always go for what I want.

Gracias a mis viejos por su apoyo todos estos años, por tratar de mantenerse al tanto de lo que sea que sea lo que estoy haciendo como trabajo, por las incontables videollamadas mientras inyectaba miles de oocitos, y por motivarme a seguir mis sueños, aún cuando mis sueños estén a 11418 km de casa. Y especialmente, gracias por esos abrazos que me recargan de pilas y que me llenan de su amor cada vez que tenemos la aislada chance de vernos. No puedo esperar a recibir los próximos.

Lastly, and taking the risk of sounding self-centred, I will thank myself. A doctoral work is in itself a challenge that is really not for everyone. Doing it over 11000 km from my family and friends has only added to that. Doing it with a world-wide pandemic hitting two months after the start of your work, and I say this with due respect to all those who suffered from it, made it an even harder challenge. When adding to the list the different personal difficulties I went through during this time, I cannot help but to thank me. So thank you Guille for the resilience, thank you for enduring, thank you for doing everything with love, thank you for keeping an open mind to learn from all experiences, and thank you for going to therapy with the excellent Martina when you felt you needed it. You made it, Guille. Thank you for bringing me here.

Tarda en llegar, y al final... al final hay recompensa.

Summary

Malaria remains the most prevalent infectious disease in the world, with over 249 million cases and over 608 thousand deaths reported in 2022. Despite enormous efforts, two vaccines have only recently been recommended for use in a handful of countries. Therefore, malaria control has focused on vector control on the one hand, and on prophylaxis and treatment with antimalarials on the other. However, control and eradication programmes have been marked by periods of immense progress followed by lapses of stagnation and relapse. For instance, it has been almost 15 years since resistance to the artemisinins was first reported in Southeast Asia, and nearly a decade since parasites resistant to the partner drug piperaquine emerged, bringing artemisinin-based combination therapies under revision. Frequently, mutations in the *Plasmodium falciparum* chloroquine resistance transporter (PfCRT) are responsible for partner drug resistance, hampering parasite clearance in treated patients. The protein lies in the digestive vacuole membrane of the parasite, where resistance-conferring mutations allow PfCRT to bind and expel drugs like chloroquine or piperaquine out of the vacuole, where they can no longer exert their antimalarial effects. While efforts are in parallel directed to designing new drugs and developing new vaccines, a further understanding of the mechanisms by which PfCRT handles drugs is necessary to extend the longevity of currently available antimalarials and to prevent the emergence of resistance to new drugs.

This doctoral thesis studied PfCRT from the point of view of its post-translational modifications and of the mutations that it carries in chloroquine and piperaquine resistant parasites. Through the employment of proteomic approaches like the chemoproteomic profiling of kinase inhibitors ML-7 and H-89, I investigated which of the protein kinases in the parasite are responsible for phosphorylation of the Ser33 residue in the cytosolic N-terminus of PfCRT. In parallel, I employed K-CLASP, a method specifically designed to determine which protein kinase in a cellular lysate can phosphorylate a given phosphosite. Both experiments pointed at PfPKA as a candidate for post-translationally modifying PfCRT at the Ser33 residue. In this work, the recombinant expression of PfPKA was attempted in *Escherichia coli* BL21 (DE3) pLysS, and in *Spodoptera frugiperda* Sf9 and Sf21 cells, though the protein was found to be either not expressed or present in the insoluble fraction. Additionally, using an established heterologous expression system, *Xenopus laevis* oocytes, the effects of

mutations H97Y, F145I, M343L and G353V on the PfCRT-mediated drug transport kinetics was studied. The findings offered an explanation to why these mutations confer resistance to the partner drug piperaquine but, in doing so, re-sensitize the parasite to chloroquine. I also probed the substrate binding cavity of PfCRT by combining substrate competition kinetics, information theory for model discrimination, graphical analyses of kinetic data, and computational docking and molecular dynamics simulations. With these, I found that chloroquine and piperaquine have separate, independent binding pockets in PfCRT, though some isoforms can have them competing for the same site. Lastly, based on the obtained results and on a suggestion to use chloroquine and piperaquine together in a combination therapy, I generated an artificial double mutant that outperformed isoforms associated with chloroquine or piperaquine resistance in terms of drug transport. I hypothesize that the protein cavity is very flexible and can evolve in ways to offer solutions to a parasite that faces varying drug challenges.

Zusammenfassung

Malaria ist nach wie vor die am weitesten verbreitete Infektionskrankheit der Welt. Im Jahr 2022 wurden mehr als 249 Millionen Fälle und über 608 Tausend Todesfälle gemeldet. Trotz enormer Anstrengungen wurden nur in letzter Zeit zwei Impfstoffe für den Einsatz in einer Handvoll Länder empfohlen. Daher konzentrierte sich die Malariabekämpfung bisher einerseits auf die Vektorkontrolle und andererseits auf die Prophylaxe und Behandlung mit Malariamitteln. Die Programme zur Bekämpfung und Ausrottung der Malaria waren durch Zeiten immenser Fortschritte gekennzeichnet, auf die jedoch Zeiten der Stagnation und des Rückfalls folgten. Es ist fast 15 Jahre her, dass in Südostasien zum ersten Mal eine Resistenz gegen Artemisinin festgestellt wurde, und fast ein Jahrzehnt ist vergangen, seit Parasiten aufgetaucht sind, die gegen das Partnerpräparat Piperaquin resistent sind, wodurch die auf Artemisinin basierenden Kombinationstherapien auf den Prüfstand kamen. Häufig sind Mutationen im Chloroquin-Resistenz-Transporter (PfCRT) von *Plasmodium falciparum* für die Resistenz gegen Partner-Medikamente verantwortlich und behindern die Beseitigung der Parasiten bei behandelten Patienten. Das Protein liegt in der Membran der Verdauungsvakuole des Parasiten, wo es nach dem Erwerb bestimmter Mutationen Medikamente wie Chloroquin oder Piperaquin bindet, und aus der Vakuole ausschleust, wo sie ihre Wirkung gegen Malaria nicht mehr entfalten können. Während parallel dazu Anstrengungen unternommen werden, um neue Medikamente zu entwerfen und neue Impfstoffe zu entwickeln, ist ein besseres Verständnis der Mechanismen, mit denen PfCRT mit Medikamenten umgeht, notwendig, um die Langlebigkeit der derzeit verfügbaren Malariamittel zu verlängern und die Entstehung von Resistenzen gegen neue Medikamente zu verhindern.

Diese Doktorarbeit untersuchte PfCRT unter dem Gesichtspunkt seiner posttranslationalen Modifikationen und der Mutationen, die es in Chloroquin- und Piperaquin-resistenten Parasiten trägt. Durch den Einsatz von proteomischen Ansätzen wie dem chemoproteomischen Profiling der Kinaseinhibitoren ML-7 und H-89 untersuchte ich, welche der Proteinkinasen im Parasiten für die Phosphorylierung des Ser33-Rests im zytosolischen N-Terminus von PfCRT verantwortlich sind. Parallel dazu habe ich K-CLASP eingesetzt, eine Methode, die speziell entwickelt wurde, um festzustellen, welche Proteinkinase in einem zellulären Lysat eine bestimmte Phosphorseite phosphorylieren kann. Beide Experimente wiesen auf PfPKA als einen

Kandidaten für die posttranslationale Modifizierung von PfCRT am Ser33-Rest hin. In dieser Arbeit wurde die rekombinante Expression von PfPKA in *Escherichia coli* BL21 (DE3) pLysS und in *Spodoptera frugiperda* Sf9- und Sf21-Zellen versucht, wobei sich herausstellte, dass das Protein entweder nicht exprimiert wurde oder in der unlöslichen Fraktion vorhanden war. Darüber hinaus wurden unter Verwendung eines etablierten heterologen Expressionssystems, *Xenopus laevis* Oocyten, die Auswirkungen der Mutationen H97Y, F145I, M343L und G353V auf die PfCRT-vermittelte Medikamententransportkinetik untersucht. Die Ergebnisse boten eine Erklärung dafür, warum diese Mutationen eine Resistenz gegen das Partner-Medikament Piperaquin verleihen, den Parasiten aber gleichzeitig wieder gegen Chloroquin sensibilisieren. Außerdem untersuchte ich den Substratbindungstasche von PfCRT, indem ich Substratkonkurrenzkinetik, Informationstheorie zur Modellunterscheidung, grafische Analysen kinetischer Daten und computergestützte Docking- und Molekulardynamiksimulationen kombinierte. Dabei stellte ich fest, dass Chloroquin und Piperaquin separate, unabhängige Bindungstaschen in PfCRT haben, obwohl sie bei einigen Isoformen um dieselbe Stelle konkurrieren können. Schließlich habe ich auf der Grundlage dieser Ergebnisse und einer Idee, Chloroquin und Piperaquin zusammen in einer Kombinationstherapie zu verwenden, eine künstliche Doppelmutante geschaffen, die Isoformen, die mit Chloroquin- oder Piperaquin-Resistenz assoziiert sind, in Bezug auf den Medikamententransport übertrifft. Ich stelle die Hypothese auf, dass der Proteinbindungstasche sehr flexibel ist und sich so entwickeln kann, dass er Lösungen für einen Parasiten bietet, der mit verschiedenen Medikamenten konfrontiert ist.

Abbreviations

°C	Degrees centigrade
A	Alanine, adenosine, or ampere
ACTs	Artemisinin-based combination therapies
AGC	Automatic gain control
AIC	Akaike Information Criterion
AIC_C	Corrected Akaike Information Criterion
AL	Artemether + lumefantrine
Amp	Ampicillin
APS	Ammonium persulfate
AQ	Amodiaquine
ARS	Artemisinin
AS	Artesunate
ATP	Adenosine triphosphate
ATP-CL	ATP-crosslinker
bp	Base pairs
BSA	Bovine serum albumin
C	Cysteine or cytidine
c	Centi
cAMP	Cyclic adenosine monophosphate
cf	Correction factor
CHMI	Controlled human malaria infection
CM	Complete medium
CP	Compound pulldown buffer
CQ	Chloroquine
cRNA	5’-capped RNA
CSP	Circumsporozoite protein
D	Aspartic acid
Da	Daltons
ddH_2O	Double-distilled water
DDT	Dichlorodiphenyltrichloroethane
df	Degrees of freedom
DHA	Dihydroartemisinin

DMSO	Dimethyl sulfoxide
DNA	Deoxyribonucleic acid
dNTP	Deoxy-nucleoside triphosphate
DV	Digestive vacuole
E	Glutamic acid
EC50	Half-maximal effective concentration
EDTA	Ethylenediaminetetraacetic acid
EM	Electron microscopy
E. coli	*Escherichia coli*
F	Phenylalanine or F-factor
Fab	Antigen-binding fragment
FDR	False discovery rate
FMP	Forward mutant primer
FPIX	Ferriprotoporphyrin IX
G	Glycine or guanosine
g	Grams or gravitational force equivalent
Gly	Glycine
H	Histidine
h	Hours
HAP	Histo-aspartic protease
H_C	Hill coefficient
HCD	Higher energy collision induced dissociation
HDP	Heme detoxification protein
hPKA	Human cAMP-dependent protein kinase
HPLC	High-performance liquid chromatography
hpi	Hours post infection
I	Isoleucine
IFA	Indirect Fluorescent Antibody
IFN-γ	Interferon γ
IL-10	Interleukin-10
IPTG	Isopropylthio-β-galactoside
JM	Juxtamembrane domain
k	Kilo
K	Lysine

K-CLASP	Kinase-catalysed crosslinking and streptavidin purification
K_D	Dissociation constant
K_D^{app}	Apparent dissociation constant
Ki	Constant of inhibition
K_M	Michaelis constant
L	Leucine or litre
LB	Luria Bertani medium
LB-Amp	Luria Bertani medium supplemented with 100 µg/mL ampicillin
LC	Liquid chromatography
LFQ	Label-free quantification
M	Methionine or molar
m	Mili or meter
µ	Micro
MBR	Match between runs
min	Minutes
MD	Molecular dynamics
MQ	Mefloquine
MS	Mass spectrometry
MS/MS	Tandem mass spectrometry
MSP-1	Merozoite surface protein-1
m/z	Mass to charge ratio
N	Asparagine
n	Nano
NCE	Normalized collision energy
OD	Optical density
OD600	Optical density at 600 nm
P	Proline
p	Pico
PBS	Phosphate buffer saline
PCR	Polymerase chain reaction
P. falciparum	*Plasmodium falciparum*
PfCRT	*Plasmodium falciparum* chloroquine resistance transporter
PKA	cAMP-dependent protein kinase

PfMDR1	*Plasmodium falciparum* multidrug resistance protein 1
POD	Horseradish peroxidase
PPM	Parasite plasma membrane
ppm	Parts per million
PPQ	Piperaquine
PSM	Peptide-spectrum match
PV	Parasitophorous vacuole
PVDF	Polyvinylidene fluoride
PVM	Parasitophorous vacuole membrane
PYR	Pyrimethamine
Q	Glutamine
QD	Quinidine
QN	Quinine
R	Arginine
RBC	Red blood cells
RMP	Reverse mutant primer
RNA	Ribonucleic acid
ROS	Reactive oxygen species
rpm	Revolutions per minute
RPMI	Roswell Park Memorial Institute
RT	Room temperature
S	Serine
s	Seconds
SB	Super broth
SDS	Sodium dodecyl sulphate
SDS-PAGE	SDS polyacrylamide gel electrophoresis
SEM	Standard error of the mean
SMA	Severe malarial anaemia
SNP	Single nucleotide polymorphism
SP	Sulfadoxine + pyrimethamine
T	Threonine or thymidine
T_a	Annealing temperature
TEMED	Tetramethyl ethylenediamine
T_m	Melting temperature

TM	Transmembrane domain
TNF	Tumour necrosis factor
TSAP	Thermosensitive alkaline phosphatase
UHPLC	Ultra-high-performance liquid chromatography
UV	Ultraviolet radiation
V	Valine or volts
v/v	Volume in volume
V_{max}	Maximal velocity of transport
VP	Verapamil
W	Tryptophan
WGA	Wheat germ agglutinin
WHO	World Health Organisation
w/v	Weight in volume
X. laevis	*Xenopus laevis*
Y	Tyrosine

Table of contents

1 Introduction

1.1 Malaria and *Plasmodium*

1.1.1 Some concepts on the disease

Malaria is the most prevalent infectious disease in the world [1]. It is estimated that almost half of the world's population is at risk of contracting the disease. Each year, the World Health Organisation (WHO) publishes a report assessing the trends in malaria control and elimination across the globe, with information coming from over 80 endemic countries in all WHO regions. According to the last World malaria report, an estimated total of 249 million malaria cases were reported worldwide in 2022. Cases are reported in the Americas, Africa, Eastern Mediterranean, Southeast Asia, and the Western Pacific region (Figure 1.1). About 94 % of all cases were reported in the WHO African region, with Nigeria (27 %) and the Democratic Republic of the Congo (12 %) accounting for almost half of the global cases.

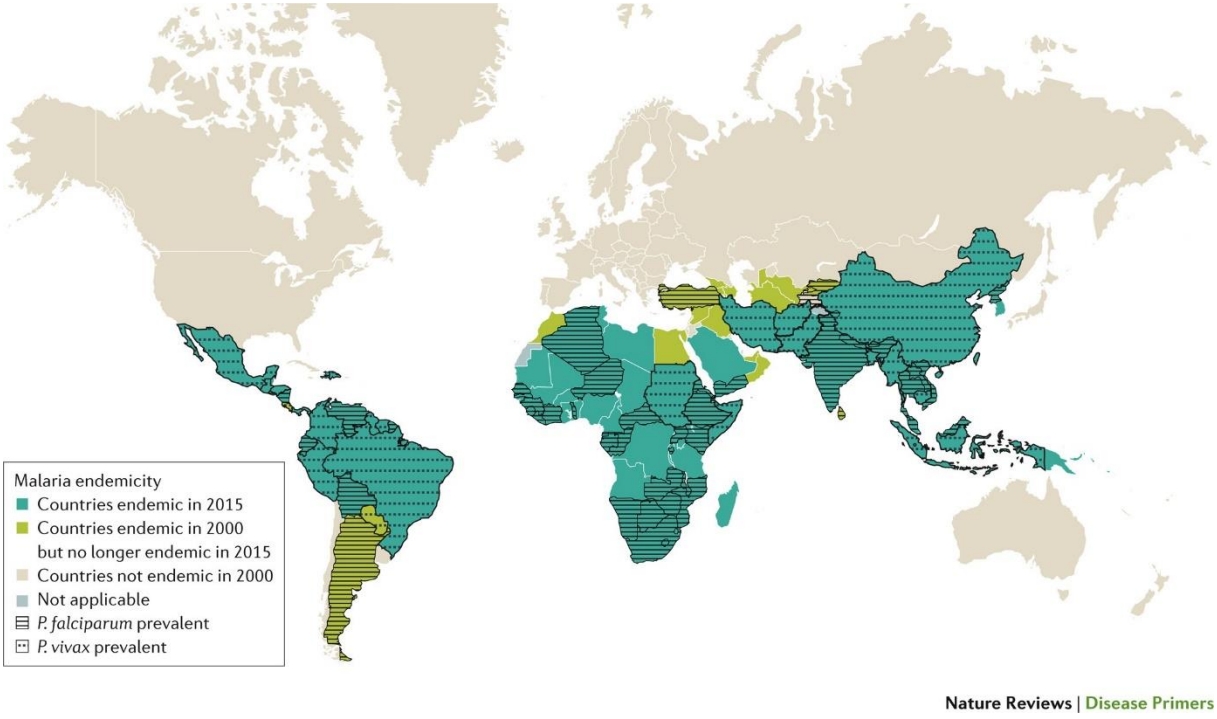

Figure 1.1. Malaria-endemic regions. Countries affected by malaria listed in the WHO malaria report [1]. Note that only *Plasmodium falciparum* and *Plasmodium vivax* are mentioned, since they are the two most common species causing malaria. Taken from [2].

Of all the reported cases, 608 thousand resulted in patient death [1]. It is also in the African region where around 95 % of malaria deaths occur, again with Nigeria (31 %)

and the Democratic Republic of the Congo (12 %) totalling almost half of them. While the incidence of the disease showed a marked decrease in the early 2000s, it stagnated from 2015 on, and has increased steeply since 2020. This resulted despite the immense efforts deployed to control and eradicate the disease. The decline in positive results combating malaria come from a combination of parasite resistance to artemisinins and its partner drugs (see below) [3-5], and mosquito resistance to the pyrethroid class of insecticides [6, 7]. An additional, unexpected difficulty was added during the COVID-19 pandemic in 2020-2022, which led to supply chain shortages and delays for the health system of all countries, and to increased procurement and shipment costs. The latter is a fact of particular importance because malaria mostly affects resource-limited countries [1]. With climate change warming former temperate regions, new niches have recently been created for mosquito breading, representing an additional challenge for malaria control [8-10].

Malaria affects people of all ages and genders, but it is particularly critical in 2 populations: i) children under the age of 5, as they have not yet fully developed a mature immune system [11], and are thus more vulnerable to infections of all kinds, and ii) pregnant individuals, since their immune system is altered during pregnancy [12], which is thought to render the unborn child exposed. In fact, placental malaria leads to poor pregnancy outcomes, such as abortions, intra-uterine growth retardation, and low birth weight [13].

1.1.2 *Plasmodium*, a complex, deadly parasite

From a European perspective, malaria is known to exist as a disease for over 2800 years, with the early Greeks Homer (850 BC) or Hippocrates (400 BC) describing the poor health conditions and enlarged spleens of people living in marshy places [14, 15]. The name “malaria” presumably comes from Italian, “mal’aria” (meaning “bad air”). For a long time, breathing miasma or drinking from stagnated water sources were considered the causes for developing the typical malaria fevers. It was only when Louis Pasteur and Robert Koch developed the germ theory of infection in 1878-1879 that a microbiological cause for malaria was proposed and sought after [16, 17].

The causative agent of malaria is a unicellular parasite, a protozoan belonging to the *Plasmodium* genus, first discovered by Charles Laveran in 1880, a French officer who was at the time working in Algeria [18]. Since then, more than 200 species of

Plasmodium have been described [19]. The different species affect different hosts, among which humans are just an example, as are other primate and non-primate mammals, reptiles and birds [19]. Only 5 *Plasmodium* species are known to infect humans in natural settings. *P. falciparum* is the deadliest, most widely spread, and causes the highest number of cases and the most severe complications, including cerebral malaria [1]. *P. vivax* is largely relevant in the WHO region of the Americas and in Southeast Asia, with its infections taking on a particular importance, since *P. vivax* forms asymptomatic, dormant species that can cause disease months or years after the primary infection [20]. *P. malariae* and *P. ovale* are less common species, limited to certain geographical regions in Africa and the Western Pacific, and are considered the least dangerous species causing malaria. Lastly, *P. knowlesi* is a species that infects primarily macaques and leaf monkeys in Southeast Asia, though it is hypothesized that non-human primates may act as a reservoir for human malaria caused by this parasite species. Because *P. knowlesi* parasites look similar to *P. falciparum* and *P. vivax*, there is evidence suggesting that human cases of *P. knowlesi* malaria have actually been underestimated because of misdiagnosis, and that the species should be deemed more important [21].

Plasmodium parasites have a very complex life cycle (Figure 1.2) [2]. Ronald Ross discovered in 1899 that mosquitoes are the vector that transmit malaria [22]. There, sporozoites reside in the salivary glands of the female *Anopheles* mosquito, waiting for the insect to take a blood meal on a human. When doing so, sporozoites are injected into the skin of the new host through the mosquito's proboscis. This form of the parasite is highly motile, which allows it to migrate through the skin, until it reaches a blood vessel. The parasite circulates the bloodstream and eventually finds the capillary network of the liver. Here, the circumsporozoite protein (CSP) plays a major role in attaching the parasite to the liver cells [23]. It then travels across an endothelial barrier to enter the hepatic parenchyma, undergoes a functional switch, and invades a hepatocyte. The liver stage is not only the stage when the parasite starts to evade the human host's immune system, but also when the first cycle of schizogony begins [24, 25]. The intrahepatic trophozoite undergoes massive cell growth and DNA replication, after which it differentiates into tens of thousands of merozoites. Liver stage development in *P. falciparum* lasts 6-15 days. In *P. vivax* infections, some trophozoites remain uni-nucleated and enter latency as hypnozoites, which can remain in the liver for months or years before they become re-activated to produce merozoites [26, 27].

The merozoites produced in the liver stages are released back to the bloodstream. Once there, the merozoite attaches to the surface of a red blood cell (RBC) via MSP-1 (merozoite surface protein-1), reorients to have the apical end juxtaposed with the erythrocyte membrane, and invades the RBC [28]. The intraerythrocytic stage is the second schizogony the parasite undergoes. First, it develops in a form that under the microscope looks like a ring, thus termed “ring-stage” [29]. Then, the parasite grows in size and prepares for DNA replication during the rest of the trophozoite stage. Later, during the schizont stage, asynchronous nuclear division occurs, and 8-20 daughter merozoite cells are formed. Lastly, merozoites rupture the RBC, entering the bloodstream, ready to find new RBCs to invade [2].

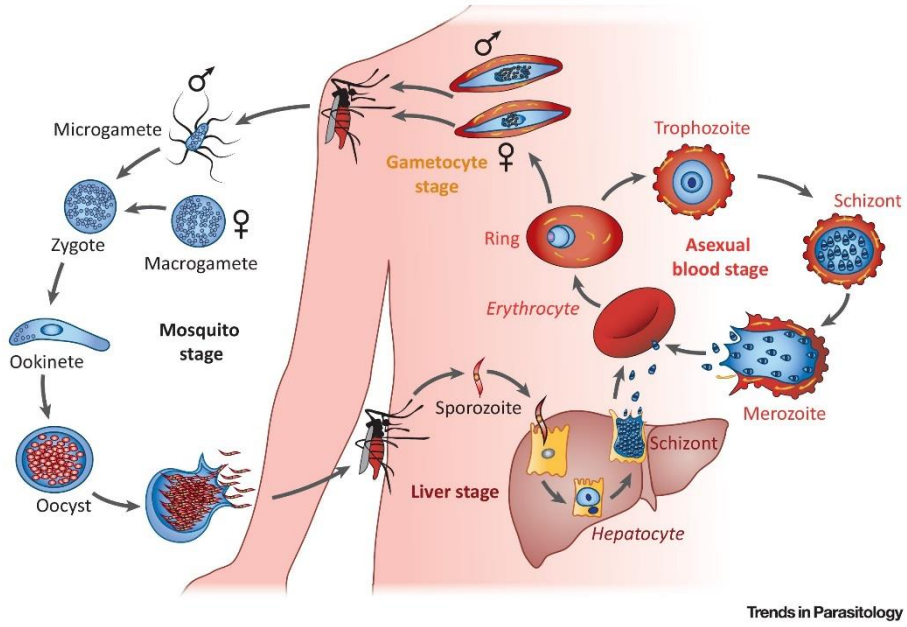

Figure 1.2. Life cycle of *P. falciparum*. The parasite transitions from a mosquito stage, where it develops sexually and asexually in the *Anopheles* mosquito vector, to a human stage, where it develops via schizogony, first in the liver and later in the blood of the host. Some parasites in the human host undergo gametocytogenesis, producing male and female gametocytes that are taken up by a mosquito to close the cycle. Taken with permission from [30].

A small proportion of blood-stage parasites commits to sexual development and undergoes gametocytogenesis [31]. When an *Anopheles* mosquito feeds on an infected human, the blood it ingests partially contains gametocytes [32]. The change in temperature and pH experienced in the transmission from vertebrate to invertebrate host is thought to trigger a further development of the male gametocyte, called exflagellation, in which 8 microgametes are formed per gametocyte [33, 34]. In the female gametocyte, further development also occurs, giving rise to 1 macrogamete per

gametocyte. Once the gametes fuse in the mosquito midgut, a zygote forms, and meiosis takes place. The resulting ookinete traverses the mosquito midgut epithelium to reach the basal lamina, where it develops into a sessile, replicative oocyst [35]. Oocysts produce thousands of sporozoites that are released into the haemocoel, through which sporozoites reach, invade and establish in the salivary glands [36]. From the moment of gametocyte ingestion by the mosquito, it takes 10-18 days for a parasite to reach the salivary glands. When this mosquito bites a human, sporozoites are injected into the new host, and the cycle begins again.

1.2 The blood stage of *Plasmodium falciparum*

1.2.1 Disease manifestation and its cellular basis

Human clinical disease is nothing more than the result of the interaction of the parasite's biology in concert with the human's pathophysiological response [37]. In complicated malaria cases, anemia and jaundice (yellow colouring of skin and eyes) typically appear. Anemia is the result of not only the recurrent destruction of infected mature RBCs by the blood-stage parasite, but also of the increased RBC sequestration by the spleen [38, 39]. The organ is a secondary lymphoid organ, adapted to inducing innate and adaptive immune responses. It also normally plays a central role in clearing the blood from senescent and damaged RBCs via their phagocytosis. During a malaria infection, it becomes the main organ involved in the development of the immune response and in the elimination of infected RBCs through splenic clearance [40-42]. The spleen of malaria patients is usually enlarged and even palpable, to the point that the size of the spleen is used as an indicator of disease progression [43]. The active spleen retains parasitized RBCs, and it removes parasites and infected RBCs from circulation [44, 45]. Naturally, as the infection becomes acute and the number of infected RBCs increases, adding to reduced erythropoiesis as commonly seen in malaria patients, symptoms of anemia become evident and even severe, as is the case in severe malarial anemia (SMA) [46-48].

The cruellest of *falciparum* malaria manifestations is possibly cerebral malaria [49]. In sub-Saharan Africa it is much more common in children under 5 years old than in adults, though the opposite is true in Southeast Asia [50, 51]. Cerebral malaria typically manifests as abrupt convulsions, impaired consciousness, and sometimes coma [52]. It is characterized by sequestration, the process of adherence of infected RBCs to the

vascular endothelium, which triggers inflammatory cytokine responses that result in vascular leakage [53]. Sequestration is mediated by a protein that the parasite produces to be localized at the infected RBC's surface: PfEMP1. This very variable protein, anchored to the RBC via knobs, binds to receptors on the surface of endothelial cells in the microvasculature, making the infected RBCs "sticky". This promotes sequestration, a mechanism that helps the parasite avoid splenic clearance [54-56]. When this occurs in the brain, obstruction of the microvasculature causes a reduction in the typical delivery of oxygen and glucose, which is suspected to be the factor triggering coma [57, 58]. Without treatment, cerebral malaria is invariably fatal; even with treatment, 15-20 % of patients still die. It accounts for at least 15 % of malaria deaths, and even those who survive it suffer from long-term neuro-cognitive impairments [59, 60].

No matter how severe the disease might get, patients mostly go to the clinic after they have suffered from fever. The characteristic feverous paroxysms of malaria [61] have long been linked to the burst of infected RBCs and consequent release of merozoites into the bloodstream. The fever lasts only a few hours, and the frequency of the febrile episodes depends on the parasite species, occurring every 48 h (tertian malaria) for *P. falciparum, P. vivax*, and *P. ovale*; every 72 h (quartan malaria) for *P. malariae*; and every 24 h (quotidian malaria) for *P. knowlesi* [62]. Fever is triggered upon merozoite release by a number of pyrogenic factors, including the production of proinflammatory stimuli like TNF (tumour necrosis factor), IL-10 (interleukin 10), and IFN-γ (interferon-γ) [63-65]. However, manifestation of disease does not take place until a certain threshold in the parasite-human interaction is surpassed, a scenario that may become more possible the larger the parasite population becomes. Then, it is only a matter of time until disease progression has gone too far.

1.2.2 Acquiring nutrients inside the red blood cell: The *Plasmodium* perspective

The RBC is a very unique, specialized type of cell in the human body. It has no nucleus and no other organelles, it is incapable of producing new biomass, and has a limited metabolism [66-68]. All those characteristics make it ideal for the transport of gases through the body, mainly oxygen and carbon dioxide. However, they also make it a very harsh environment for an invading organism like the malaria parasite. When a merozoite invades the RBC, it invaginates the erythrocyte membrane and envelopes itself in a parasitophorous vacuole (PV). There, the parasite develops hidden from the

human host's immune system and, when in the form of gametocytes, awaits for a mosquito blood meal to secure its transmission. However, the RBC and the parasitophorous vacuole membrane (PVM) represent barriers that must be crossed by nutrients for the parasite to utilize for its own growth and development. This is accomplished by two major mechanisms. One involves the uptake of nutrients into the RBC and parasite via *Plasmodium*-encoded channels and transporters, the so-called "new permeation pathways" [69-71]. The other one is the continuous endocytosis of the host cell's cytoplasm [72].

P. falciparum endocytoses the RBC cytoplasm in what seems to be a non-selective process (Figure 1.3) [72, 73]. The uptake begins early in the intraerythrocytic parasite, with the parasite engulfing part of the host cell's cytoplasm soon after invasion. With this first engulfment, termed the "Big Gulp" [74], 40 % of the parasite's volume is represented by a hemoglobin-containing structure that originates from and remains connected with the host cell [75]. As the parasite transitions through the trophozoite stage (18-30 hpi), a different process is observed, though it is to date not fully understood. It is generally accepted that the process involves the formation of cytostomes and phagophores [76-78]. The former is an invagination of the PVM and of the parasite plasma membrane (PPM) that has an opening of ~100 nm, through which it remains connected to the RBC cytoplasm, surrounded by an electron dense collar. A phagophore is instead an invagination of the PVM and PPM without an associated collar and with a wider opening. While some models propose that vesicles pinch off from these invaginated structures, others suggest that the structures themselves become endocytic vesicles after their openings close. Regardless, vesicles filled with host cell cytoplasm originate from cytostomes and phagophores inside the intraerythrocytic parasite. At some point in the transition through the trophozoite stage, the hemoglobin-containing vesicles inside the parasite coalesce to form a single, large vacuole, termed digestive vacuole (DV) or food vacuole [75]. Throughout the rest of the intraerythrocytic stage, RBC cytoplasm endocytosis continues through the fusion of newly formed vesicles with the DV. It is remarkable that the trophozoite stage lasts only some hours, and still the parasite manages to consume 60-80 % of the RBC's cytoplasmic content, most of which is hemoglobin [68].

1.2.3 Hemoglobin metabolism in the malaria parasite

In adult humans, hemoglobin consists of two chains of α-globin and two chains of β-globin, each complexing a heme moiety as a prosthetic group, resulting in a total of four per hemoglobin molecule [79]. Its main function is the binding of O_2 at the lungs and its release at peripheral tissues and organs, and the binding of carbon dioxide in tissues for its release in the lungs. Hemoglobin binds these gases through the iron present in the heme groups. Cooperative binding takes place until all four heme groups in hemoglobin are loaded with oxygen molecules [80]. This happens mostly in the lungs, where there is abundance of oxygen and hemoglobin is in the *relaxed* (R) state. When the oxygenated RBC reaches a peripheral tissue, factors like low pH and the concentration of carbon dioxide or 2,3-diphosphoglycerate, all of which are indicative of cellular metabolic activity, favour the *taut* (T) form of hemoglobin. In it, the protein has low affinity for oxygen, promoting its release at the tissue site [81]. In parallel, carbon dioxide binds in allosteric sites in hemoglobin, further facilitating oxygen release [82]. Hemoglobin represents around 90 % of the RBC's dry weight [68], highlighting that the main function of the erythrocyte is the transport and exchange of respiratory gases in the human body.

With the endocytosis of the RBC cytoplasm, the intraerythrocytic parasite creates space for its own growth. It also incorporates a great amount of hemoglobin that *P. falciparum* uses as a source of amino acids (Figure 1.3) [83]. Hemoglobin catabolism is performed by a concert of proteases, including the aspartic proteases plasmepsins I-IV, and the cysteine proteases falcipain 2, 2b, and 3 [84]. While there are other plasmepsins and falcipains encoded in the genome of *P. falciparum*, the aforementioned are the only ones expressed in the intraerythrocytic cycle that localize to the DV [84]. Most of them are firstly exported as proenzymes to the parasitophorous vacuole membrane thanks to signal peptides and hydrophobic patches, which target the proteins for export. When anchored to the membrane, the C-terminus (from which the active enzyme is derived) ends up in the RBC cytoplasmic side [85, 86]. They later get internalized in the parasite upon cytostome-derived vesicle formation [87]. Fusion of these vesicles with the DV exposes the pro-enzymes to the acidic pH of this lysosome-like compartment, which is required for maturation and activation of the anchored proteases, mainly by falcipain-2 and -3 [88].

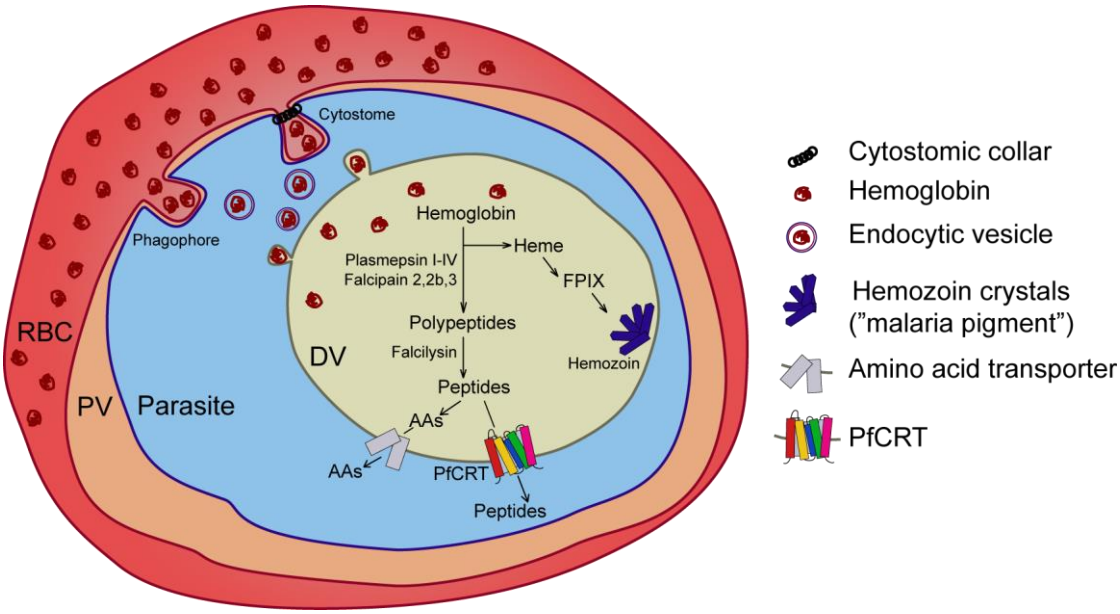

Figure 1.3. Nutrient uptake in *P. falciparum*. When the parasite is inside the red blood cell (RBC), it resides surrounded by a parasitophorous vacuole (PV). This constitutes a barrier for the acquisition of nutrients. With the formation of cytostomes and phagophores [76-78], *P. falciparum* ingests the RBC's cytoplasm, which consists mostly of hemoglobin. Endocytic vesicles are thought to pinch off from cytostomes and phagophores, carrying their load and later fusing with the digestive vacuole (DV) of the parasite, releasing their content in this lysosome-like compartment. There, a concert of proteases breaks hemoglobin down to small peptides and amino acids [83, 86, 88], which are then transported to the parasite's cytosol by different vacuolar transporters. As a by-product of hemoglobin catabolism, heme is released, which is then processed into inert hemozoin crystals in lipid environments [89, 90]. Other parasitic organelles have been omitted for simplicity.

Plasmepsins are aspartic acid proteases, meaning they have two aspartic acid residues in their active site (plasmepsin III, also known as histo-aspartic protease or HAP, has one of the catalytic aspartic acids replaced by a histidine) [91]. One acts as a proton donor, while the other one serves as a proton acceptor, in a reaction that results in the cleavage of the peptide bond. The different plasmepsins differ in the specificity of their cleavage site. In the digestive vacuole, plasmepsins I and II cleave between residues Phe33 and Leu34 of the α-globin chains of hemoglobin [92, 93]. This is thought to denature and render the globin chains more accessible to protease action, facilitating further cleavages by these and other plasmepsins, as well as by falcipains [94]. Falcipains are cysteine proteases that rely on a catalytic cysteine for mediating peptide bond hydrolysis. Some studies suggest that they too can initiate hemoglobin digestion, though many indicate otherwise, and point at falcipains acting on the globin

chains only after cleavage initiation by plasmepsins I and II [95, 96]. The metalloprotease falcilysin further digests the long polypeptides to generate smaller oligopeptides. The end product is oligopeptides of approximately 8 residues in length. A number of amino peptidases were found to localize in the DV, suggesting that free amino acids are produced in this compartment for later transport to the parasite's cytosol by transporters in the DV membrane.

Hemoglobin catabolism is not limited to feeding the amino acid pools of the parasite. Important argumentation for this came when research showed that only 16 % of globin-derived amino acids end up in parasitic proteins [97]. Additionally, hemoglobin lacks isoleucine. It is nowadays generally accepted that hemoglobin digestion serves yet another function while the parasite is growing, the so-called "colloid-osmotic balance hypothesis" [98]. When the parasite expresses the new permeation pathways' channels and transporters, it makes the RBC more permeable to organic and inorganic ions. This would normally lead to water intake that would end up destroying the RBC. Because hemoglobin is processed to short peptides and amino acids, what the parasite achieves with its digestions is the reduction of the concentration of hemoglobin, an impermeant component, thus preventing water intake and the consequent hemolysis [98, 99].

Mutations in any or some of the 4 copies of the α-globin gene, and/or in any or both of the two copies of the β-globin gene, are increasingly common. In fact, hemoglobinopathies are the most common monogenic disorders in the world [100, 101]. Normally, these mutations, which commonly are point mutations or deletions, result in clinical manifestations like thalassemia, sickle cell disease, hemolytic anemia, erythrocytosis or polycythemia [100]. Interestingly, hemoglobinopathic patients are usually more protected against malarial infections than non-hemoglobinopathic ones, though the mechanism of protection is not understood [102-106]. Hemoglobinopathies are more prevalent in malaria endemic regions, which feeds an increasing body of evidence that suggests that natural selection favours hemoglobinopathic carriers in malaria-endemic regions [107]. Hemoglobin is therefore a central player in malaria pathogenesis.

1.2.4 Hemozoin, aka “the malaria pigment”

At the expense of profiting from hemoglobin catabolism in the digestive vacuole, the intraerythrocytic parasite encounters a great challenge: heme. With the breakdown of the hemoglobin molecules, the prosthetic groups bound to the globin chains are released. In a proteinaceous environment, the Fe^{2+} in heme is rather stable, but when set free from hemoglobin into an aqueous medium, it quickly becomes oxidized to Fe^{3+}, forming ferriprotoporphyrin IX (FPIX; Figure 1.3). In this form, iron is highly reactive [108], and has the potential to induce severe oxidative damage to numerous cellular components in the form of lipid peroxidation, formation of protein-protein crosslinks, oxidation of polypeptide backbones, and even DNA breaks [109]. The parasite counts with means to avoid the toxicity of heme, the most important one being the formation of hemozoin, an insoluble, inert crystal made of heme units. This heme-detoxification product can be seen as brown structures inside the DV of *P. falciparum*, thus it is often called “the malaria pigment” [83]. In fact, Laveran found that the parasite developed in the RBCs after, in his own words, “looking for the pigment” in the fresh, unstained blood of malaria patients, based on the known fact that the spleen of malaria patients had a pigment [110].

Hemozoin formation is the target of immense research efforts [111]. The crystals consist of FPIX units that first dimerize, and later are added to cap the end of a pre-existing crystal [112]. Yet, whether it is an enzymatic-driven process or not is still a matter of debate. It is known for years that different lipids, which appear to be present in the DV of the parasite, trigger the nucleation of hemozoin dimers that later extend to form the crystals [89, 90]. In fact, hemozoin deposits are usually found associated with or in close proximity to lipid structures, such as the DV membrane. However, based on hemozoin formation having a rate corresponding to an enzymatic process, some work has suggested a protein, or a protein complex including the heme detoxification protein (HDP), to be responsible for such job [113-115]. In fact, the HDP is highly conserved among *Plasmodium* species, and it’s refractory to gene knock-out, consistent with it having an essential role in the parasite. The recombinantly expressed protein, as well as the protein purified from parasitic extract, is able to catalyse hemozoin formation at a rate similar to the one expected *in vivo*. Having such an essential and conserved function among *Plasmodium* species, efforts are made to

design drugs that specifically target and inhibit the HDP [116]. Attempts to design new antimalarials are necessary given the current scenario of multi-drug resistant malaria.

1.3 Drug resistance in *falciparum* malaria

1.3.1 Antimalarials anti malaria

The repertoire of drugs available for the prophylaxis and treatment of malaria is broad. Different classes have been approved, distributed and used in the past century, including quinolines, arylaminoalcohols, antifolates, artemisinins, antibiotics, and inhibitors of the respiratory chain, among others. Recommended prophylaxis and treatment varies depending on the infecting species, which have different patterns of geographical distribution [1]. Furthermore, in parts of each of the WHO malaria regions, some strains, mainly of *P. falciparum* and of *P. vivax*, have developed resistance to the available antimalarials.

1.3.1.1 Quinolines

The stereoisomers quinine (QN) and quinidine (QD) are present in the bark of the cinchona tree (*Cinchona pubescens*) [117], which was used since at least the 1500s to treat malaria, and possibly even earlier by the Incas in Peru [118]. In the late 1800s, the source for cinchona bark was replaced for the Javan tree, which is richer in QN. Since then, QN became the mainstay of malaria treatment for decades. Winston Churchill once proclaimed “gin and tonic has saved more Englishmen’s lives and minds than all the doctors in the Empire”, clearly referring how the prescription of QN-rich gin and tonic beverage helped expand the British Empire in Asia and the islands in the Western Pacific Ocean [119]. The search for synthetic QN led to the development of many chemicals, including some that ended up being used as dyes for microscopy, like methylene blue, or for the textile industry. Chloroquine (CQ) was first produced in 1934 (Figure 1.4), but its initial evaluation deemed it too toxic for human use. It was re-evaluated in 1943 and, since then, it became the single drug of choice for malaria treatment and prophylaxis. CQ is safe, affordable, efficacious, tolerable, and has few side effects at the dosage prescribed for malaria treatment [120, 121]. In 1955, the WHO launched the Global Malaria Eradication campaign, which first consisted of massive indoor spraying with the recently developed DDT (dichlorodiphenyltrichloroethane) insecticide. Later, after DDT-resistance reports, the program incorporated mass administration of CQ, even introducing it in cooking salt

[122, 123]. Resistance to CQ emerged soon after in Thailand, Africa, and South America, and, nowadays, can be found almost everywhere where there is *P. falciparum* [1, 124, 125]. In the search for yet new antimalarials, the bisquinoline piperaquine (PPQ) was developed in the 1960s by the Chinese National Malaria Elimination Programme [126], as a substitute for CQ. It was tested as a monotherapy, but resistance emerged and its use dropped during the 1980s.

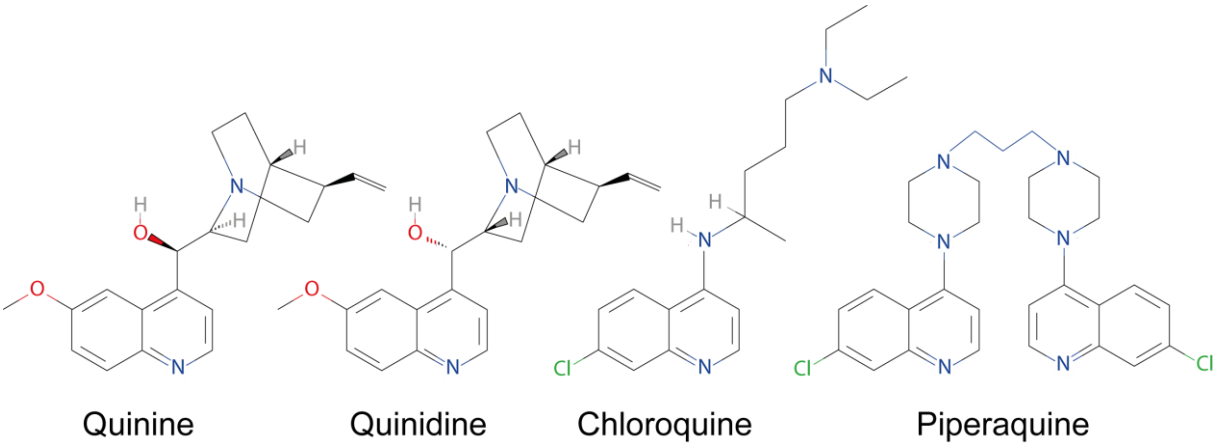

Figure 1.4. Structure of quinoline antimalarials. The chemical structure of the antimalarials quinine, quinidine, chloroquine, and piperaquine is shown. The quinoline ring that is common to the 4 drugs is at the base of each drug for easier comparison. Nitrogen atoms are coloured in blue; oxygen atoms are coloured in red; hydrogen atoms are coloured in grey.

It is generally accepted that QN, CQ and PPQ act by interfering with the heme detoxification process. These alkaline drugs are neutral in the cytoplasm of the parasite, so they can readily diffuse across membranes. When they enter the DV of the parasite, where the pH is 5.2, they become protonated and positively charged, which prevents them from leaving the compartment. In fact, these drugs accumulate in the DV approximately 1000-fold relative to their concentration in the surrounding medium [127]. Once there, they cap hemozoin crystals, hindering the deposition of oncoming FPIX molecules. It also seems that CQ forms a complex with free FPIX, accumulating at the DV membrane surface, and possibly perforating the membrane, leading to spillage of the complex into the parasite cytoplasm [111]. Inhibiting heme detoxification is thus expected to lead to severe oxidative damage in the parasite, resulting in parasite death.

Nowadays, QN is still used as a second-line treatment for uncomplicated malaria, either when first-line treatment is not available or in cases of drug resistance [128]. It must be taken 3 times daily, for a total of 7 days. Such a demanding regime, adding to

unpleasant adverse effects (nausea, headache, tinnitus), often leads to low patient adherence. QN can also be administered in the first trimester of pregnancy and may be administered for severe malaria cases when parenteral artesunate is not available. When used, CQ is administered once daily for 3 days, with great tolerance and few to none side effects, which leads to high patient compliance [120]. It can also be used for prophylaxis alone or in combination with proguanil, either daily (lower dose) or weekly (higher dose). CQ is considered suitable for use in all three trimesters of pregnancy and can be given to breast-feeding individuals [128]. It is not recommended in areas where there is widespread CQ-resistant *P. falciparum.* PPQ was used as a monotherapy against malaria in China for 10 years in the late 1980s, with the regime consisting of 5 doses divided in 2 days [126, 129]. Despite general tolerability, side effects were mild, including headaches, dizziness, vomiting and diarrhea [130, 131]. Pregnant individuals were advised to use it with caution. Resistance emerged rapidly, so its use reduced. Nowadays it is only used in combination with dihydroartemisinin.

1.3.1.2 Artemisinins and combination therapies

Artemisinin (ARS) is present in the *Artemisia* plants, which have been used as medicinal herbs in Traditional Chinese Medicine since at least the times of the Eastern Jin Dynasty (317-420 AD) [132]. When CQ resistance became the norm after the Global Malaria Eradication campaign, the search for new antimalarial drugs began. Nobel-prize winner Prof. Youyou Tu found the antimalarial properties of extracts of *Artemisia* plants, isolated and tested its active component ARS, and produced ARS derivatives that were later also tested and employed in China to treat malaria patients. In the 1990s, numerous studies showed that ARS-based therapy, especially in combination with slower-acting antimalarials like PPQ or mefloquine, rapidly diminished symptoms for both uncomplicated and severe *P. falciparum* infections. In 2006, the WHO changed its strategy, and artemisinin-based combination therapies (ACTs) became the first-line treatment against malaria, although many countries were already employing them [133]. To this date, 5 ACTs have been approved and used to treat malaria: artemether + lumefantrine (AL), artesunate + amodiaquine (AS+AQ), artesunate + mefloquine (AS+MQ), artesunate + sulfadoxine-pyrimethamine (AS+SP), and dihydroartemisinin + piperaquine (DHA+PPQ). Soon after, studies reported reduced ACT efficacy in western Cambodia (border with Thailand) [3, 134]. Partial ARS resistance became apparent in the following years, setting ground for the current

scenario where the parasite is able to survive ACT treatment and has developed resistance to some of the partner drugs, like PPQ [135, 136]. In recent years, ARS resistance and low ACT efficacy are becoming increasingly evident and worrisome in Africa [5].

The mode of action of the artemisinins is not fully clear, though it is well understood that their activation through breakage of their endoperoxide bridge is essential. The activation seems to be catalysed in the DV by FPIX and/or free Fe^{2+} that result from hemoglobin metabolism [137, 138]. Activated artemisinins have been reported to prevent hemozoin formation by alkylating FPIX, making the latter both the activator and the target of the drug. Given the redox nature of the endoperoxide bridge, artemisinins are expected to generate reactive oxygen species (ROS), leading to the alkylation of numerous proteins [139-141]. Thus, it seems that ARS does not have *one* target in the parasite, but rather a promiscuous mechanism in which multiple cellular components are affected.

Artemisinins are well tolerated and are very safe, thanks to rapid elimination after oral intake [142-145]. ACT regimes involve a 1-daily-dose 3-day course, with variations on the dosage for infants under 5 years old, pregnant, and breast-feeding individuals. It can be accompanied by a single dose of primaquine to reduce transmission in low-transmission areas. In severe *P. falciparum* cases, intravenous AS or intramuscular artemether can be given daily [133].

1.3.2 PfCRT *et al.*

The main determinant of resistance to the quinoline class of antimalarials in *P. falciparum* is the *Plasmodium falciparum* chloroquine resistance transporter (PfCRT) [146-150], a member of the drug/metabolite transporter (DMT) superfamily [151, 152]. Such proteins are expected to have 10 transmembrane domains (TM) with an internal two-fold pseudo-symmetry. The latter is suspected to arise from a gene duplication event, whereby TM1-5 have significant homology to TM6-10 [153]. The N- and C-termini are predominantly positively charged, and so are expected to have cytoplasmic localization, following the positive-inside rule [154, 155]. The structure of the PfCRT isoform 7G8 was solved in 2019 [156], confirming the expected characteristics of the protein (Figure 1.5). In particular, 5 helical pairs were identified, arranged as two-helix hairpins with inverted antiparallel topology. The structure was solved with the protein

in an open-to-vacuole conformation, thanks to a strategy that involved an antigen-binding fragment (Fab) that is inserted in the cavity of the protein from the vacuolar side. The other conformations, namely the occluded and the open-to-cytoplasm conformations, have so far only been computationally modelled based on homology to other proteins [157, 158]. However, information on inter-helical loops is often lacking due to low homology.

a

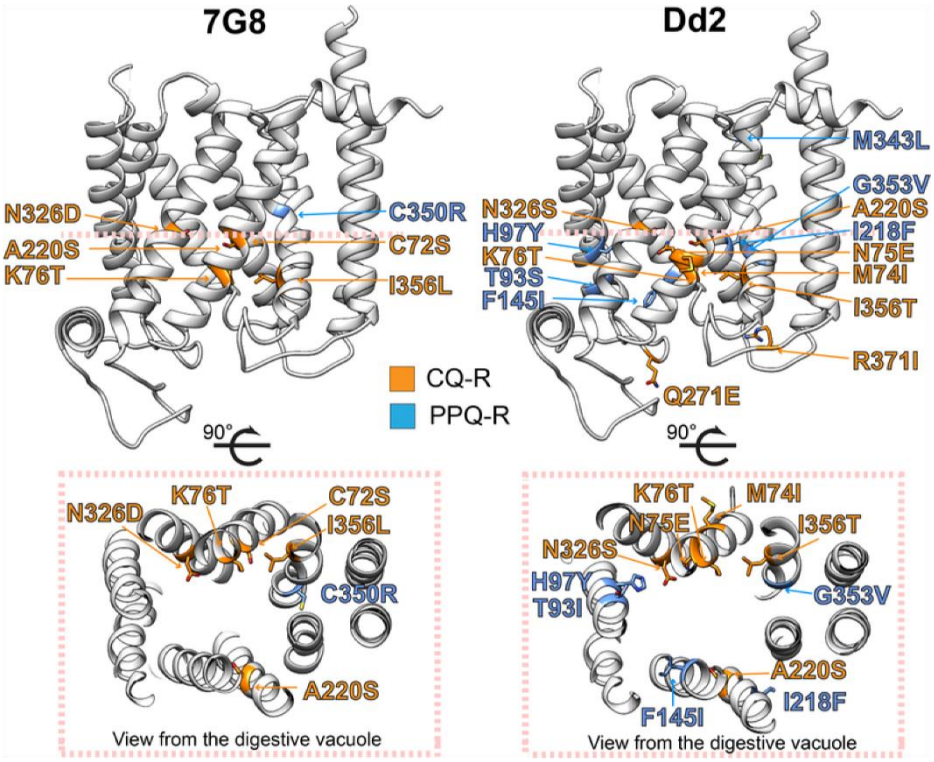

b

PfCRT variant	Status	Origin	Year reported	Amino acid position in PfCRT								
				72	74	75	76	220	271	326	356	371
HB3	CQ-S	Honduras	1984	C	M	N	K	A	Q	N	I	R
3D7	CQ-S	The Netherlands	1987	C	M	N	K	A	Q	N	I	R
Dd2	CQ-R	Indochina	1988	C	I	E	T	S	E	S	T	I
7G8	CQ-R	Brazil	1984	S	M	N	T	S	Q	D	L	R

Figure 1.5. Structure and CQ resistance profile of PfCRT. a, The structure and model of the CQ resistant isoforms 7G8 ($PfCRT^{7G8}$) and Dd2 ($PfCRT^{Dd2}$), respectively. The mutations known to confer resistance to CQ (orange) or to PPQ (blue) relative to the CQ sensitive $PfCRT^{3D7}$ isoform are indicated. Note that many of these mutations lie in the cavity of the transporter, as seen in the view from the DV panel. Taken with permission from [156]. **b,** Isoforms of PfCRT from parasites isolated in different parts of the world. The sequence differences between CQ resistant and CQ sensitive-related variants are highlighted in grey [168-171]. CQ-S: CQ sensitive; CQ-R: CQ resistant.

The protein is essential for the intraerythrocytic parasite [159, 160]. PfCRT localizes to the membrane of the parasite's DV (Figure 1.3) [161, 162], where it resides to transport oligopeptides that result from hemoglobin catabolism, from the DV lumen to the cytoplasm of the parasite [160, 163]. Based on its localization, other substrates have been suggested for PfCRT, like glutathione [164], cationic amino acids, polyamines [165], and iron ions [166]. After much debate, Shafik *et al.* [163] showed that PfCRT mediates the transport of hemoglobin-derived peptides of 4-11 residues in length from the DV, where they are generated, to the cytosol of the parasite. This has been confirmed by employing fluorescently labelled peptides, which accumulated in the DV after conditional knock-down of PfCRT [160]. The transport of these oligopeptides is pH-dependent, which contributes to the question of whether substrate translocation is coupled to H^+ symport, taking advantage of the H^+ gradient across the vacuolar membrane [166, 167].

PfCRT on its own is not able to mediate drug resistance, which is why for decades different antimalarials were effective in treating malaria patients. However, in scenarios of drug misuse where the plasma concentration of the drug does not reach lethal levels, parasites that carry mutations permitting drug tolerance possess an advantage over wild type parasites. Over the years, additional mutations that increase that advantage, for example by compensating for side effects of former mutations (e.g. growth defects), are selected for, and their prevalence increases [172]. CQ resistance emerged first in Thailand in 1957, spread through Southeast Asia, and reached Africa in the late 1970s [173, 174]. It developed independently in South America. The CQ resistant *P. falciparum* Dd2 strain from Indochina carries 8 point mutations in PfCRT ($PfCRT^{Dd2}$) relative to the drug sensitive 3D7 strain ($PfCRT^{3D7}$) [170]. A key amino acid substitution is the K76T, which eliminates a positive charge from the central cavity of the carrier, a necessary step for the transport of positively charged substrates like the quinolines CQ and PPQ (Figure 1.5) [156, 172, 175]. The rest of the mutations seem to signify a compensation of the fitness cost that the K76T replacement causes to the parasite [176, 177]. In fact, PfCRT from CQ resistant parasites handles oligopeptides less efficiently than that of drug sensitive strains [163, 178]. Mostly, the mutations that confer CQ resistance lie in the central cavity of the protein, generating an environment that facilitates interactions with a range of substrates, from natural ones to drugs, while still permitting the conformational transition that leads to substrate translocation [156]. Nowadays, several PfCRT isoforms are prevalent across the world, many of which are

responsible for widespread CQ resistance [170]. In recent years, with the deployment of ACTs in Southeast Asia, in particular of DHA-PPQ in Cambodia, parasites with acquired partial resistance to the artemisinins have gained an extra, 9th mutation over their PfCRT^{Dd2}, conferring PPQ resistance. These comprise the H97Y, F145I, M343L, and G353V mutations, among others of lesser prevalence [178-182]. Of them, the F145I mutation (PfCRT^{Dd2_F145I}) confers the highest degree of PPQ resistance. Surprisingly, parasites with any of these extra mutations are re-sensitised to CQ, though the reasons have remained unclear. The re-sensitisation phenomenon has promoted the idea of a new combination regime comprising both CQ and PPQ, since the parasite seems to not be able to handle both drugs simultaneously [156, 179]. Concerns about potential mutations that would render the parasite resistant to the two drugs is however noteworthy.

Protein phosphorylation plays a crucial role on the functioning of transporters in many organisms [183-185], of which *P. falciparum* and PfCRT are no exceptions. The transporter is phosphorylated in cytosolic loops at Ser33, Ser411, Thr416, and possibly at Ser420 [186, 187]. Phosphorylation at Thr416 serves as a trafficking and sorting signal without which the protein is incorrectly directed from the endoplasmic reticulum to the parasite plasma membrane [188]. Instead, phosphorylation of Ser33 increases the tolerance of Dd2 parasites to CQ and QN by increasing the V_{max} of PfCRT-mediated transport [187]. Owing to the divergent kinome, i.e. the protein kinases, of the malaria parasite, it is difficult to predict the identity of the protein kinases responsible for phosphorylating PfCRT [189-191]. However, that characteristic can be exploited, since targeting the malarial kinases that activate key proteins like PfCRT would potentially have little to no side effects, as a certain degree of specificity is expected thanks to that evolutionary distance [192]. The malarial kinome consists of approximately 90 protein kinases, with members belonging to most of the known protein kinase families, and additional proteins belonging to a family unique to *Plasmodium*, the FIKK kinases [189, 191]. Regardless, most protein kinases in the malaria parasite have escaped thorough investigation, which makes them both attractive and difficult targets of research.

Other proteins have also been linked to drug resistance in malaria. The *P. falciparum* multidrug resistance protein 1 (PfMDR1) is another vacuolar transporter that, after acquiring mutations, either SNPs or gene duplication events, modulates the tolerance

of the parasite to different antimalarials [193-195]. The protein is homologous to the P-glycoprotein in humans, a known mediator of multidrug resistance in cancer cells. By expressing PfMDR1 in *X. laevis* oocytes, Shafik *et al.* [196] showed that the protein mediates the transport of several antimalarials more or less efficiently, depending on the set of mutations the protein has. Additionally, duplication events in the plasmepsin genes seems to modulate resistance to PPQ, potentially by reducing the rate at which the toxic products of hemoglobin catabolism are generated [197-199]. Similarly, because the artemisinins are activated and target products of hemoglobin metabolism, mutations in PfKelch13 that reduce its abundance and/or function provide tolerance to this class of antimalarials. The protein function remains unknown, though it is somewhat clear that it participates in RBC cytoplasm ingestion by interacting with cytostomes [200, 201].

1.4 Perspectives and aims of this study

Different vaccines for malaria are being developed and tested, with some using attenuated whole parasites and others focusing on single antigens [202-204]. Blood-stage malaria vaccine candidates have shown, however, no more than 60-70 % efficacy [205, 206]. Two pre-erythrocytic vaccine candidates, RTS,S/AS01 and R21/Matrix-M, have completed phase III trials, and have been recently recommended for use in children in sub-Saharan Africa who are at risk of infection with *P. falciparum* [207, 208]. The vaccine candidate PfSPZ for pre-erythrocytic stages has shown promising results in controlled human malaria infections (CHMI), though its efficacy was only approximately 50 % when tested in malaria-exposed adults [209, 210]. Other vaccines, like those for preventing placental malaria or for blocking transmission, have also been tested with similar results. Efforts for an erythrocytic malaria vaccine, like those relying on full-length MSP-1, are ongoing [211].

In the current scenario, multidrug resistant parasites have gained ground in Southeast Asia [179], and are becoming established in Africa [5]. In countries where treatment failure with an ACT is above 10 %, the strategy is usually changed to a different ACT to which the parasite does not have known cross-resistance [133]. However, it appears that it will not be long until new antimalarials with novel mechanisms of action are needed. Despite having a range of antimalarials in the pipeline, many are still in their first pre-clinical and clinical trial phases [212]. This means that in the short term, we

can only count on the currently available antimalarials, as long as they are still effective in combating the disease. Extending their longevity while finding new drug targets are thus critical parts of the immense scaffolding built to eradicate malaria.

With this in mind, this doctoral work intends to contribute to a better mechanistic understanding of the functioning of the *Plasmodium falciparum* chloroquine resistance transporter, PfCRT. Mutations in this protein have repeatedly stalled and complicated all progress made towards the eradication of malaria, thanks to its ability to mediate resistance to chloroquine and other first-line antimalarial drugs. Firstly, this thesis aims at functionally understanding how the novel PfCRT mutations that appeared in Southeast Asia, namely H97Y, F145I, M343L, and G353V, shift the susceptibility of the parasite from chloroquine resistance and piperaquine sensitivity, to chloroquine sensitivity and piperaquine resistance. This was done by expressing the different PfCRT variants in a heterologous expression system, *Xenopus laevis* oocytes, and investigating how the mutations impacted chloroquine and piperaquine transport from a Michaelis-Menten perspective. An additional goal is to probe the binding cavity of the protein to uncover how chloroquine and piperaquine compete for binding to PfCRT, which involved extensive kinetics analyses and computational simulations. Finally, this work tries to shed light on the identity of the protein kinases that phosphorylate PfCRT on Ser33, with the objective of offering new drug targets for antimalarial drug development.

2 Materials and Methods

2.1 Materials

2.1.1 Equipment

Equipment	Company
Analytical scale	Kern and Sohn, Balingen, Germany
Bandelin sonopuls HD 2070	BANDELIN electronic, Berlin, Germany
Biofuge fresco/pico	Heraeus Instruments, Hanau, Germany
Blot Scanner C-DiGit	LiCor, Bad Homburg, Germany
Confocal Leica TCS SP5	Leica Microsystems CMS, Jena, Germany
Digital camera DC120 Zoom	Kodak, New York, USA
Electroporator Gene Pulser II	Biorad, Munich, Germany
Gas burner gasprofi 1 micro	WLD-TEC
Heat block NoeBlock Mono I	NeoLab, Heidelberg, Germany
Incubator Heraeus B12/UB12	Thermo Fisher Scientific, Dreieich, Germany
Incubator for oocytes	Memmert, Schwabach, Germany
J2-MC Centrifuge	Beckman, Krefeld, Germany
KL 1500 LCD cold light source	Schott, Mainz, Germany
Leica S4-E	Leica Microsystems CMS, Jena, Germany
Light optical microscope Axiolab.A1	Zeiss, Jena, Germany
Liquid Scintillation Analyzer Tri-Carb 4910 TR	PerkinElmer, Rodgau, Germany
MACS D column	Miltenyi Biotec, Bergisch Gladbach, Germany
Megafuge 1.0 R	Heraeus Instruments, Hanau, Germany
Megafuge 2.0 R	Heraeus Instruments, Hanau, Germany
Micropipette puller Flaming/Brown, Model P-1000	Sutter Instruments, Tuttlingen, Germany
Microinjector Nanoject II	Drummond, Broomall, USA
Microwave oven	Sharp, Düsseldorf, Germany
MiliQ water system Purist ultrapure	Rephile, Germany

NanoDrop One	Thermo Fisher Scientific, Dreieich, Germany
Nanoject II injector	Drummond Scientific, Broomall, USA
pH-meter pH 7110	WTW, Weilheim, Germany
Pipetman Gilson P10/P20/P200/P1000	Abimed, Langenfeld, Germany
Pipetus Forty/Standard	Hirschmann Labortechnik, Eberstadt, Germany
Plate reader FLUOstar OPTIMA	BMG Labtech, Ortenberg, Germany
Power Pac 200/300	Biorad, München, Germany
RC5BPlus	Sorvall, Langenselbold, Germany
Rotors JA20.0, JA20.1	Beckman Instruments, Palo Alto, CA, USA
Rotor GS-3	DuPont Instruments, Bad Homburg, Germany
Semi-dry transfer cell Trans blot SD	BioRad, München, Germany
Shaker KS 501 digital	IKA, Staufen, Germany
Spectrophotometer UVIKON 923	Kontron Instruments, München, Germany
Sterile workbench HeraSafe	Heraeus Instruments, Hanau, Germany
Thermocycler Labcycler	Sensoquest, Göttingen, Germany
UV table TFX-35M	Vilber Lourmat, Eberhardzell, Germany
Vacuum workstation	QUIAGEN, Hilden, Germany
SuperMACS II Separator	Miltenyi Biotec, Bergisch Gladbach, Germany
Vortex Genie 2	Roth, Karlsruhe, Germany
Water bath Julabo 7A	Julabo, Seelbach, Germany
Zeiss Image Examiner	Zeiss, Jena, Germany

2.1.2 Disposables

Disposable	**Company**
Capillaries GB 100 F10	Drummond, Broomall, USA
Cryovials	Nalgene, Wiesbaden, Germany
Electroporation cuvettes Gene Pulser	Biorad, München, Germany
Eppendorf tubes	Sarstedt, Nümbrecht, Germany

Falcon tubes (15, 50 mL)	Corning incorporation, Bodenheim, Germany
Filter systems 500 mL	Corning, Kaiserslautern, Germany
Filters Millex GS (0.2 µm)	Merck Millipore, Darmstadt, Germany
Gloves TouchNTuff	Ansell, München, Germany
Immersion oil	Zeiss, Jena, Germany
Object slides	Marienfeld, Lauda-Königshofen, Germany
PCR soft tubes 0.25 mL	Biozym Scientific
Petri dishes (100x20 mm; 145x20 mm)	Greiner Bio-one, Frickenhausen, Germany
Pipette tips	Corning incorporation, Bodenheim, Germany
Plastic pipettes (1 mL; 5 mL; 10 mL; 25 mL)	Corning incorporation, Bodenheim, Germany
PVDF membrane	Biorad, München, Germany
Scalpel 11	Feather, Osaka, Japan
Snaptwist Scintillation Vials 6.5 mL	Simport, Beloeil, Canada
Stitches Novosyn 4/0 45 cm	B|Braun, Melsungen, Germany

2.1.3 Chemicals

2.1.3.1 Solid chemicals

Chemical	**Catalogue number**	**Company**
ML-7.HCl	BML-EI197	Enzo Life Sciences
H-89.2HCl	BML-EI196	Enzo Life Sciences
Chloroquine.$2H_3PO_4$	C6628	Sigma Aldrich
Piperaquine.$4H_3PO_4.4H_2O$	C7874	Sigma Aldrich

The rest of non-radioactive solid chemicals used in this study were purchased directly from companies Applichem, Merck, Roth, Serva, Sigma Aldrich, or Thermo Fisher Scientific, or through the Heidelberg Medical Faculty, unless indicated otherwise.

2.1.3.2 Radioactive chemicals

Chemical	Radioactivity	Concentration	Company
[^{3}H]Chloroquine	25 Ci/mmol	1 mCi/mL	GE Healthcare, Munich, Germany
[^{3}H]Piperaquine	15 Ci/mmol	1 mCi/mL	American Radiolabeled Chemicals, St. Louis, USA

2.1.3.3 Buffers, media and solutions

Buffer/medium/solution	Composition
Agarose for DNA electrophoresis gel	1 % (w/v) agarose in TAE buffer
Albumax	5 % (w/v) Albumax II in RPMI 25 mM HEPES L-glutamine (Gibco)
Anaesthetic solution	0.3 % (w/v) ethyl 2-aminobenzoate methanesulfonate pH 7 with $NaHCO_3$
Collagenase solution	0.1 % (w/v) Collagenase D 0.5 % (w/v) BSA 9 mM Na_2HPO_4 in OR2 buffer
Coomassie staining	50 % (v/v) methanol 10 % (v/v) acetic acid 0.5 % (w/v) Coomassie Blue R-250
Coomassie de-staining	20 % (v/v) methanol 7 % (v/v) acetic acid
E. coli lysis buffer	50 mM Tris pH 7.5 500 mM NaCl 10 % glycerol 5 mM β-mercaptoethanol 5 mM MgCl2 10 mM imidazole

	sm nuclease
	1x cOmplete Protease Inhibitor Cocktail (Roche)
Freezing solution	6.2 M glycerol
	0.14 M sodium lactate
	0.5 mM KCl
	pH 7.2 with $NaHCO_3$
K-CLASP lysis buffer	25 mM HEPES pH 7.4
	10 % (v/v) glycerol
	1.5 mM $MgCl_2$
	150 mM NaCl
	1 mM Na_3VO_4
	25 mM NaF
	0.8 % (v/v) IGEPAL
	1 mM DTT
	1x cOmplete Protease Inhibitor Cocktail (Roche)
Kinobeads lysis buffer	50 mM Tris pH 7.5
	5 % (v/v) glycerol
	1.5 mM $MgCl_2$
	150 mM NaCl
	1 mM Na_3VO_4
	25 mM NaF
	0.8 % (v/v) IGEPAL
	1 mM DTT
	1x cOmplete Protease Inhibitor Cocktail (Roche)
LB	1 % (w/v) tryptone/peptone
	0.5 % (w/v) yeast extract
	0.5 % (w/v) NaCl
LB-agar	LB
	1.5 % (w/v) agar-agar
MACS buffer	PBS
	0.5 % (w/v) BSA
	2 mM EDTA
ND96 pH 7.5	10 mM HEPES pH 7.5

	10 mM Tris
	96 mM NaCl
	2 mM KCl
	1 mM $MgCl_2$
	1.8 mM $CaCl_2$
	50 µg/mL gentamycin
ND96 pH 6.0	10 mM MES pH 6.0
	10 mM Tris
	96 mM NaCl
	2 mM KCl
	1 mM $MgCl_2$
	1.8 mM $CaCl_2$
	50 µg/mL gentamycin
NZY^+	1 % (w/v) casein hydrolysate
	0.5 % (w/v) yeast extract
	0.5 % (w/v) NaCl
	12 mM $MgCl_2$
	12 mM $MgSO_4$
	20 mM glucose
	To pH 7.5 with NaOH
Oocyte lysis buffer	10 mM HEPES pH 7.4
	150 mM NaCl
	1 % (v/v) IGEPAL
	0.5 % sodium deoxycholate
	0.1 % SDS
	1x cOmplete Protease Inhibitor Cocktail (Roche)
OR2 buffer	10 mM HEPES pH 7.5
	10 mM Tris
	96 mM NaCl
	2 mM KCl
	1 mM $MgCl_2$
	50 µg/mL gentamycin
PBS	1 tablet of phosphate-buffered saline solution

	in 200 mL of ddH_2O
PBST	PBS
	0.1 % Tween®20
Protein loading buffer	250 mM Tris pH 6.8
	3 % (w/v) SDS
	20 % (v/v) glycerol
	0.1 % (w/v) bromophenol blue
RPMI CM	5 % (v/v) A+ human serum
	5 % (v/v) Albumax
	0.2 mM hypoxanthine
	0.2 µg/mL gentamycin
	in RPMI 25 mM HEPES L-glutamine (Gibco)
RNA running buffer	20 mM MOPS
	2 mM sodium acetate
	0.25 mM EDTA
SB	3.5 % (w/v) tryptone/peptone
	2 % (w/v) yeast extract
	0.5 % (w/v) NaCl
	2 mM NaOH
SDS-PAGE running buffer	25 mM Tris
	250 mM glycine
	0.1 % (w/v) SDS
SDS-PAGE transfer buffer	39 mM Tris
	48 mM glycine
	0.038 % (w/v) SDS
SOB medium	2 % (w/v) tryptone/peptone
	0.5 % (w/v) yeast extract
	0.05 % (w/v) NaCl
	0.5 % (w/v) $MgSO_4.7H_2O$
SOC medium	SOB
	20 mM D-glucose
TAE buffer	4 mM Tris-acetate
	1 mM EDTA pH 8

Thawing solution I	12 % (w/v) sodium chloride
Thawing solution II	1.6 % (w/v) sodium chloride
Thawing solution III	0.9 % (w/v) sodium chloride 0.2 % (w/v) glucose

2.1.4 Biological and biologically-related materials

2.1.4.1 Enzymes

Enzyme	**Company**
Collagenase D	Roche, Penzberg, Germany
EconoTaq polymearse	Lucigen, Middleton, USA
Phusion polymerase	Thermo Fisher Scientific, Dreieich, Germany
Restriction Enzymes	New England Biolabs, Frankfurt am Main, Germany
T4 DNA ligase	Thermo Fisher Scientific, Dreieich, Germany
Thermosensitive alkaline phosphatase (TSAP), Shrimp	New England Biolabs, Frankfurt am Main, Germany

2.1.4.2 Antibodies

Antibody	**Company**
Donkey anti-guinea-pig-POD	Jackson ImmunoResearch, Suffolk, UK
Donkey anti-mouse-POD	Jackson ImmunoResearch, Suffolk, UK
Goat anti-rabbit-POD	Jackson ImmunoResearch, Suffolk, UK
Guinea pig anti-PfCRT polyclonal (raised against PfCRT's N-terminus peptide sequence MKFASKKNNQKNSSK)	Eurogentec, Cologne, Germany
Mouse anti-α-tubulin monoclonal (clone B-5-1-2)	Sigma Aldrich, Munich, Germany
Mouse anti-V5 monoclonal (1:1000; clone SV5-Pk1)	Thermo Fisher Scientific, Dreieich, Germany
Rabbit anti-PfCRT	Kindly provided by Prof. David Fidock

Wheat Germ Agglutinin Alexa Fluor 633 conjugate	Thermo Fisher Scientific, Dreieich, Germany

2.1.4.3 Organisms

Strain	Origin
Escherichia coli PMC 103	Provided by Prof. Cowman [213]
Escherichia coli BL21 DE3	Merck (Cat. Nr. 69450)
Plasmodium falciparum Dd2	Indochina [170]
Xenopus laevis	NASCO, Fort Atkinson, WI, USA Xenopus1, Dexter, MI, USA
XL10-Gold ultracompetent cells	Agilent Technologies, Waldbronn, Germany

2.1.4.4 Plasmids

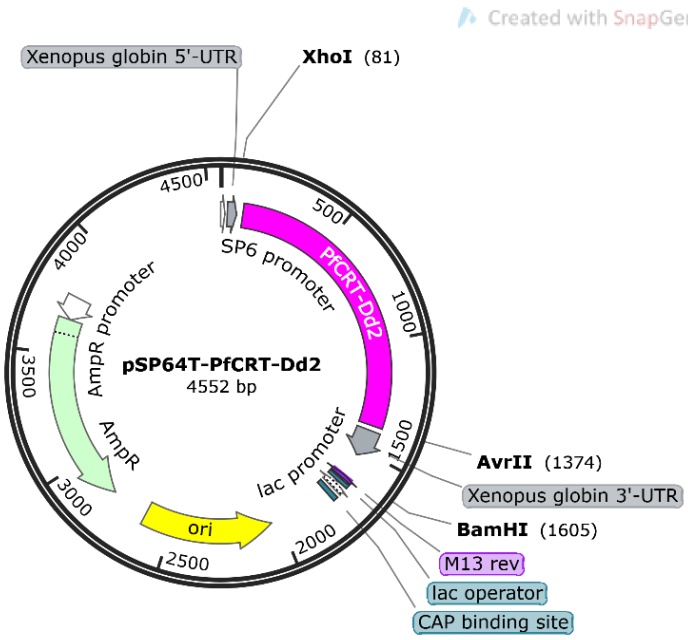

Figure 2.1. Plasmid map of the plasmid pSP64T-PfCRT-Dd2 for cloning and *in vitro* transcription of PfCRT. Shown is the plasmid map with its size in bp, and the features present in it. Arrows indicate the direction of reading. AmpR: ampicillin resistance cassette; ori: origin of replication; CAP: catabolite activator protein. Map created with SnapGene 6.0.2.

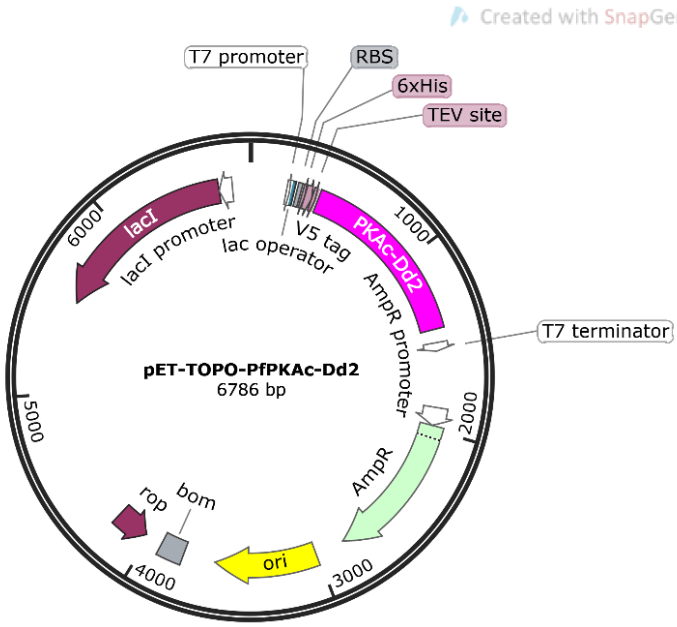

Figure 2.2. Plasmid map of the plasmid pET-TOPO-PfPKAc-Dd2 for expression of PfPKAc in *E. coli* BL21 (DE3). Shown is the plasmid map with its size in bp, and the features present in it. Arrows indicate the direction of reading. AmpR: ampicillin resistance cassette; ori: origin of replication; bom: basis of mobility; rop: rop protein gene; RBS: ribosome binding site; TEV: TEV protease cleavage site. Custom made by Invitrogen. Map created with SnapGene 6.0.2.

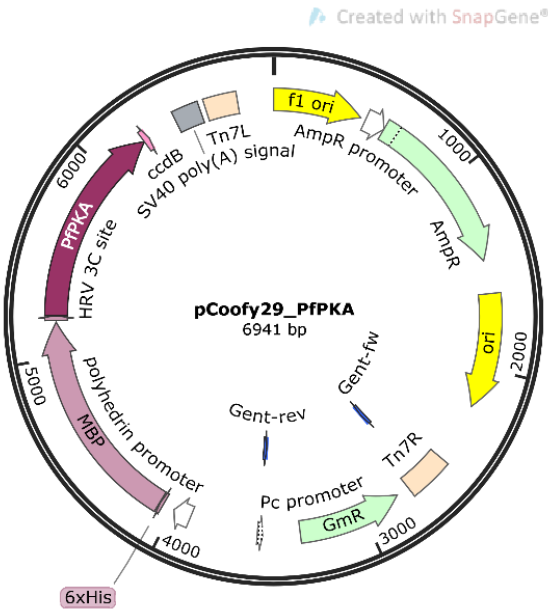

Figure 2.3. Plasmid map of the plasmid pCoofy29_PfPKA for expression of PfPKAc in insect cells. Shown is the plasmid map with its size in bp, and the features present in it. Arrows indicate the direction of reading. AmpR: ampicillin resistance

cassette; f1 ori: f1 bacteriophage origin of replication; ori: origin of replication in bacteria; Tn7: transposon Tn7; GmR: gentamycin acetyltransferase; MBP: maltose binding protein; HRV 3C: human rhinovirus 3C protease cleavage site; ccdB: bacterial toxin. pCoofy29 was a gift from Sabine Suppmann (Addgene plasmid # 44005 ; http://n2t.net/addgene:44005 ; RRID:Addgene_44005) [214]. Map created with SnapGene 6.0.2.

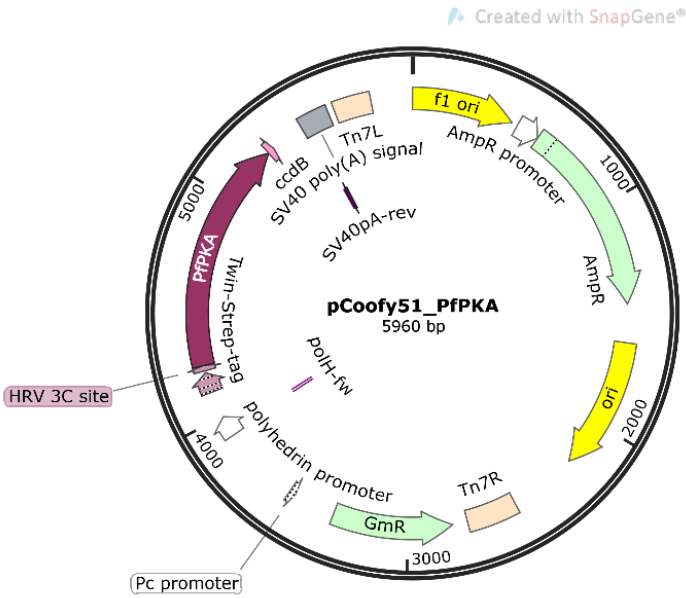

Figure 2.4. Plasmid map of the plasmid pCoofy51_PfPKA for expression of PfPKAc in insect cells. Shown is the plasmid map with its size in bp, and the features present in it. Arrows indicate the direction of reading. AmpR: ampicillin resistance cassette; f1 ori: f1 bacteriophage origin of replication; ori: origin of replication in bacteria; Tn7: transposon Tn7; GmR: gentamycin acetyltransferase; HRV 3C: human rhinovirus 3C protease cleavage site; ccdB: bacterial toxin. pCoofy51 was a gift from Sabine Suppmann (Addgene plasmid # 122005 ; http://n2t.net/addgene:122005 ; RRID:Addgene_122005) [214]. Map created with SnapGene 6.0.2.

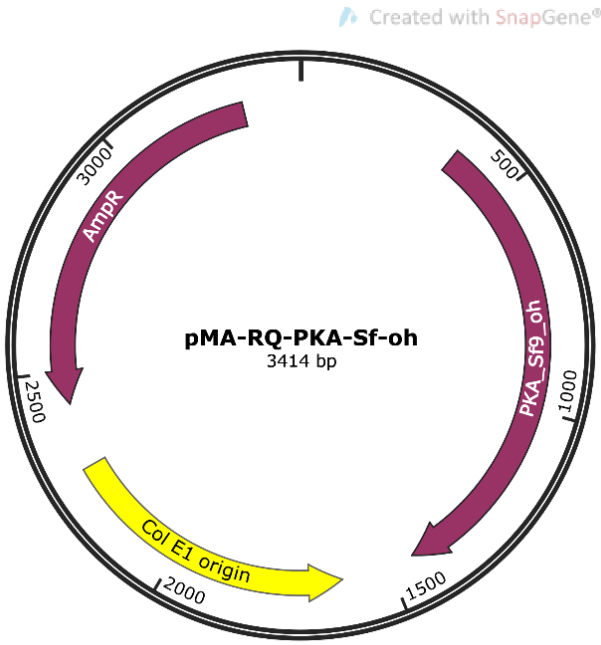

Figure 2.5. Plasmid map of the plasmid pMA-RQ-PKA-Sf-oh as a template for *pfpkac*, codon-optimized for expression in *Spodoptera frugiperda* Sf9 and Sf21 cells. Shown is the plasmid map with its size in bp, and the features present in it. Arrows indicate the direction of reading. AmpR: ampicillin resistance cassette; Col E1 origin: origin of replication. Custom made by Invitrogen. Map created with SnapGene 6.0.2.

2.1.4.5 Primers

Number	Name	Sequence (5’ → 3’)
1	5’Globin-for	GCAGAAGCTCAGAATAAACG
2	3’Globin-rev	GTAGCTTAGAGACTCCATTCG
3	H97Y-for	CCTCTGAAACCTATAACTTCATCTG
4	H97Y-rev	CAGATGAAGTTATAGGTTTCAGAGG
5	V141A-for	GCCTGCTCTGCTATTTTGGC
6	V141A-rev	GCCAAAATAGCAGAGCAGGC
7	F145I-for	TATTTTGGCTATCATCGGTTTGAC
8	F145I-rev	TCAAACCGATGATAGCCAAAATAAC
9	S257A-for	CAATTATTCACCGCCTGCTTGA
10	S257A-rev	TCAAGCAGGCGGTGAATAATTG
11	I260A-for	CTCCTGCTTGGCTTTGCCAG

12	I260A-rev	CTGGCAAAGCCAAGCAGGAG
13	M343L-for	TCTCCACTCTGACCTAC
14	M343L-rev	GTAGGTCAGAGTGGAGA
15	G353V-for	GCATTCAAGTTCCAGCTAC
16	G353V-rev	GTAGCTGGAACTTGAATGC
17	LP1-3C-vector-for	GGGCCCCTGGAACAGAACTTCCAG
18	LP2-ccdB-vector-rev	CGCCATTAACCTGATGTTCTGGGG
19	LP1-3C-overhang-for	AAGTTCTGTTCCAGGGGCCC
20	LP2-ccdB-overhang-rev	CCCCAGAACATCAGGTTAATGGCG
21	polH-for	AAATGATAACCATCTCGC
22	SV40pA-rev	GAAATTTGTGATGCTATTGC

2.1.4.6 Peptides

Name	**N-modification**	**Sequence (N → C)**
33-S	Biotin	ELDNLVQEGNGSRLGGGSCLGK
33-K	Biotin	ELDNLVQEGNGKRLGGGSCLGK

2.1.5 Software and databases

Program/Database	**Version**	**Developer/Source**
Chromas	2.6.6	Technelysium Pty Ltd
ImageJ	1.52	NIH
Jupyter (anaconda3)	1.0.0	Anaconda
PlasmoDB		http://plasmodb.org/plasmo/
Protein Data Bank		http://rcsb.org/pdb/home/home.do
Serial Cloner	2.6.1	SerialBasics
SigmaPlot	14.0	Systat Software Inc.
SnapGene Viewer	6.0.2	SnapGene
UniProt		https://www.uniprot.org/

2.2 Methods

2.2.1 Parasitology

2.2.1.1 *In vitro* cultures of *P. falciparum*

Intraerythrocytic stages of *P. falciparum* were kept in a blood culture following standard protocols, with slight modifications [215]. Cultures were kept in an incubator at 37 °C with a fixed atmosphere of 5 % O_2, 3 % CO_2, 92 % N_2, and 95 % humidity. They were kept in RPMI CM at a hematocrit of 2-4 %. The development of parasites was monitored regularly by microscopic inspection of Giemsa-stained thin blood smears. The parasitemia (percentage of infected red blood cells) was maintained between 0.5 % and 20 %, depending on the experimental requirements. To avoid accumulation of toxic metabolites, the medium was changed at least every second day.

2.2.1.2 Freezing and thawing of parasites

For long-term storage, parasites were cryopreserved. A culture at 3-5 % parasitemia consisting mostly of ring-stage parasites was pelleted by centrifugation at 900 g at RT for 2 min. The pellet was treated with 1/3 volume (compared to pellet size) of Freezing solution. After incubating 5 min at RT, 4/3 volumes (compared to pellet size) of Freezing solution were used to carefully resuspend the pellet. The suspension was distributed in cryogenic vials, and frozen at -80 °C or in liquid nitrogen.

To thaw parasites, the frozen cryogenic vials were thawed at 37 °C, before resuspending with 200 µL of Thawing solution I. The suspension was transferred to a 15 mL falcon tube, and 9 mL of Thawing solution II were slowly added. The sample was centrifuged at 900 g at RT for 2 min, and the pellet was slowly re-suspended with 7 mL of Thawing solution III. The cells were pelleted once again at 900 g at RT for 2 min. After that, they were re-suspended in RPMI CM and transferred to a Petri dish containing 500 µL of fresh erythrocytes.

2.2.1.3 Parasite synchronization with sorbitol (ring stages)

During intraerythrocytic development, parasites express different proteins that increase the permeability of the host red blood cell membrane. Upon sorbitol treatment, trophozoite- and schizont-infected red blood cells, permeable to the sugar, get destroyed by osmotic shock. In contrast, ring-infected and non-infected red blood cells

are impermeable to sorbitol and, thus, survive the treatment [216]. Briefly, the red blood cells in the culture were re-suspended in 10 mL pre-warmed 5 % sorbitol, and incubated 5-10 min at 37 °C. Then, the suspension was centrifuged at 900 g at RT for 2 min. The pellet was re-suspended in RPMI CM and transferred to a fresh Petri dish.

2.2.1.4 Parasite synchronization through magnetic purification (trophozoite and schizont stages)

Late intraerythrocytic parasite stages show accumulation of iron-containing hemozoin crystals in their digestive vacuoles. Based on that, trophozoite- and schizont-infected red blood cells have paramagnetic properties. Thus, a magnetic activated cell sorting (MACS) system can be used to separate these from ring-infected and uninfected red blood cells. A MACS D column was washed twice with MACS buffer and inserted into the SuperMACS II separator. The parasite culture was loaded into the column, and the elution rate was adjusted to 1 drop every 2-3 seconds. The column was then washed with MACS buffer until a colourless flow-through was observed. Then, the column was removed from the separator, and the late stage-infected red blood cells were eluted with 10 mL MACS buffer into a 15 mL falcon tube. Cells were pelleted at 900 g at RT for 2 min, re-suspended in 1 mL PBS, and transferred to a 1.5 mL Eppendorf tube. They were centrifuged at 16000 g at 4 °C for 1 min. If the supernatant presented colour, the washing step with PBS and the subsequent centrifugation were repeated. Otherwise, they were immediately used or frozen at -80 °C until use.

2.2.1.5 Parasite lysis for kinobead pull-down and K-CLASP assays

After MACS purification of late stage-infected red blood cells, the red blood cells were lysed to release the parasites by incubation at 37 °C for 30 s in 0.07 % (w/v) saponin in PBS. The parasites were pelleted by centrifugation at 16000 g at 4 °C for 1 min and washed with 1 mL PBS, and then centrifuged again under the same conditions. The washing step was repeated as long as the supernatant presented colour. The parasite pellet was then re-suspended in appropriate volume (depending on pellet size) of Kinobeads lysis buffer or K-CLASP lysis buffer. The suspension was sonicated to lyse the parasites. Each sample was sonicated thrice, each time with 8 pulses at 20 % and minimum power (Bandelin sonopuls HD 2070), with resting periods of at least 1 min on ice in between sonication cycles. The lysates were centrifuged at 16000 g at 4 °C for 30 min, and the supernatants were stored at -80 °C until use.

2.2.1.6 Kinobead-based identification of drug-binding protein kinases

The identification of parasitic protein kinases that bind to the kinase inhibitors ML-7 and H-89 was carried out by Dr. Polina Prokofeva and Dr. Guillaume Médard from the Technical University of Munich, Germany. A parasite lysate prepared in Kinobeads lysis buffer was diluted with 1 volume of CP buffer (50 mM Tris pH 7.5, 5 % glycerol, 1.5 mM $MgCl_2$, 150 mM NaCl, 1 mM Na_3VO_4, 20 mM NaF, 1 mM DTT, 1x cOmplete Protease Inhibitor Cocktail (Roche)). For competition pulldowns in 96-well plates, 500 µL of diluted lysates were pre-incubated with 1 of 9 concentrations of either ML-7 or H-89 (vehicle DMSO, 30 nM, 100 nM, 300 nM, 1 µM, 3 µM, 10 µM, 30 µM, or 300 µM) at 4 °C for 45 min in an end-over-end shaker [217]. Kinobeads were added to a 96-well filter plate (17 µL settled beads per well) and pre-equilibrated with 1 mL CP buffer, followed by a washing step with CP buffer supplemented with 0.4 % IGEPAL. Then, compound-lysate mixtures were incubated with kinobeads at 4 °C for 30 min in an end-over-end shaker.

To assess the degree of protein depletion from the lysates, a second pulldown was performed with fresh beads and the unbound protein flow through of the vehicle DMSO control mixtures. The beads were then washed with 1 mL of CP buffer supplemented with 0.4 % IGEPAL, then with 2 mL of CP buffer supplemented with 0.2 % IGEPAL, and lastly with 3 mL of CP buffer. Proteins were denatured by incubation with 40 µL denaturing buffer (40 mM Tris pH 7.4, 8 M urea, 10 mM DTT) at 4 °C for 30 min, and alkylated by incubating a RT for 30 min with 4 µL 550 mM chloroacetamide. Urea was diluted to 1 M by the addition of 250 µL 40 mM Tris pH 7.4. Proteins were digested overnight with 30 µL 10 ng/µL trypsin. Digested peptides were eluted, acidified with 7 µL 10 % formic acid, and subjected to C18 StageTip desalting. For that, acidified peptides were loaded twice onto StageTip columns and centrifuged at 500 g. Columns were washed twice with 200 µL 0.1 % formic acid in deionized water. Peptides were collected by double elution with 40 µL 0.1 % formic acid in 50 % acetonitrile, frozen and dried in vacuum prior to LC-MS/MS analysis.

For analysis, an Orbitrap Fusion Lumos (Thermo Fisher Scientific) mass spectrometer coupled to a Dionex UltiMate 3000 HPLC was used. Peptides were delivered to a trap column within 10 min in 0.1 % formic acid in HPLC grade water at 5 µL/min. Peptides were then separated on an analytical column over a 50 min gradient ranging 4-32 % solvent B (0.1 % formic acid, 5 % DMSO in acetonitrile) in solvent A (0.1 % formic acid,

5 % DMSO in HPLC grade water) at 300 nL/min. The mass spectrometer operated in data dependent mode, and MS1 spectra were acquired over a mass-to-charge ratio of 360-1300 m/z at a resolution of 60000 in the Orbitrap. Maximum injection time was set to 50 ms and automatic gain control (AGC) target value to $5x10^5$. Top 12 most abundant peptide precursors were isolated (isolation window of 1.7, maximum injection time of 22 ms, AGC value of $1x10^5$), fragmented by higher energy collision induced dissociation (HCD) using 28 % normalized collision energy (NCE) and analysed in the Orbitrap at a resolution of 15000. The dynamic exclusion was set to 20 s.

Peptide and protein identification and quantification was performed with MaxQuantv1.5.3.30. Acquired raw MS data was searched against all canonical protein sequences annotated in Swissprot reference *Plasmodium falciparum* (isolate 3D7) database using the integrated search engine Andromeda. Trypsin/P was specified as the proteolytic enzyme with up to two missed cleavage sites allowed. Cysteine carbamidomethylation was set as fixed modification, methionine oxidation and protein N-terminal acetylation were set as variable modifications. IBAQ, label-free quantification (LFQ) and match between runs (MBR) were enabled. All searches were performed with 1 % Peptide-spectrum match (PSM) and protein false discovery rate (FDR). Other search parameters were set as default.

Relative binding for every compound concentration and correction factor (cf) for protein depletion was calculated as the ratio of a protein group LFQ intensity for every compound concentration to the DMSO vehicle control. The correction factor was calculated as the ratio of LFQ intensities from the second consecutive pulldown done with the flow through of the DMSO vehicle control pulldown to the LFQ intensities in the DMSO vehicle control. EC50 values were derived from dose-response curves. Apparent binding constants (K_D^{app}) were calculated by multiplying EC50 values with the respective correction factor. Potential compound interactors were annotated manually if the resulting binding curve showed typical sigmoidal shape. Unique peptides and acquired MS/MS spectral counts for each condition that showed a dose-dependent decrease were used as additional level of evidence for binder annotation.

2.2.1.7 Kinase-catalysed crosslinking and streptavidin purification (K-CLASP)

The identification of protein kinases from the parasite that can phosphorylate peptides containing the phosphosite Ser33 of PfCRT was carried out by Eric Davis and Prof.

Mary Kay Pflum from the Wayne State University, USA. A parasite lysate was prepared as described above, with the lysis done in K-CLASP lysis buffer. The lysate was incubated with 5 mM ATP-ArN_3 and 4.1 mM N-biotinylated peptide (see section 2.1.4.6 Peptides) in a total volume of 60 µL, for 2 h at 31 °C with shaking at 300 rpm under UV irradiation at 365 nm [218, 219]. Control reactions were performed without ATP-ArN_3, no UV irradiation, or with 4.1 mM mutant N-biotinylated peptide. Excess N-biotinylated peptide and endogenous biotin were removed by filtration using 3 kDa centriprep spin columns (Millipore). The filtered samples were then incubated with streptavidin resin (250 µL, Genscript) for 20 min at room temperature with rotation in phosphate binding buffer (0.1 M phosphate pH 7.2, 0.15 M NaCl) in a total volume of 250 µL. The resin was washed 10 times with 250 µL phosphate binding buffer, and then four times with 250 µL water. Proteins were eluted by boiling in 250 µL 2 % SDS for 8 min. The elution was concentrated and excess SDS was partially removed by filtering using a 3 kDa centriprep spin column. The concentrated samples were boiled at 95 °C for 1 min in Laemmli sample buffer and separated on 10 % SDS-PAGE gels. Total proteins were visualized with SPYRO Ruby stain. Kinases were visualized with Streptavidin CY5 (Thermo Fisher Scientific, catalogue number: 434316) after transfer onto PVDF membranes.

Proteins were in-gel digested from three independent trials as previously described [220]. Digested peptides were separated by reverse-phase chromatography in 0.1 % formic acid using and EASY nLC-1000 UHPLC system (Thermo). MS1 profiling was carried out over a 375-1600 m/z range at a resolution of 70000. MS2 fragmentation was performed using higher energy collision induced dissociation (HCD) on the top 15 ions using a 1.6 m/z window and normalized collision energy (NCE) of 29 %. Dynamic exclusion was set to 15 s. MS raw data was processed using Proteome Discoverer v2.2 against three *Plasmodium falciparum* UniProt (downloaded 05.13.2022; 16679 entries). Searches included up to 2 missed tryptic cleavages. Mass tolerances for parent ions were 20 ppm for the first search, 4.5 ppm for the second search, and 20 ppm for fragment ions. The S5 iodoacetamide derivative was set as a fixed modification. Oxidation of methionine and acetylation of protein N-termini were set as variable modifications. Minimum protein and peptide identification probabilities were set at ≤1 % false discovery rate (FDR), as determined by a reversed database search, and proteins required just 1 unique peptide. All other parameters were left at default

settings. Fold enrichment was calculated by dividing the peptide intensity observed for N-biotinylated peptide by that observed for the mutant N-biotinylated peptide. A hit list was constructed by identifying proteins with at least 1.5-fold enrichment in N-biotinylated peptide compared to the non-UV irradiated samples in at least two replicates.

2.2.2 Molecular biology of nucleic acids

2.2.2.1 Agarose gel electrophoresis

To separate DNA molecules according to their size, agarose gel electrophoresis was performed. The agarose was boiled until complete dissolution in TAE buffer to a final concentration of 1 % (w/v; for 1 to 10 kb fragments) or 2 % (w/v; for 0.1 to 1 kb fragments). The liquid agarose was mixed with ROTI GelStain Red (Carl Roth) and used to cast the gel. The GeneRuler 1 kb Plus DNA-ladder (Thermo Fisher Scientific) was used as a size marker. The samples were mixed with 6x DNA Loading Dye (Thermo Fisher Scientific) and loaded into the wells. Gels were run at 90-140 V and 400 mA for 45-60 min. UV illumination was used to visualize the DNA bands, and images were taken with a DC120 Zoom Digital Camera (Kodak).

Similarly, the quality of RNA molecules was assessed by agarose gel electrophoresis. RNAse-free agarose was boiled until complete dissolution in 1.5x RNA running buffer to a final concentration of 0.9 % (w/v). The liquid agarose was supplemented with ROTI GelStain Red (Carl Roth) and used to cast the gel. The solidified gel was incubated for 1 min with 37 % formaldehyde to prevent the formation of RNA secondary structures. Samples were incubated at 65 °C for 3 min with RNA Loading buffer (Thermo Fisher Scientific). Gels were run at 60 V for 60 min. Visualization of RNA bands was done as described above for DNA bands.

2.2.2.2 DNA purification from agarose gel

The QIAquick Gel Extraction Kit was used to extract DNA molecules from agarose gels, following the manufacturer's instructions. The desired agarose gel fragments were cut out and solubilized in 3 volumes relative to gel weight of QG buffer at 56 °C. Then, 1 volume relative to gel weight of isopropanol was added. The mixture was transferred to a QIAquick TM column and spun down at 16000 g at RT for 1 min. The column was washed once with 700 µL PE buffer and centrifuged twice in the same

conditions as before. DNA was eluted with 22 µL pre-warmed (56 °C) ddH_2O. The purified fragments were stored at -20 °C until use.

2.2.2.3 Generation of *pfpkac* insert with overhangs and of linear pCoofy vectors

For expression of PfPKAc in insect cell lines Sf9 and Sf21, a codon-optimized version of the *pfpkac* gene was purchased as part of the pMA-RQ-PKA-Sf-oh plasmid (Figure 2.5). The gene was amplified, and overhangs were incorporated on both ends, by running the following PCR:

***pfpkac* with LP overhangs PCR**

Reagent	**Volume**	**Settings**		
		T °C	**time**	
ddH_2O	32 µL			
5x HF buffer	10 µL	98 °C	3 min	
2 mM dNTPs	5 µL	98 °C	20 s	x30
pMA-RQ-PKA-Sf-oh	1 µL	52 °C	20 s	
LP1-3C-overhang-for 50 µM	0.5 µL	70 °C	30 s	
LP2-ccdB-overhang-rev 50 µM	0.5 µL	70 °C	3 min	
Phusion polymerase 2 U/µL	1 µL	4 °C	∞	

In parallel, the vectors pCoofy29 and pCoofy51 were linearized with the following PCR:

pCoofy vector linearization PCR

Reagent	**Volume**	**Settings**		
		T °C	**time**	
ddH_2O	32 µL			
5x HF buffer	10 µL	98 °C	3 min	
2 mM dNTPs	5 µL	98 °C	20 s	x30
pCoofy29 or pCoofy51	1 µL	70 °C	20 s	
LP1-3C-vector-for 50 µM	0.5 µL	70 °C	20 s	
LP2-ccdB-vector-rev 50 µM	0.5 µL	70 °C	3 min	
Phusion polymerase 2 U/µL	1 µL	4 °C	∞	

All the PCR products were run on a 1 % agarose gel and purified from the gel using the QIAquick Gel Extraction Kit, as described above. Products were stored at -20 °C until use.

2.2.2.4 In-Fusion cloning of *pfpkac* into pCoofy vectors and transformation of ultracompetent cells

The PCR products that were purified from agarose gels were thawed on ice, and their concentrations were determined using a NanoDrop. Using the In-Fusion cloning kit (Takara Bio), the cloning of *pkpkac* into pCoofy vectors was performed at 50 °C for 15 min as follows. After the reaction was completed, the samples were placed on ice.

In-Fusion cloning

Reagent	**Volume**
ddH_2O	x µL (to 10 µL)
pfpkac-overhang (insert)	y µL (50 ng)
Linear pCoofy29 or pCoofy51 (vector)	z µL (to 8:1 molar ratio of insert:vector)
5x In-Fusion Mix	2 µL

In parallel, XL10-Gold Ultracompetent cells (Agilent Technologies, USA) were thawed on ice, and β-mercaptoethanol was added as suggested by the manufacturer. The mixture was incubated on ice for 10 min, before transforming DNA was added and mixed gently. The new mixture was incubated on ice for 30 min. A heat pulse at 42 °C for 30 s followed, and the cells were then place on ice for 2 min. A total of 900 µL pre-warmed (42 °C) NZY^+ medium was added, and the cells were grown at 37 °C under shaking for 1 h. At least 200 µL of the culture was plated onto LB-Agar plates supplemented with 100 µg/mL ampicillin, and incubated overnight at 30 °C.

The transformant colonies were screened for the presence of the *pfpkac* gene by colony screening PCR, where part of the colonies was submerged in the PCR mixture:

pCoofy-PfPKAc screening PCR

Reagent	Volume
ddH_2O	16.5 µL
10x EconoTaq buffer	2.5 µL
2 mM dNTPs	2.5 µL
25 mM $MgCl_2$	2.5 µL
LP1-3C-overhang-for 50 µM	0.5 µL
LP2-ccdB-overhang-rev 50 µM	0.5 µL
EconoTaq 5 U/µL	0.25 µL

PCR settings		
T °C	**time**	
98 °C	3 min	
98 °C	20 s	x30
56 °C	20 s	
70 °C	1 min 15 s	
70 °C	3 min	
4 °C	∞	

PCR products were run on a 1 % agarose gel, and the presence of insert was confirmed by the presence of a band at 1.3 kbp. Positive colonies were used for plasmid mini prep (see section 2.2.2.10 Plasmid preparation (Mini prep)), which were sent to sequencing (see section 2.2.2.11 DNA sequencing) using primers 21 and 22 see section 2.1.4.5 Primers).

2.2.2.5 Overlap extension PCR for site-directed mutagenesis

To introduce point mutations in *pfcrt* in the pSP64T-PfCRT-Dd2 plasmid, the overlap extension PCR method was used [221]. PCR 1 was run using 5'Globin-for and a reverse mutant primer (RMP; see section 2.1.4.5 Primers), while PCR 2 was run using 3'Globin-rev and a forward mutant primer (FMP). The annealing temperature (T_a) of the PCR cycles was that of the lowest primer T_m + 4 °C, as recommended by the manufacturer for Phusion polymerase. The reactions were set as follows:

Reagent	Volume	
	PCR 1	**PCR 2**
ddH_2O	32 µL	32 µL
5x HF buffer	10 µL	10 µL
2 mM dNTPs	5 µL	5 µL
Template DNA	1 µL	1 µL
5'Globin-for 50 µM	0.5 µL	—
RMP 50 µM	0.5 µL	—
3'Globin-rev 50 µM	—	0.5 µL
FMP 50 µM	—	0.5 µL
Phusion polymerase 2 U/µL	1 µL	1 µL

Settings		
T °C	**time**	
98 °C	3 min	
98 °C	20 s	x30
T_a	20 s	
70 °C	20 s	
70 °C	3 min	
4 °C	∞	

The PCR 1 and PCR 2 products were run on a 1 % agarose gel and purified from the gel using the QIAquick Gel Extraction Kit, as described above. Then, they were used to run PCR 3:

PCR 3

Reagent	**Volume**
ddH_2O	32 µL
5x HF buffer	10 µL
2 mM dNTPs	5 µL
PCR 1 product	0.5 µL
PCR 2 product	0.5 µL
5'Globin-for 50 µM	0.5 µL
3'Globin-rev 50 µM	0.5 µL
Phusion polymerase 2 U/µL	1 µL

Settings		
T °C	**time**	
98 °C	3 min	
98 °C	20 s	x30
58 °C	20 s	
70 °C	30 s	
70 °C	3 min	
4 °C	∞	

The PCR 3 products were run on a 1 % agarose gel and purified from the gel using the QIAquick Gel Extraction Kit, as described above. The DNA fragments were stored at -20 °C until use.

2.2.2.6 Sticky end generation and ligation

To introduce the PCR 3 products into the backbone of the pSP64T vector, both the PCR 3 product and the plasmid pSP64T-PfCRT-Dd2 were digested overnight at 37 °C with the same pair of restriction enzymes:

	PCR 3	**pSP64T-PfCRT-Dd2**
Reagent	**Volume**	
DNA sample	22 µL	5 µL
ddH_2O	—	17 µL
10x CutSmart buffer	2.5 µL	2.5 µL
AvrII	0.25 µL	0.25 µL
XhoI	0.25 µL	0.25 µL

The next day, 1 µL of thermosensitive alkalyne phosphatase (TSAP) was added to the plasmid sample, followed by an incubation at 37 °C for 30 min. Then, the enzyme TSAP was inactivated by incubating at 65 °C for 15 min. Both the digested PCR 3 product (from here on, "insert") and the digested, dephosphorylated plasmid (from here

on, “open vector”) were run on a 1 % agarose gel, and later extracted from the gel as described before.

The concentration of purified insert and open vector were measured by using a NanoDrop One. A ligation between them was run overnight at 16 °C in the following conditions:

Ligation

Reagent	**Volume**	Use volumes such that the molar ratio of insert:vector is 1:1, and total volume of 10 µL
Insert	x µL (100 ng)	
Open vector	y µL	
5x T4 DNA Ligase buffer	2 µL	
T4 DNA Ligase	1 µL	

2.2.2.7 Preparation of electrocompetent *Escherichia coli*

Electrocompetent *E. coli* PMC103 was inoculated and grown overnight in 10 mL Super Broth (SB) medium at 37 °C while shaking at 200 rpm. The next day, 6 mL of the overnight culture were used as a starter to inoculate 600 mL SB medium, and the culture was grown at 37 °C for 3.5 h while shaking at 200 rpm. The bacteria were harvested by centrifugation at 6000 g at 4 °C for 15 min. From here on, all steps were done on ice, using ice-cold solutions, under sterile conditions. The pellet was washed with 600 mL ddH_2O, and centrifuged at 6000 g at 4 °C for 15 min. The washing step was repeated, and the bacteria were centrifuged under the same conditions. The pellet was then washed with 10 % (v/v) glycerol and centrifuged under the same conditions. The pellet was then re-suspended in 2 mL 10 % (v/v) glycerol, aliquoted, and snap-frozen at -80 °C. The bacteria were stored at -80 °C until use.

2.2.2.8 Transformation of electrocompetent *Escherichia coli*

First, the ligated DNA was purified from the ligation mixture to increase transformation efficiency. To do that, 1 volume (1 µL) of 3.5 M sodium acetate (pH 4.5) and 2.5 volumes (25 µL) of 100 % ethanol were added to the ligation mixture. The DNA precipitation was further promoted by incubating at -80 °C for at least 30 min. Then, the ligation product was pelleted by centrifugation at 16000 g at 4 °C for 30 min. The pellet was washed with 50 µL 70 % ethanol, and the centrifugation step was repeated. The DNA pellet was allowed to air-dry, and then dissolved in 10 µL ddH_2O.

For the transformation of bacteria, 50 µL of cells were thawed on ice, mixed with 200 µL sterile 10 % glycerol (v/v) and with the purified ligated product. Electroporation was carried at 2500 V (Electroporator Gene Pulser II). Cells were mixed with 1 mL pre-warmed (37 °C) SOC medium and incubated at 37 °C for 1 h with shaking at 180 rpm. Bacteria were pelleted by centrifugation at 6000 g for 5 min, resuspended in 100 µL LB, and plated onto LB-Agar plates supplemented with 100 µg/mL ampicillin. Plates were incubated overnight at 30 °C.

2.2.2.9 Colony screening PCR of *pfcrt*

To confirm the presence of insert in colonies, colony screening PCR was carried out by submerging part of the colonies in PCR mixture, and running the PCR reactions as follows:

Colony screening

Reagent	**Volume**
ddH_2O	16.5 µL
10x EconoTaq buffer	2.5 µL
2 mM dNTPs	2.5 µL
25 mM $MgCl_2$	2.5 µL
5'Globin-for 50 µM	0.5 µL
3'Globin-rev 50 µM	0.5 µL
EconoTaq 5 U/µL	0.25 µL

PCR settings		
T °C	**time**	
98 °C	3 min	
98 °C	20 s	x30
56 °C	20 s	
70 °C	1 min 15 s	
70 °C	3 min	
4 °C	∞	

PCR products were run on a 1 % agarose gel, and the presence of insert was confirmed by the presence of a band at 1.4 kbp.

2.2.2.10 Plasmid preparation (Mini prep)

Plasmid preparation was done in small scale for control and sequencing purposes using the High Pure Plasmid Isolation Kit (Roche). A transformant colony with the desired plasmid was grown overnight at 37 °C while shaking at 180 rpm in 10 mL LB medium supplemented with 100 µg/mL ampicillin. The next day, the bacteria were harvested by centrifugation at 6000 g for 8 min, resuspended in 300 µL buffer P1, and lysed with an extra 300 µL buffer P2 at RT for 5 min. Then, 300 µL of buffer P3 were added, and the suspension was mixed and incubated on ice for 5 min. The sample was centrifuged at 16000 g at 4 °C for 10 min, and the supernatant was transferred to a DNA-binding column provided in the kit. The sample was allowed to pass through

the column by centrifugation at 16000 g at RT for 1 min. The column was first washed with 700 µL of buffer P4 and centrifuged under the same conditions as before, and then with 500 µL buffer P5, centrifuging again in same conditions. The DNA was eluted with 50 µL pre-warmed (56 °C) ddH_2O by centrifuging in the same conditions as before.

As a control, a digestion was run at 37 °C for 30 min as follows:

Digestion

Reagent	**Volume**
ddH_2O	5 µL
Plasmid mini prep	3 µL
10x CutSmart buffer	1 µL
AvrII	0.5 µL
XhoI	0.5 µL

The digested samples were run on a 1 % agarose gel, and bands at approximately 3.2 kbp and 1.3 kbp were expected.

2.2.2.11 DNA sequencing

The sequencing of DNA samples was performed by Eurofins Genomics (Ebersberg, Germany) using the cycle sequencing technology, a modification of the traditional Sanger sequencing [222]. Serial Cloner software was used to analyse the sequences obtained. The used primers are listed in section 2.1.4.5 Primers. The samples were prepared as follows:

Plasmids 20 µL, 30-100 ng/µL
Primers 20 µL, 10 pmol/µL

2.2.2.12 Plasmid preparation (Maxi prep)

Plasmid preparation was done in large scale for preparative purposes using the QIAGEN Plasmid Maxi Kit. A colony carrying the desired plasmid was grown overnight at 37 °C shaking at 180 rpm in 400 mL SB medium supplemented with 100 µg/mL ampicillin. The next day, the bacteria were harvested by centrifugation at 2700 g at 4 °C for 15 min. The pellet was resuspended in 10 mL buffer P1 and lysed by mixing and incubating for 10 min at RT with 10 mL buffer P2. Then, 10 mL buffer P3 were added, mixed, and the suspension was incubated for 20 min on ice. A centrifugation step at 17400 g at 4 °C for 30 min followed. To clear it out of any debris, the supernatant

was centrifuged again at 17400 g at 4 °C for 15 min. The supernatant was loaded onto a previously equilibrated column and allowed to flow through it. The column was washed twice with 20 mL washing buffer. The DNA was then eluted with 15 mL elution buffer, and 10.5 mL isopropanol were added. The DNA was pelleted by centrifuging at 14200 g at 4 °C for 30 min. The pellet was washed with 1 mL 70 % ethanol and centrifuged at 16000 g at 4 °C for 10 min. After air-drying, DNA was dissolved in appropriate volume of ddH_2O (100-200 µL) and stored at -20 °C until use.

2.2.2.13 Plasmid linearization and phenol/chloroform extraction

Plasmid DNA from Maxi preps was linearized by incubating 20 µg DNA at 37 °C overnight with a restriction enzyme as follows:

Linearization

Reagent	**Volume**
Plasmid Maxi prep	x µL (20 µg DNA)
ddH_2O	y µL (to 50 µL)
10x CutSmart buffer	5 µL
BamHI-HF	4 µL

The next day, the DNA was purified by phenol/chloroform extraction. First, 300 µL ddH_2O were added to the linearization mixture. Then, 1 volume (350 µL) Roti phenol/chloroform/isoamylalcohol (Carl Roth) were added, and the mixture was vortexed. It was then centrifuged at 16000 g at RT for 2 min. The upper, aqueous phase was recovered, and 1 volume (350 µL) Roti phenol/chloroform/isoamylalcohol were added and mixed thoroughly. The mixture was centrifuged under same settings as before. The upper phase was recovered and mixed with 1 volume of a 25:1 mixture of chloroform:isoamylalcohol, and later centrifuged in same conditions. The upper phase was again recovered, and DNA was precipitated by adding 0.1 volumes (35 µL) 3.5 M sodium acetate (pH 4.5) and 2.5 volumes (875 µL) of 100 % ethanol, and by incubating at -80 °C for at least 30 min. The DNA was then pelleted by centrifuging at 16000 g at 4 °C for 10 min, washed with 70 % ethanol, and centrifuged again. After air-drying, the DNA was dissolved in 20 µL nuclease-free H_2O (Thermo Fisher Scientific).

2.2.2.14 Capped RNA synthesis

The *in vitro* synthesis of 5'-capped RNA (cRNA) was carried using the *in vitro* RNA transcription kit mMessage mMachine SP6 (Thermo Fisher Scientific). The phenol-chloroform-purified, linearized plasmid DNA was used as a template, and the reaction was allowed to run at 37 °C for 2 h as follows:

cRNA synthesis

Reagent	**Volume**
2x NTP/CAP	10 µL
Linearized DNA	x µL (1 µg DNA)
Nuclease-free H_2O	y µL (to 20 µL)
10x Buffer	2 µL
Enzyme Mix	2 µL

Then, 1 µL DNAse was added to degrade the DNA at 37 °C for 15 min. The reaction was stopped and cRNA was precipitated by addition of 30 µL LiCl and 30 µL nuclease-free H_2O. The precipitation was aided by incubating overnight at -80 °C. The next day, cRNA was pelleted by centrifuging at 16000 g at 4 °C for 30 min. The pellet was washed with 100 µL 70 % ethanol and centrifuged again, but for 15 min. After air-drying, the cRNA was dissolved in 12 µL nuclease-free H_2O. The concentration of the sample was determined with a NanoDrop to dilute it with nuclease-free H_2O to a final concentration of 0.6 µg/µL and stored at -80 °C until use.

2.2.2.15 Transformation of *E. coli* (DE3) pLysS competent cells

Competent *E. coli* (DE3) pLysS cells (Merck) were transformed with pET-TOPO-PfPKAc-Dd2 as suggested by the manufacturer. Briefly, cells were thawed on ice, and incubated on ice for 10 min with 2 ng pET-TOPO-PfPKAc plasmid. Cells were subjected to a heat pulse at 42 °C for 30 s before letting them recover 2 min on ice. A volume of 100 µL SOC medium was added, and cells were incubated at 37 °C under shaking for 1 h. The culture was plated onto LB-Agar plates supplemented with 100 µg/mL ampicillin, and incubated overnight at 30 °C. Transformant colonies were screened for the presence of the *pfpkac* gene by running a colony screening PCR:

pET-PfPKAc screening PCR

Reagent	Volume
ddH_2O	16.5 µL
10x EconoTaq buffer	2.5 µL
2 mM dNTPs	2.5 µL
25 mM $MgCl_2$	2.5 µL
T7 promotor-for 50 µM	0.5 µL
T7 terminator-rev 50 µM	0.5 µL
EconoTaq 5 U/µL	0.25 µL

PCR settings		
T °C	**time**	
98 °C	3 min	
98 °C	20 s	x30
56 °C	20 s	
70 °C	1 min 15 s	
70 °C	3 min	
4 °C	∞	

PCR products were run on a 1 % agarose gel, and the presence of insert was confirmed by the presence of a band at 1.3 kbp.

2.2.3 *Xenopus laevis* oocytes

Ethical approval of the work performed with the *Xenopus laevis* frogs was obtained from the Regierungspräsidium Karlsruhe (Aktenzeichen 35-9185.81/G-31/11 and 35-9185.81/G-21/23) in accordance with the German “Tierschutzgesetz”.

2.2.3.1 *Xenopus laevis* maintenance

Frogs (female, at least 2 years old) were purchased from NASCO (USA). The animal facility at Heidelberg University (IBF - Interfakultäre Biomedizinische Forschungseinrichtum) performed basic caring for the frogs. The temperature of the aquariums was kept at 18 °C and the frogs were fed 3 times a week with food pellets.

2.2.3.2 Surgical isolation of ovaries from *X. laevis*

The frog was transferred from the aquarium to a tank filled with 0.3 % (w/v) ethyl 3-amino benzoate methanesulfonate (pH 7 with $NaHCO_3$) to anaesthetize. After 15-20 min, the frog was laid on a moisturized paper, and absence of reflexes was confirmed. A small incision (1.5 cm) was made with a scalpel on the skin and underlying muscle layer in the lower part of the abdomen. The ovary laying underneath was pulled out gently through the incision using tweezers. Part of it was cut out and transferred to a container filled with OR2 buffer. The incisions in the muscle and skin were individually stitched, and the frog was allowed to recover in tap water while keeping the head above water level. After 30-45 min, the frog was checked for reflexes and the water was changed. After 2 h, the frog was returned to the aquarium. The surgery was performed

up to 4 times on each frog, giving the frogs at least 2 months to recover between successive surgeries.

2.2.3.3 Collagenase digestion of ovary sacs

On the same day of surgery, the ovary was fractioned into pieces of 10-20 oocytes using tweezers and washed repeatedly with OR2 buffer, until the solution remained clear upon addition to the flask containing the ovary pieces. The fragments were then incubated overnight at 18 °C in 0.1 % (w/v) D-collagenase in OR2 buffer under gentle agitation. The next day, when the oocytes were free from collagen, they were washed several times with OR2 buffer, and then several times with ND96 buffer at pH 7.5. Oocytes were stored at 18 °C in ND96 buffer at pH 7.5.

2.2.3.4 cRNA injection of *X. laevis* oocytes

Glass capillaries were pulled to yield a tapered end before the day of injection (puller settings: heat, 515; pull, 30; velocity, 30; delay, 250; pressure, 500). Defolliculated oocytes in stages V or VI of development and without signs of rupture or apoptosis were manually selected for injection, and randomly grouped. Each oocyte was injected with 50 µL (30 ng) of cRNA, or with 50 µL nuclease-free H_2O, in the vegetal pole using a Nanoject II injector. Injected oocytes were kept at 18 °C in ND96 buffer at pH 7.5. The buffer was changed twice daily until oocytes were used. Damaged and dead oocytes, visible by rupture, loss of shape, and/or loss of pigmentation in the animal pole, were manually removed.

2.2.3.5 Drug uptake assays using *X. laevis* oocytes

Drug uptake assays were performed 48-72 h after cRNA injection. Oocytes in groups of 10 were washed with buffer ND96 pH 6.0, and then transferred to a 2 mL Eppendorf tube, to which 100 µL of uptake buffer were added to start the experiment. The uptake buffer consisted of buffer ND96 pH 6.0, supplemented with 42 nM [^{3}H]CQ or 40 nM [^{3}H]PPQ, and different concentrations of cold CQ and/or PPQ, depending on the experiment. When testing the effect of verapamil (VP), the drug was added to the uptake buffer at a final concentration of 100 µM. All drug transport assays were performed at RT. After the desired incubation time in uptake buffer, the oocytes were washed 3 times with ice-cold ND96 pH 6.0. Each individual oocyte was then transferred to a scintillation vial pre-filled with 200 µL 5 % SDS. Oocytes were lysed by vortexing, and 2 mL scintillation liquid (Ultima Gold, PerkinElmer, USA) were added to each vial.

After mixing, counting was done using a liquid scintillation counter, which measured the amount of radioactive label incorporated into each oocyte in counts per minute. To convert counts per minute to pmol of drug, 10 µL of uptake buffer was measured in duplicate in independent vials, each containing 200 µL 5 % SDS and 2 mL scintillation liquid. For each condition tested, water-injected oocytes were tested in parallel. The PfCRT-mediated drug transport was calculated by subtracting the amount of drug incorporated into water-injected oocytes from the amount of drug incorporated into PfCRT-expressing oocytes. All the equations used for data analysis can be found in [223].

2.2.3.6 Immunofluorescence microscopy (IFA) of injected oocytes

IFA was started on the same day as drug uptake assays. Oocytes were fixed for 4 h with 4 % (v/v) paraformaldehyde in PBS. They were then washed 3 times with 3 % (w/v) BSA in PBS, and later permeabilized for 60 min in 0.05 % (w/v) Triton-X 100 in PBS. After that, oocytes were washed 3 times as described above. They were incubated at 4 °C overnight with rabbit anti-PfCRT antiserum (1:500 dilution). After washing 3 times as before, the secondary antibody anti-rabbit Alexa Fluor 488 (1:1000 dilution) was added and allowed to incubate for 45 min. Another 3 washing steps were done, and then the antibody that served as an internal control, wheat germ agglutinin Alexa Fluor 633 (5 µg/mL) was added, incubating at 4 °C for 10 min. After 3 washing steps, the oocytes were analysed by fluorescence microscopy. Images were taken with a Zeiss LSM 510 confocal microscope and processed with ImageJ.

2.2.4 Protein biochemistry

2.2.4.1 Protein concentration determination via the Bradford assay

Protein concentration in the extracts was determined using the Bradford assay [224]. The Bio-Rad Dye Reagent Concentrate (Bio-Rad) was used according to manufacturer's instructions. A standard curve (0, 1, 2.5, 5 and 10 µg of BSA) was built in duplicate in a final volume of 800 µL ddH_2O. Then, 200 µL of the Dye Reagent Concentrate were added, samples were vortexed and allowed to evolve at RT for 5 min, and absorbance at 595 nm was measured. Protein samples were prepared and processed accordingly, and their concentrations were calculated using the fresh standard curve.

2.2.4.2 Heterologous expression of PfPKAc

For the expression in *E. coli* BL21 (DE3) pLysS, a colony positive for the *pfpkac* gene was used to start an overnight starter culture at 37 °C under shaking at 180 rpm in LB medium supplemented with 100 µg/mL ampicillin. The next day, 0.5 mL of the culture was transferred to a 50 mL LB medium (supplemented with 100 µg/mL ampicillin). The new culture was incubated at 37 °C under shaking. Aliquots were taken at different time points to monitor the OD600. When the OD600 reached 0.7-1.0, 0.5 mM IPTG was added to the culture to induce protein expression. The culture was then transferred to a shaker working at either 22 °C or 18 °C, for 6 h. Cells were harvested by centrifugation for 10 min at 3000 g at 4 °C, and the pellets were stored at -80 °C until use. Bacterial pellets were resuspended in 5 mL *E. coli* lysis buffer, and 3 freeze/thaw cycles were used to lyse the cells (liquid N_2 vs waterbath at 37 °C). Lysates were centrifuged at 10000 g at 4 °C for 10 min. Supernatants were incubated for 1.5 h with 50 µL Ni-NTA beads, and then washed 3 times with washing buffer (50 mM Tris/HCl pH 7.5, 500 mM NaCl, 10 % glycerol, 5 mM β-mercaptoethanol). The beads were incubated 1 h with 200 µL elution buffer (50 mM Tris/HCl pH 7.5, 500 mM NaCl, 10 % glycerol, 5 mM β-mercaptoethanol, 350 mM imidazole), with end-to-end rotation. The proteins were transferred to a spin column and the flow-through was stored at -20 °C until use.

2.2.4.3 SDS polyacrylamide gel electrophoresis (SDS-PAGE) of proteins

Protein samples were analysed by SDS-PAGE electrophoresis for various purposes. The molecular weight marker Page Ruler pre-stained plus (Thermo Fisher Scientific) was loaded on the gels alongside the samples. Each gel was run at 200 V and 40 mA for 45 to 60 min in SDS-PAGE running buffer. The percentage of acrylamide in the resolving gel depended on the resolution needed.

	Resolving gel				Stacking gel
	8 %	10 %	12 %		5 %
Reagent	**Volume**			**Reagent**	**Volume**
ddH_2O	4.68 mL	3.96 mL	3.35 mL	ddH_2O	3.46 mL
1.5 M Tris pH 8.8	2.50 mL	2.50 mL	2.50 mL	1 M Tris pH 6.8	630 µL
10 % SDS	100 µL	100 µL	100 µL	10 % SDS	50 µL
30 % acrylamide	2.66 mL	3.33 mL	4.00 mL	30 % acrylamide	830 µL
10 % APS	100 µL	100 µL	100 µL	10 % APS	50 µL
TEMED	6 µL	6 µL	6 µL	TEMED	5 µL

After the run, the gel was incubated in Coomassie staining solution at 50 rpm at RT for 5 min. Then, the gel was washed with distilled water and left overnight at 50 rpm at RT in Coomassie de-staining solution.

2.2.4.4 Western Blot of cellular lysates

Western blot of oocyte lysates was started the same day of drug uptake assays. Total lysates from *X. laevis* oocytes were prepared by addition of 20 µL oocyte lysis buffer (10 mM HEPES pH 7.4, 150 mM NaCl, 1 % IGEPAL, 0.5 % sodium deoxycholate, 0.1 % SDS, 1x cOmplete Protease Inhibitor Cocktail (Roche)) per oocyte. Cells were mechanically broken while on ice. Cellular debris was separated by centrifugation at 16000 g at 4 °C for 15 min.

Cellular lysates were mixed with sample buffer (250 mM Tris pH 6.8, 3 % SDS, 20 % glycerol, 0.1 % bromophenol blue), heated to 70 °C for 3 min, and stored at -20 °C until use. Lysates were then size-fractioned using 10 % SDS-PAGE and transferred to a PVDF membrane. After the transfer, the membrane was cut un two halves below the 55 kDa marker band, at around 50 kDa, and blocked by incubating at RT on a roller for 30 min in 5 % milk/PBS. The membrane was incubated at 4 °C on a roller overnight with a primary antibody, depending on the protein to detect:

Antigen to detect	**Primary antibody**
PfCRT	Guinea pig anti-PfCRT antiserum (1:1000 dilution)
α-tubulin	Mouse anti-α-tubulin antiserum (1:1000 dilution; clone B-5-1-2)
V5 epitope	Mouse anti-V5 (1:1000; clone SV5-Pk1)

The next day, the membrane was washed 3 times, each with 10 mL PBST at RT on a roller. The membrane was then incubated at RT on a roller for 1 h with a secondary antibody:

Antigen to detect	Secondary antibody
Mouse	Goat anti-mouse POD antibody (1:10000 dilution)
Guinea pig	Donkey anti-guinea pig POD antibody (1:10000 dilution)

The membrane was washed 3 times as described above. Then, it was incubated at RT for 5 min with 3 mL Luminescent substrate solution A and 30 µL Substrate solution B, from the BM Chemiluminescence Western Blotting Substrate Blot (POD) kit (Roche). After incubation, the membrane was placed on a digital blot scanner (C-DiGit), and the signal intensities were captured and quantified using Image Studio Digits version 4.0 (LiCor). All antibodies were diluted in 1 % (w/v) BSA in PBS.

2.2.5 Computational simulations

2.2.5.1 Molecular docking studies

Docking and molecular dynamics (MD) simulations were run by Dr. Giulia D'Arrigo from the Heidelberg Institute for Theoretical Studies (HITS), in Heidelberg. The cryo-EM structure of the PfCRT 7G8 isoform (PDB ID: 6UKJ; 3.2 Å) [156] was used as a template for homology modelling. The SWISS-MODEL Protein Modelling server [225] was used to generate the model. The structure of $PfCRT^{Dd2}$ model was then prepared using the Protein Preparation Wizard in Maestro [226] and protonated at pH 6.0 using PROPKA [227]. Prior to docking calculations, the two drugs, CQ and PPQ, were prepared with LigPrep and ionized at pH 6.0 using Epik [228]. Induced-fit docking (IFD) [229] was performed using the default options unless specificed otherwise. The same docking box was used for both compounds and built by selecting Q235, S90, Q156, L221, W352, L83, and F145 as centroids. For both CQ and PPQ, 10 poses were generated. The first docking pose of PPQ and the third docking pose of CQ were then merged when embedded into a POPC (1-palmitoyl-2oleoyl-phosphatidylcholine) lipid bilayer, built with the CHARMM GUI webserver [230] using the Amber Lipid14 force field [231]. The systems were then solvated in a periodic box of TIP3P [232] water molecules and neutralized at an ion concentration of 150 mM NaCl. The GAFF [233] force field was used for parameterizing the two compounds along with AM1-BCC for assigning partial charges [234]. The Amber ff14SB force field [233] was used to assign

protein parameters. MD simulations were run using the Amber20 software [235]. The systems were first energy-minimized with 10 consecutive runs (1000 steps each) of decreasing restraints from 1000 to 0.01 kcal mol^{-1} $Å^{-2}$ with the Langevin thermostat (NVT), and then up to 310 K with restraints of 5 kcal mol^{-1} $Å^{-2}$. A 4 ns equilibration with restraints of 5 kcal mol^{-1} $Å^{-2}$ was then performed. Additionally, 10 consecutive simulations (5 ns each) without restraints were run to equilibrate the system's periodic boundary dimensions. Finally, a production of 1 µs under the NPT ensemble (Langevin thermostat at 310 K with a Berendsen barostat at 1 bar) was run. A time step of 2 fs was used for all simulations, and bonds with hydrogens were constrained using the SHAKE algorithm.

3 Results

3.1. The phosphorylation of PfCRT

Previously, my group and colleagues investigated the role of phosphorylation at a serine residue at position 33 in PfCRT (Ser33) [187]. Using a repertoire of protein kinase inhibitors with different protein kinase specificity, they found some that led to a 2.7- to 3.5-fold increased accumulation of CQ in CQ resistant *P. falciparum* Dd2 parasites, relative to untreated control. They later linked the action of those small molecules to PfCRT, because parasites treated with one of the tested kinase inhibitors, ML-7, were sensitized to CQ and QN, two drugs against whom resistance is mediated by PfCRT. Instead, ML-7 did not sensitize parasites to pyrimethamine (PYR), whose mechanism of resistance is independent of PfCRT. They also generated mutant *P. falciparum* Dd2 parasites using CRISPR-Cas9 technology, and showed that substituting Ser33 for alanine (S33A) significantly sensitized the parasites to CQ and QN. Instead, replacing Ser33 for aspartic acid (S33D), a mimic of phosphoserine, restored CQ and QN resistance. Functional transport studies in *Xenopus laevis* oocytes revealed that the S33A replacement impacts the V_{max} of PfCRT-mediated CQ transport, suggesting an involvement of the phosphorylation event at Ser33 in the mechanism of drug translocation across the vacuolar membrane.

Here, I worked on uncovering the parasite's protein kinases that phosphorylate PfCRT, with a particular focus on the phosphorylation on Ser33. Because predictive bioinformatic tools are lacking or underdeveloped for *P. falciparum*, I focused instead on two proteomic approaches that work on independent principles. The goal was to find overlapping hits in both methods, which could provide an insight into the nature and identity of the desired protein kinase.

3.1.1. Chemoproteomic profiling of ML-7 and H-89 in competitive pulldown assays with kinobeads suggests PKA phosphorylates Ser33 in PfCRT

Both ML-7 and H-89 re-sensitized Dd2 parasites to CQ and QN, a phenomenon causatively linked to Ser33 phosphorylation and PfCRT-mediated drug resistance [187]. It is thus possible that both kinase inhibitors act on the same protein kinase, e.g. the protein kinase phosphorylating Ser33 in PfCRT. Therefore, the possibility exists to use ML-7 and H-89 to identify the protein kinase acting on the malarial transporter. To

do so, competition pulldown experiments using either ML-7 or H-89 were performed [217]. In a vehicle control DMSO pulldown experiment, the lysate is incubated with kinobeads to let the parasite's proteins interact with the drugs attached to the beads (Figure 3.1.1a). After washing, the eluted proteins will be those which could bind to the kinase inhibitors covalently bound to the beads. In a competition pulldown assay, the parasite lysate is pre-incubated with ML-7 or H-89, and then with the kinobeads. Now, proteins that can bind to kinase inhibitors (ML-7, H-89, or the kinobead-attached inhibitors) do not fully bind to the kinobeads. Instead, a triple equilibrium is formed in which a proportion of these proteins will remain in solution, bound to ML-7 or H-89, and will be washed out and therefore not be detected after elution. The extent of that proportion depends on the ratio of the affinities a protein has for the soluble inhibitor and for the kinobead-attached inhibitors, and on the concentration of ML-7 or H-89 used for pre-incubation. Thus, performing competition pulldown experiments at different concentrations of ML-7 or H-89 will lead to a dose-response curve in which the readout signal is the abundance of a certain protein after its elution from the kinobeads.

Parasite lysates prepared in kinobeads lysis buffer were used by Dr. Polina Prokofeva during her doctoral work under the supervision of Dr. Guillaume Médard, from the Technical University of Munich. These lysates were subjected to competition pulldown experiments, in which they were pre-incubated with 1 of 9 concentrations of either ML-7 or H-89 (vehicle DMSO, 30 nM, 100 nM, 300 nM, 1 µM, 3 µM, 10 µM, 30 µM, or 300 µM) before being incubated with the kinobeads. The beads were washed, and bound proteins in each condition were later eluted, denatured, alkylated, trypsin-digested, and analysed by MS/MS using an Orbitrap Fusion Lumos (Thermo Fisher Scientific) coupled to HPLC. A total of 717 proteins were enriched with the kinobeads after pre-incubation with ML-7, and a total of 837 proteins when H-89 was used for the pre-incubation step. The resulting dose-response curves for each protein and for each inhibitor were filtered according to the following criteria: (a) the curve must follow a sigmoidal shape with at least 1 point under 50 % label-free quantitation (LFQ) intensity relative to DMSO control; (b) the abundance of the protein in the lysate, measured as the $\log_{10}$ of the LFQ intensity of the protein in the vehicle DMSO sample, has to be above 6.5; (c) the MSMS count and unique peptide dose-response curves must also follow sigmoidal shapes; and (d) the MSMS count and unique peptides in the vehicle DMSO control should not be less than 10. These criteria were set to increase the

confidence of the binding between the protein and the small molecule [217]. Applying the filter to the enriched proteins led to only 2 hits, which were the same for ML-7 and H-89 samples: *Plasmodium falciparum* cAMP-dependent protein kinase catalytic subunit (PfPKAc) and *Plasmodium falciparum* cAMP-dependent protein kinase regulatory subunit (PfPKAr). The dose-response curve revealed EC50 values of 44.2 µM and 35.9 µM with ML-7 for the regulatory and catalytic subunit, respectively, and of 3.7 µM and 3.3 µM with H-89 (Figure 3.1.1b,c).

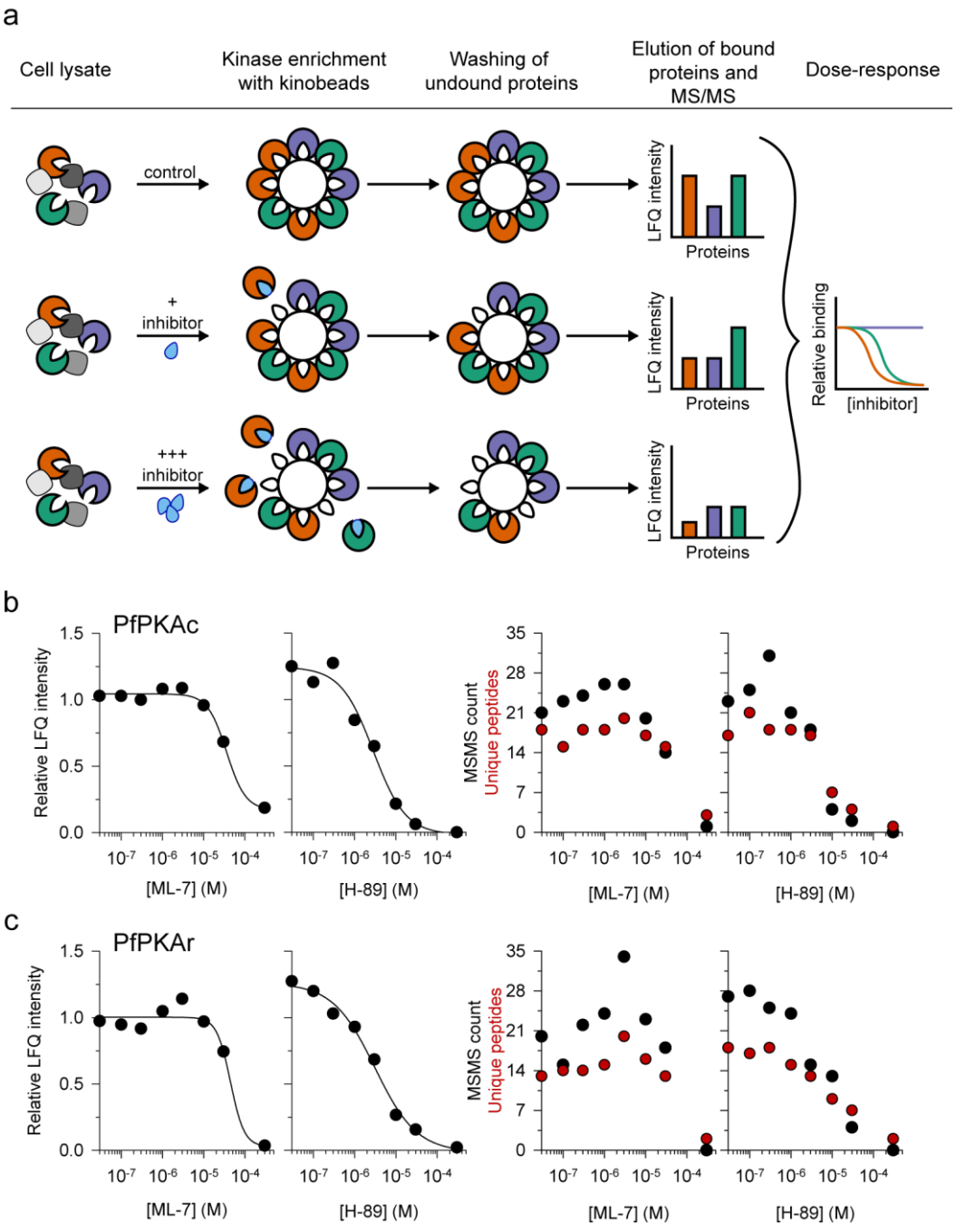

Figure 3.1.1. Malarial PKA binds both ML-7 and H-89. a, Schematics of the competition pulldown experiment workflow. Protein kinases present in a lysate (open

circles) are enriched by kinobeads (white circles) and, depending on their capacity to bind to them or to inhibitor molecules (light blue) of ML-7 or H-89, and on the concentration of the latter, its quantification by mass spectrometry leads to an LFQ readout. **b**, Dose-response curves for the enrichment of PfPKAc with ML-7 or H-89. **c**, Same as (**b**), but for PfPKAr. The data was produced by Dr. Paulina Prokofeva and Dr. Guillaume Médard. The parameters from the curves are summarized in Table 3.1.1.

For the calculation of apparent dissociation constant (K_d^{app}) between a protein and ML-7 or H-89, the EC50 from the dose-response curve was used. However, the K_d^{app} is for the equilibrium between free protein, free inhibitor, and the protein-inhibitor complex, and the EC50 value is a result of the presence of kinobeads in the system. Binding of the proteins to the affinity matrix depletes the free protein species in the aforementioned equilibrium. As a consequence, EC50 values are shifted towards higher drug concentrations. The level of depletion, and thus the shift of the EC50 values, depends on the protein's abundance in the lysate, its affinity to the kinobead matrix, and the effective kinobead probe concentration. Because these are not known beforehand, depletion must be determined experimentally for each protein. To do so, the correction factor (cf) is calculated for each protein. The eluate from the vehicle DMSO sample was subjected to a second, consecutive pulldown assay, and the intensity obtained for each protein after the second pulldown is relativized to the intensity obtained for that protein after the first pulldown. The cf can vary between 0 and 1, with values closer to 0 indicating a higher level of depletion. By multiplying the EC50 values by the cf, the apparent affinities (K_d^{app}) were obtained, resulting in 44.2 µM and 22.6 µM for ML-7 and the regulatory and catalytic subunits, respectively, and in 1.8 µM and 0.9 µM for H-89 (Table 3.1.1).

Table 3.1.1. Kinase-ligand binding parameters. Shown are the parameters derived from the dose-response curves of PKAc and PKAr with ML-7 and H-89, together with the derived apparent affinity constant after calculation of the correction factor. EC50, half-maximal effective concentration; cf, correction factor; K_d^{app}, apparent dissociation constant.

	PKAc			**PKAr**		
	EC50	cf	K_d^{app}	EC50	cf	K_d^{app}
ML-7	35.9 µM	0.63	22.6 µM	44.2 µM	1.08	44.2 µM
H-89	3.3 µM	0.29	0.9 µM	3.7 µM	0.47	1.8 µM

Of note, FIKK-10.1 was also enriched in the competition pulldown assays performed with both drugs. Despite meeting all the criteria set above, the FIKK protein kinases are believed to be all (except for FIKK8) exported to the host red blood cell's cytoplasm [236]. Thus, it appeared unlikely that FIKK-10.1 phosphorylates PfCRT in a natural setting, and was therefore dismissed as a candidate.

3.1.2. Kinase-catalyzed crosslinking and streptavidin purification (K-CLASP) supports PKA as a candidate

I then decided to complement the competition pulldown results with an independent approach, employing the kinase-catalysed crosslinking and streptavidin purification (K-CLASP) methodology [220]. To do this, I worked in collaboration with Eric Davis and Prof. Mary Kay Pflum from the Wayne State University, USA. K-CLASP relies on the fact that kinases efficiently accept γ-phosphate-modified ATP analogues as co-substrates, including ATP-crosslinkers (ATP-CL) such as ATP-arylazide [218]. In K-CLASP, a biotin-tagged peptide substrate containing the phosphosite of interest is incubated with lysate in the presence of ATP-CL and UV irradiation. The biotin-tagged peptide substrate covalently attaches to its respective protein kinase in the lysate via kinase-catalyzed crosslinking (Figure 3.1.2a). The covalently crosslinked peptide-kinase complex is then enriched using a streptavidin resin and analysed by liquid chromatography-tandem mass spectrometry (LC-MS/MS) to identify the captured kinase. Because substrate-kinase interactions are transient, allowing diffusion of the substrate after transfer of the photo-crosslinking group, the biotin-tagged peptide can conjugate to proteins that are nearby the protein kinase, including directly and indirectly associated proteins (AP). Thus, both target protein kinases and kinase-associated proteins are observed in a K-CLASP experiment.

Here, a protein extract prepared from Dd2 parasites was incubated with ATP-CL and an N-biotinylated peptide containing the Ser33 phosphosite (biotin-ELDNLVQEGNGSRLGGGSCLGK, where Ser33 is underlined), in the presence of UV irradiation. Negative controls were used to assess unspecific background crosslinking, and included 1) exclusion of UV irradiation, ATP-CL, or peptide, from the reaction mixture, as a bead binding control; 2) exclusion of UV irradiation; and 3) replacing the peptide for a mutant peptide in which the Ser has been replaced for Lys (biotin-ELDNLVQEGNGKRLGGGSCLGK, where the mutated site is underlined). Two independent biological replicates with two technical replicates each were analysed by

LC-MS/MS and LFQ, and a total of 2505 proteins were observed. Fold enrichment values were calculated by dividing the LFQ intensities observed in the samples with UV light by those observed without UV light for the same samples in each technical replicate. A hit list was constructed by identifying proteins with at least a 1.5-fold enrichment value in at least 1 trial, in addition to lower intensities in the negative controls relative to test samples (Figure 3.1.2b). PfPKAc was identified in 2 out of 4 trials (1 from each biological replicate). However, it did not meet the criteria to be undoubtedly considered a hit. Instead, PfPKAr was enriched in the 4 trials, meeting the hit criteria in 1 of them. These independent results support the competition pulldown assays, suggesting that PKA interacts with the Ser33 phosphosite.

a

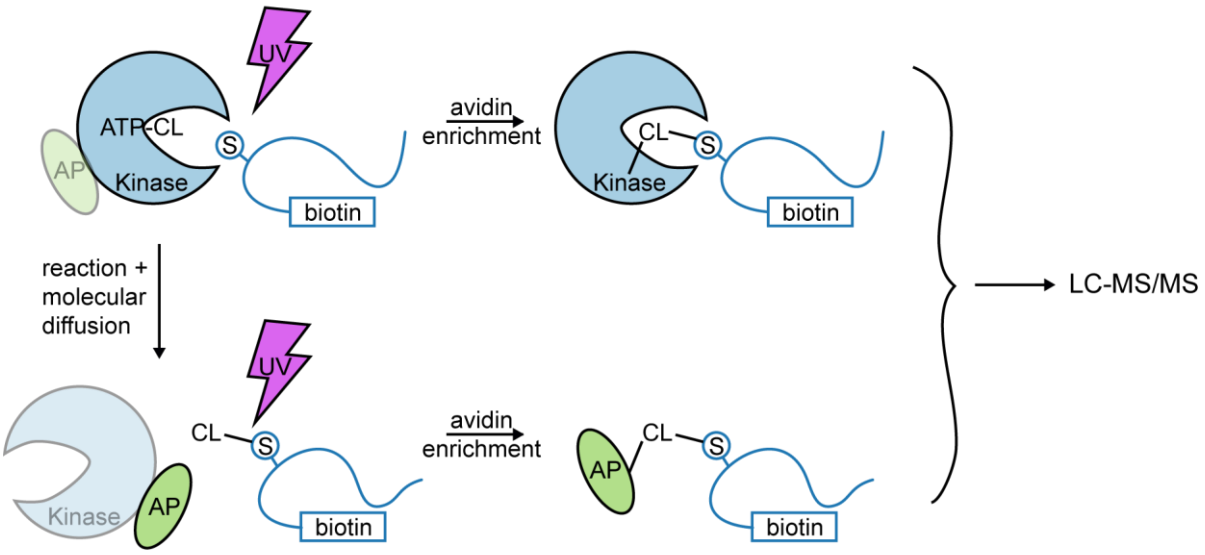

b

Hit proteins	Gene ID	Trials enriched	Met criteria	Enrichment value
PKAc	PF3D7_0934800	2/4	0/4	—
PKAr	PF3D7_1223100	4/4	1/4	1.57
CK I	PF3D7_1136500	4/4	1/4	1.54

Figure 3.1.2. K-CLASP experiment supports PKA as the candidate protein kinase. a, Schematics of the principle behind the K-CLASP method. *Top,* The kinase, bound to the ATP-crosslinker (ATP-CL) catalyses the transfer of the CL to the Ser residue in a user-designed peptide (S). Because the reaction takes place under UV light, the CL reacts forming a covalent bond with what is nearby, namely the enzyme. *Bottom*, Because enzyme-peptide interactions are transient, the kinase has time to diffuse after phosphorylating the peptide. When the CL reacts because of UV light, it forms a covalent bond with a nearby protein, often those proteins associated (AP) with the kinase. **b**, Shown are the protein kinases that were enriched and met the decision-

making criteria, apart from PKAc. The data was produced by Eric Davis and Prof. Dr. Mary-Kay Pflum.

3.1.4. Recombinant expression of PfPKA leads to an insoluble protein

Two independent approaches pointed at PfPKA as the responsible enzyme for Ser33 phosphorylation, so the next aim was to prove a direct interaction between the protein kinase and Ser33. With that in mind, the recombinant expression of PfPKA was attempted by Dr. Kim Remans and Yexin Xie from the European Molecular Biology Laboratory (EMBL) in Heidelberg, Germany. After cloning of the codon-optimised version of the *pfpkac* gene into the pCoofy29 and into the pCoofy51 vectors (see section 2.1.4.4 Plasmids) [214], the expression was tested in two different insect cell lines of *Spodoptera frugiperda*, namely Sf9 and Sf21. Although different extraction conditions were tested (see Annex I), the protein was either not overexpressed or localised to the insoluble fraction. Previously, only one work achieved the successful expression of PfPKAc in *E. coli* BL21 (DE3) pLysS cells [237]. Thus, as a follow-up step, the expression of PfPKAc was tried in *E. coli* BL21 (DE3) pLysS cells using the pET-TOPO-PfPKAc-Dd2 (see section 2.1.4.4 Plasmids) following the protocol of Wurtz *et al.* (2009) [237]. Once again, protein expression was unsuccessful (see Annex I). Efforts to produce recombinant PfPKAc are still ongoing in my group, with this part of the project taken over by Dr. Cecilia Sanchez.

3.2. The mechanisms of drug transport by PfCRT

By the 1990s, malaria had developed resistance to chloroquine, to the combination of sulfadoxine + pyrimethamine, and independently to practically all antimalarials in Southeast Asia [174, 238, 239]. Throughout the decade, different countries started pointing at the efficacy of a drug that had been recently discovered and isolated: artemisinin. In a scenario where *P. falciparum* could evidently develop resistance to drugs used in monotherapy, a decision was made to combine two antimalarials with different modes of action and half-lives: the artemisinin-based combination therapies (ACTs) were born [240, 241]. Soon, most countries in Southeast Asia started adopting ACTs, and in the early 2000s, the WHO recommended them as the standard antimalarial strategy [133]. Different combinations have been approved so far: artemether + lumefantrine (AL), artesunate + sulfadoxine-pyrimethamine (AS+SP), artesunate + amodiaquine (AS+AQ), artesunate + mefloquine (AS+MQ), and dihydroartemisinin + piperaquine (DHA+PPQ). Unfortunately, mutations in PfKelch13 made the parasite more tolerant to the artemisinins [200, 201], which left room for development of resistance to the partner drugs of the ACTs. That was the case with piperaquine (PPQ), to which resistance was reported in the Thai-Cambodia border only some years after its introduction [179, 181, 182, 197].

The main driver of PPQ resistance is point mutations in PfCRT. In 2015, a retrospective study testing field isolates found mutations H97Y, M343L and G353V in PfCRT from *P. falciparum* Dd2 parasites as markers for piperaquine resistance [242]. Later, Agrawal *et al*. (2017) found an association between mutation F145I and PPQ resistance [243]. Lastly, through genetically editing CQ resistant Dd2 parasites, Ross *et al.* (2018) showed that any of the aforementioned mutations were sufficient to confer resistance to that antimalarial, and that the F145I substitution did so at the highest levels [179]. Upon PPQ selection, parasites became re-sensitised to chloroquine (CQ). That was surprising, given the structural resemblance of both drugs (PPQ is essentially 2 CQ-like 4-aminoquinoline moieties with a central linker), and the fact that these parasites still carried the PfCRT K76T substitution that was until then thought to be critical for CQ resistance [172].

Here, I worked on the kinetic characterization of $PfCRT^{Dd2}$ and its novel mutant forms carrying the H97Y, F145I, M343L or G353V substitutions, in terms of CQ and PPQ transport. Additionally, I created an artificial double mutant that outperforms the other

isoforms above certain substrate concentrations, posing a risk to therapeutic suggestions that recommend combining CQ and PPQ [244]. I also probed the binding cavity of PfCRT to investigate how and where the two drugs interact with the transporter, providing information for the first time on where these antimalarials bind in the cavity of the protein.

3.2.1 The amino acid substitution F145I changes how PfCRT^{Dd2} interacts and translocates CQ and PPQ

Over the past decade, mutations in PfCRT have been linked to slow parasite clearance after treatment with dihydroartemisinin-piperaquine (DHA-PPQ), and to overall high rates of treatment failure in Southeast Asia [179, 181, 182, 197, 242, 243]. These mutations arose in parasites expressing the Dd2 isoform of PfCRT (PfCRT^{Dd2}), and that already carried other genomic changes that reduced their susceptibility to DHA. However, in parallel to becoming resistant to PPQ, the mutant parasites normally become susceptible to other common antimalarials, like chloroquine (CQ) [156, 179, 182]. To understand how these amino acid changes lead to PPQ resistance and to CQ re-sensitization, I introduced the F145I mutation into the coding sequence of PfCRT^{Dd2} for expression in *Xenopus laevis* oocytes to generate the PfCRT^{Dd2_F145I} mutant (see Annex II).

Oocytes expressing PfCRT^{Dd2} or PfCRT^{Dd2_F145I} were exposed to ND96 pH 6.0 buffer supplemented with either total 50 µM CQ (radiolabelled plus unlabelled) or total 50 µM PPQ (radiolabelled plus unlabelled), and the amount of radioactivity incorporated per oocyte was evaluated at different time points (Figure 3.2.1). As controls, oocytes expressing the PfCRT^{HB3} isoform from the CQ and PPQ sensitive *P. falciparum* HB3 strain, as well as water-injected oocytes, were tested in parallel. Both PfCRT^{Dd2}- and PfCRT^{Dd2_F145I}-expressing oocytes accumulated significantly more CQ and PPQ than control oocytes. On the one hand, that meant that PfCRT^{Dd2} can transport significant amounts of PPQ, despite it not conferring PPQ resistance; on the other hand, PfCRT^{Dd2_F145I} can transport significant amounts of CQ, even when it does not confer resistance to CQ. By subtracting the amount of drug accumulated in water-injected oocytes from that in PfCRT-expressing oocytes at each time point, the PfCRT-mediated drug uptake was obtained and evaluated. PfCRT^{Dd2} had a CQ half-saturation time of 150 ± 30 min, compared to PfCRT^{Dd2_F145I} with 66 ± 15 min, indicating that the mutant isoform reaches half-saturation more than twice as fast. Instead, PfCRT^{Dd2} had

a PPQ half-saturation time of 65 ± 10 min, compared to PfCRT^{Dd2_F145I} with 180 ± 40 min.

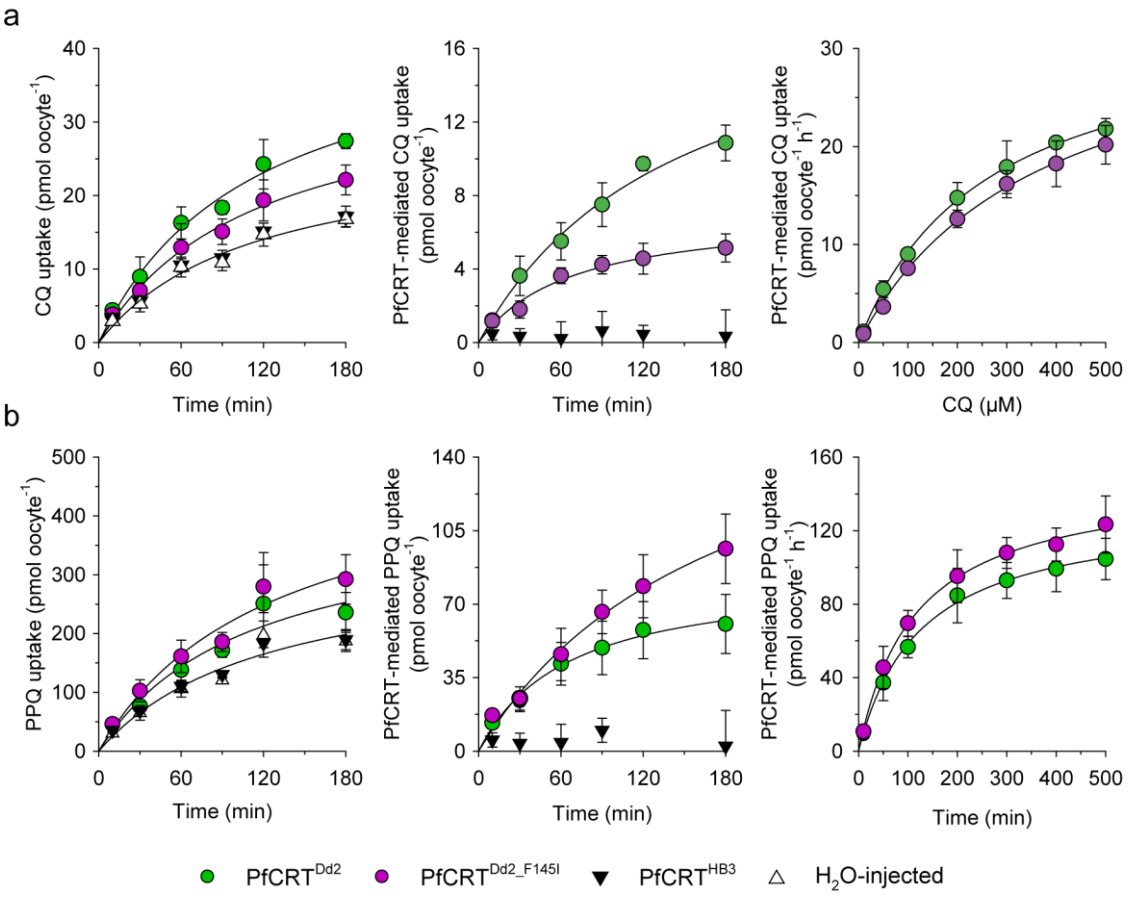

Figure 3.2.1. The effect of the F145I mutation on PfCRT^{Dd2}-mediated drug transport. a, **b**, PfCRT^{Dd2} and PfCRT^{Dd2_F145I} mediate CQ and PPQ uptake. *Left*, Time course for the uptake of CQ (**a**) or PPQ (**b**) into H_2O-injected oocytes (open triangles) and oocytes expressing PfCRT^{Dd2} (green circles), PfCRT^{Dd2_F145I} (purple circles), or PfCRT^{HB3} (filled triangles), from a medium containing 50 μM drug (radiolabelled plus unlabelled). *Middle*, The PfCRT-mediated uptake was calculated by subtracting the uptake into H_2O-injected oocytes from that of PfCRT-expressing oocytes, at each time point. *Right*, Concentration-dependence of the PfCRT-mediated uptake of CQ (**a**) or PPQ (**b**) from a medium containing 10-500 μM drug (radiolabelled plus unlabelled). The Henri-Michaelis-Menten equation was fit to the data, resulting in the parameters summarized in Table 3.2.1. Data is shown as the mean ± SEM of at least 3 independent biological replicates. Each biological replicate consists of measurements done on 10 oocytes coming from the same frog. Taken from Gomez *et al.* (2023) [223].

To investigate the saturability of CQ and of PPQ transport by both PfCRT variants, I conducted kinetic studies. The uptake of radiolabelled drug was determined from an external medium consisting of ND96 pH 6.0 supplemented with 1 of 7 total concentrations of CQ or of PPQ (10 μM, 50 μM, 100 μM, 200 μM, 300 μM, 400 μM, or 500 μM). Water-injected oocytes were tested in parallel in each condition, and the

uptake into these control oocytes was subtracted from that of PfCRT-expressing oocytes to obtain the PfCRT-mediated drug uptake at each drug concentration. Transport in both cases followed a hyperbole, consistent with transport taking place via a saturable mechanism. The Henri-Michaelis-Menten equation was fit to the data, and the parameters K_M and V_{max} were derived. The mutation F145I resulted in a 44 % increase in the K_M^{CQ}, suggesting a role for F145 in CQ binding, while it did not affect the V_{max}^{CQ}. The mutation also increased the V_{max}^{PPQ} by 14 %, without significantly impacting the K_M^{PPQ}.

Table 3.2.1. Kinetic parameters of CQ and PPQ transport by different PfCRT isoforms. The parameters for the transport of CQ (red) or PPQ (light-blue) were obtained by fitting the Henri-Michaelis-Menten or the Hill equation to the data in Figure 3.2.1 and Figure 3.2.2. V_{max}, maximal velocity of drug transport; K_M, Michaelis constant; H_C, Hill coefficient. Taken from Gomez *et al*. (2023) [223].

Parameter	PfCRT^{Dd2}	Mutation evaluated				
		F145I	H97Y	M343L	G353V	H97Y +F145I
V_{max} (pmol.oocyte^{-1}.h^{-1})	**33 ± 1**	**35 ± 2**	**24 ± 1**	**31 ± 2**	**23 ± 3**	**35 ± 4**
K_M (µM)	**260 ± 10**	**370 ± 30**	**184 ± 16**	**530 ± 60**	**270 ± 80**	**240 ± 40**
H_C						**1.6 ± 0.2**
V_{max} (pmol.oocyte^{-1}.h^{-1})	**131 ± 3**	**149 ± 3**	**131 ± 6**	**163 ± 9**	**134 ± 10**	**131 ± 10**
K_M (µM)	**125 ± 9**	**115 ± 7**	**106 ± 14**	**80 ± 16**	**90 ± 20**	**170 ± 20**
H_C						**2.0 ± 0.3**

3.2.2 Mutations conferring PPQ resistance shape the kinetics of CQ and PPQ binding and transport

Next, I extended the kinetics studies to include other mutant forms of PfCRT that in the field confer resistance to PPQ and re-sensitize to CQ: H97Y, M343L, and G353V (Figure 3.2.2). First, I generated the mutant isoforms PfCRT^{Dd2_H97Y}, PfCRT^{Dd2_M343L}, and PfCRT^{Dd2_G353V} (see Annex II). Oocytes expressing these mutant isoforms were used for kinetic studies like the ones described above, with water-injected oocytes being analysed in parallel. The H97Y mutation drastically reduced the V_{max}^{CQ}, though it also reduced the K_M^{CQ}, relative to PfCRT^{Dd2} (Table 3.2.1). In parallel, it had a slight impact on PPQ transport, by reducing the K_M^{PPQ} mildly. The M343L substitution was

the mutant with the highest K_M^{CQ}. It also had the lowest K_M^{PPQ} and the highest V_{max}^{PPQ} of all isoforms tested. Lastly, the G353V mutation significantly reduced the V_{max}^{CQ}, and it moderately reduced the K_M^{PPQ}. An inspection of the kinetic parameters revealed a strong positive correlation between the V_{max}^{PPQ} and the K_M^{CQ}.

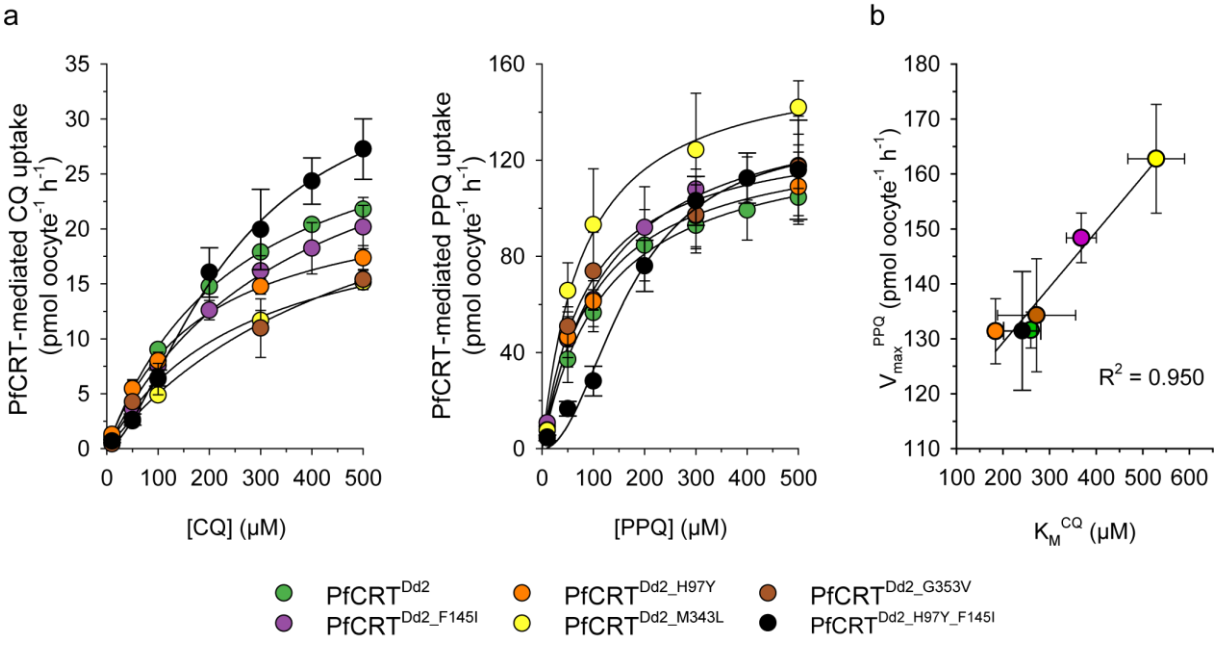

Figure 3.2.2. Kinetics of CQ and PPQ transport by PfCRT isoforms associated with CQ or PPQ resistance. a, The PfCRT-mediated uptake of CQ (*left*) or PPQ (*right*) was evaluated over a drug concentration range of 10-500 μM in oocytes expressing $PfCRT^{Dd2}$ (green), $PfCRT^{Dd2\_F145I}$ (purple), $PfCRT^{Dd2\_H97Y}$ (orange), $PfCRT^{Dd2\_M343L}$ (yellow), $PfCRT^{Dd2\_G353V}$ (brown), or the artificial double mutant $PfCRT^{Dd2\_H97Y\_F145I}$ (black). The derived kinetic parameters are summarized in Table 3.2.1. Data is shown as the mean ± SEM of at least 3 biological replicates, each resulting from measurements done on 10 oocytes coming from the same frog. **b**, Correlation analysis between the V_{max}^{PPQ} and the K_M^{CQ} of the different isoforms under study. The parameter values were taken from Table 3.2.1. The R^2 value of the correlation is indicated. Taken from Gomez *et al.* (2023) [223].

I next tested the ability of the CQ resistance reverser verapamil to inhibit the uptake of CQ or PPQ into oocytes expressing any of the PfCRT variants. Verapamil (VP) is an L-type calcium channel blocker, and is known to inhibit CQ transport mediated by $PfCRT^{Dd2}$ [150, 176, 245]. Oocytes were exposed to a medium containing a final concentration of CQ or PPQ (radiolabelled plus unlabelled) of 50 μM, in the presence or absence of 100 μM VP. The latter was able to significantly reduce both CQ and PPQ uptake in all cases. $PfCRT^{Dd2}$ was the most affected by the presence of VP when evaluating CQ transport (58 % inhibition), with $PfCRT^{Dd2\_G353V}$ being the least affected (26 % inhibition). In the case of PPQ transport, the most inhibited isoform was

$PfCRT^{Dd2\_F145I}$ (75 % inhibition), and $PfCRT^{Dd2\_G353V}$ was again the least affected (45 % inhibition).

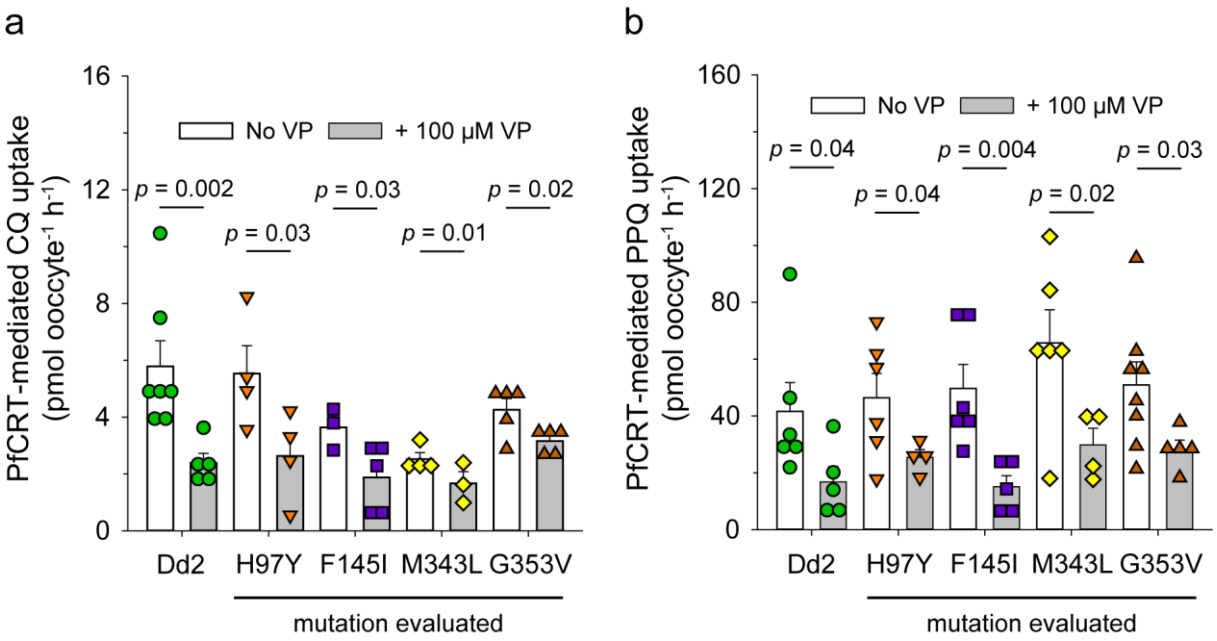

Figure 3.2.3. Verapamil inhibits PfCRT-mediated transport of CQ and PPQ. The inhibitory effect of adding 100 µM verapamil (VP) to an extracellular medium containing a total concentration of 50 µM **a**, CQ, or **b**, PPQ, was evaluated in oocytes expressing $PfCRT^{Dd2}$ (green), $PfCRT^{Dd2\_H97Y}$ (orange), $PfCRT^{Dd2\_F145I}$ (purple), $PfCRT^{Dd2\_M343L}$ (yellow), or $PfCRT^{Dd2\_G353V}$. Water-injected oocytes were analysed in parallel, and their drug uptake value was subtracted from that of PfCRT-expressing oocytes to calculate the uptake attributable to PfCRT. Data is shown as individual biological replicates (coloured symbols) overlaid onto bars representing the mean ± SEM of at least 3 biological replicates. A one-tailed Student's t-test was performed between untreated (no VP) and treated (+ 100 µM VP) conditions, and the obtained *p* values are indicated. Taken from Gomez *et al.* (2023) [223].

When inspecting the kinetic parameters of all the isoforms, it caught my attention that the H97Y mutation reduced the K_M^{CQ}. The amino acid H97 is in TM2, in close proximity to F145 in TM3, according to the cryo-EM structure of the 7G8 isoform [156]. The F145I mutation, as mentioned before, increased the K_M^{CQ}. Assuming rapid equilibrium kinetics, a reduced K_M translates into an increased affinity for CQ binding, and the opposite is true for an increased K_M [246]. Both mutations involve an aromatic side chain: the H97Y mutation introduces an aromatic side chain, while the F145I mutation eliminates one. Thus, it seemed likely to me that an aromatic side chain in the pocket comprised by TM1, 2, 3, 7 and 8, is important for CQ binding. I also wondered whether the H97Y mutation could compensate for the loss of affinity seen in the F145I mutation. I thus generated an artificial double mutant containing both mutations,

$PfCRT^{Dd2\_H97Y\_F145I}$ (see Annex II). Kinetics studies performed with the double mutant and CQ or PPQ revealed surprising and novel characteristics (Figure 3.2.2). Firstly, the data did not follow a hyperbole, but instead deviated from Michaelis-Menten kinetics. The Hill equation provided a notoriously better fit, in accordance with the sigmoidal appearance of the data points. Secondly, the kinetic parameters for CQ transport were in line with my expectations (Table 3.2.1). $PfCRT^{Dd2\_H97Y\_F145I}$ had a K_M^{CQ} comparable to that of $PfCRT^{Dd2}$, consistent with a compensatory effect of the individual mutations on that parameter. The V_{max}^{CQ} was also comparable to that of $PfCRT^{Dd2}$ and $PfCRT^{Dd2\_F145I}$. The Hill coefficient, H_C, was 1.6 ± 0.2. In terms of PPQ transport, the double mutant had a V_{max}^{PPQ} similar to that of the parental $PfCRT^{Dd2}$ and $PfCRT^{Dd2\_H97Y}$. Strikingly, the K_M^{PPQ} was higher than that of any other isoform I tested. Lastly, the double mutant outperformed $PfCRT^{Dd2}$ (the best performing CQ transporter, and the one that confers CQ resistance) at CQ transport when substrate concentration was above ~200 µM. A similar observation was made in the case of PPQ, with $PfCRT^{Dd2\_H97Y\_F145I}$ outperforming $PfCRT^{Dd2}$ at such substrate concentrations, where it performed similarly to the PPQ resistance-conferring $PfCRT^{Dd2\_F145I}$.

3.2.3 Semi-quantitative Western Blots and immunofluorescence microscopy confirm expression and localization of all PfCRT isoforms in *X. laevis* oocytes

In all uptake assays performed, water-injected oocytes are used in parallel to account for intrinsic drug uptake. In all cases, PfCRT-mediated CQ or PPQ uptake into PfCRT-expressing oocytes is calculated by subtracting the uptake into non-expressing oocytes from that into expressing ones. Despite that control, nothing guarantees that oocytes expressing different variants of PfCRT produce it at similar levels. Furthermore, a mutation could have the undesired effect of leading to protein mislocalization.

To control for PfCRT localization and expression levels, I performed immunofluorescence assay (IFA) with fluorescence microscopy as well as semi-quantitative Western Blots with Dr. Cecilia Sanchez. IFA images revealed co-localization of all PfCRT isoforms with the oocyte plasma membrane marker wheat germ agglutinin (WGA) (Figure 3.2.4a). Expression levels, as exemplified by the ratio of PfCRT expression to α-tubulin expression, were comparable for all isoforms (Figure 3.2.4b). Water-injected oocytes analysed in parallel did not react with the PfCRT-specific antiserum.

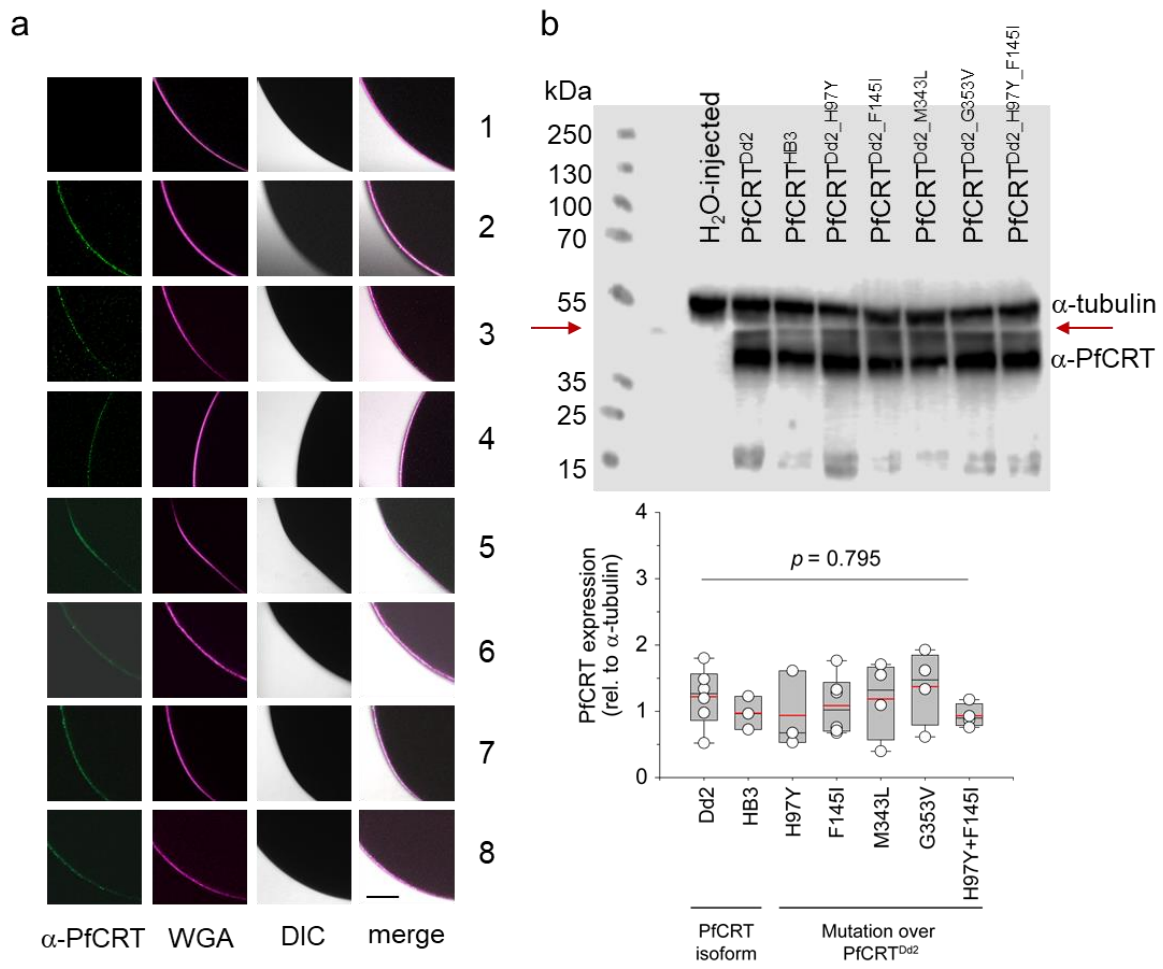

Figure 3.2.4. PfCRT localizes to the oocyte plasma membrane at similar levels. **a**, Immunofluorescence images of fixed H_2O-injected and PfCRT-expressing oocytes. *First panel from the left*, fluorescence image of PfCRT using guinea pig antiserum primary antibody (α-PfCRT) and the Alexa Fluor^{TM}488 anti-guinea pig secondary antibody. *Second panel*, fluorescence image of wheat germ agglutinin (WGA) conjugated to Alexa Fluor^{TM}488. *Third panel*, differential interference contrast (DIC) image. *Fourth panel*, overlay. Scale bar, 135 µm. Contrast was enhanced for visualization purposes. 1, H_2O-injected; 2, PfCRT^{Dd2}; 3, PfCRT^{HB3}; 4, PfCRT^{Dd2_H97Y}; 5, PfCRT^{Dd2_F145I}; 6, PfCRT^{Dd2_M343L}; 7, PfCRT^{Dd2_G353V}; 8, PfCRT^{Dd2_H97Y_F145I}. **b**, Western blot analysis of total lysates from H_2O-injected and PfCRT-expressing oocytes, using a polyclonal guinea pig antiserum specific to PfCRT and, as a loading control, mouse monoclonal anti-α-tubulin antibody. The place where the membrane was cut is indicated with red arrows. The luminescent signals from 4 independent Western blots were quantified, yielding the PfCRT expression levels relative to α-tubulin. A box plot analysis is overlaid over the individual data points (independent biological replicates), with the median (black line), mean (red line), and 25 and 75 % quartile ranges shown. Taken from Gomez *et al.* (2023) [223].

3.2.4 CQ and PPQ do not compete for binding to PfCRT^{Dd2}

In the work by Kim et al. (2019) in which the cryo-EM structure of the CQ resistant 7G8 isoform of PfCRT (PfCRT^{7G8}) was solved [156], the authors tested how binding of CQ

or PPQ inhibited binding of the other drug. Using proximity-based binding assays, they found that CQ and PPQ compete for binding to $PfCRT^{7G8}$, suggesting they bind to the same binding pocket. Previously in my group, Bellanca et al. (2014) showed that CQ has partially overlapping sites with quinine, quinidine, and VP, in $PfCRT^{Dd2}$ [150].

In an attempt to corroborate the findings by Kim and colleagues [156], I performed the Competition Plot experiment with $PfCRT^{Dd2}$ (Figure 3.2.5) [247]. To this end, I used the Henri-Michaelis-Menten equation derived from the fit in Figure 3.2.1 to find a concentration of CQ and a concentration of PPQ that would yield the same rate of drug transport. Because CQ is the less-efficiently transported substrate of the two, its concentration in the experiment had to be as close as saturation as possible. The chosen concentrations were $[CQ]^{Dd2}$ = 400 µM and $[PPQ]^{Dd2}$ = 23.1 µM. The expected uptake value was 19.8 pmol h^{-1} $oocyte^{-1}$. A number of reaction buffers were assembled, in which ND96 pH 6.0 buffer was supplemented with [CQ] = (1—*P*) x $[CQ]^{Dd2}$ and [PPQ] = *P* x $[PPQ]^{Dd2}$, with *P* = 0, 0.25, 0.5, 0.75, 0.9, or 1.

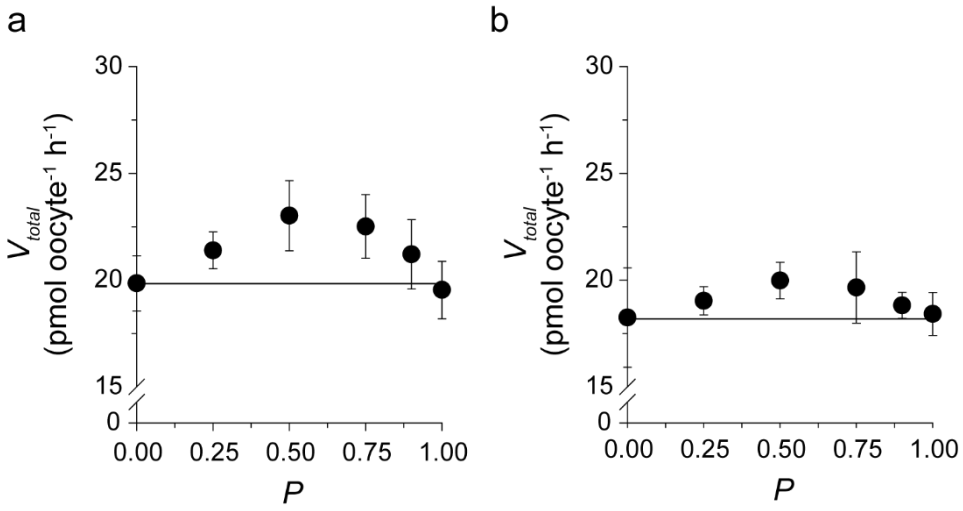

Figure 3.2.5. Competition plot of PfCRT with CQ and PPQ. The competition plot experiment was performed with CQ and PPQ and (**a**) $PfCRT^{Dd2}$-expressing oocytes, or (**b**) $PfCRT^{Dd2\_F145I}$-expressing oocytes. The horizontal lines represent the values expected if CQ and PPQ competed for binding to PfCRT. Data is shown as the mean ± SEM of at least 3 independent biological replicates. Each biological replicate is defined as measurements done on 10 oocytes originating from the same frog. Taken from Gomez *et al.* (2023) [223].

The rates of CQ and of PPQ transport were measured in pairwise experiments by the addition of either [^{3}H]CQ or [^{3}H]PPQ to each of the mixtures. The uptake values of CQ and of PPQ for each mixture (e.g. for each *P*) were mathematically added to obtain V_{total}, and V_{total} was plotted as a function of *P.* If CQ and PPQ compete for the same

binding pocket, then V_{total} is independent of *P*, and the data points are expected to fall on a horizontal line. Instead, if they do not compete, the data is expected to follow a concave shape. As seen in Figure 3.2.5a, the Competition Plot for $PfCRT^{Dd2}$ and the drugs CQ and PPQ gave a curve with a maximum, indicating the substrates do not bind at the same site. Then, I repeated the experiment using $PfCRT^{Dd2\_F145I}$, $[CQ]^{F145I}$ = 400 µM, and $[PPQ]^{F145I}$ = 18.2 µM. Again, V_{total} was independent of *P*, with the data following a concave curve with a maximum.

3.2.5 Substrate competition kinetics suggest an allosteric binding model

While the Competition Plot is useful to distinguish between an interaction that is competitive and one that is not, it does not provide information about what model of not competitive interaction truly applies [247]. To shed light on it, I performed substrate competition kinetics assays, in which the kinetics of transport of one substrate is determined at different concentrations of a second substrate, termed “inhibitor” [150, 246]. Thus, $PfCRT^{Dd2}$-expressing oocytes were exposed to ND96 pH 6.0 medium supplemented with one of seven concentrations of total (radiolabelled plus unlabelled) CQ (10, 50, 100, 200, 300, 400, or 500 µM) and one of six concentrations of unlabelled PPQ (0, 50, 125, 200, 350, or 500 µM). Water-injected oocytes were tested in parallel in each condition, and their uptake was subtracted from PfCRT-expressing oocytes to obtain the PfCRT-mediated CQ uptake. The latter was plotted as a function of CQ concentration.

Uptake decreased with increasing concentrations of PPQ, but only to a moderate extent (Figure 3.2.6a). However, the rate at which it decreased was lower at higher increments of the concentration of PPQ. To determine then how the two drugs interact with $PfCRT^{Dd2}$, I globally fit each of 16 different substrate competition model equations to the data. This was done with a Python script that I wrote with the help of Augusto Masetti [158, 223]. The script performed the fits using the least-squares method, and calculated the corrected Akaike Information Criterion (AIC_C) for each model [248]. Models were then ranked by likelihood based on their AIC_C difference (ΔAIC_C) and their Akaike weight, with the most likely model having the lowest AIC_C ($\Delta AIC_C = 0$) and the highest Akaike weight. The two best ranking models for the interaction between CQ, PPQ, and $PfCRT^{Dd2}$ were partial noncompetitive inhibition and partial mixed-type inhibition (Figure 3.2.6b). An F-test statistically favoured the partial noncompetitive

inhibition model (p = 0.89, F = 0.021, df = 37). The kinetic parameters derived from both models are summarized in Table 3.2.2.

a

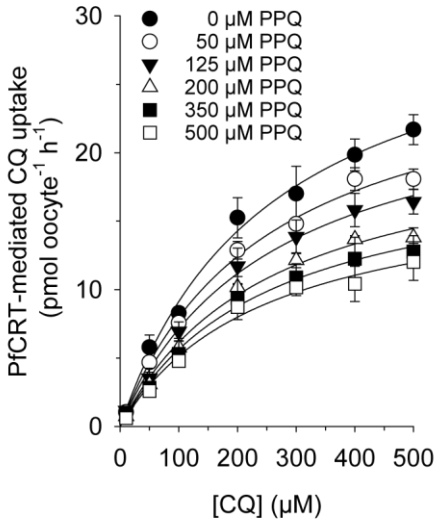

b

	Proposed mechanism	ΔAIC$_c$	Akaike weight
1	Noncompetitive (partial)	0.00	0.79
2	Mixed (partial)	2.71	0.20
3	Two-site pure competitive	13.2	0.00
4	Cooperative binding 2	16.94	0.00
5	Noncompetitive (full)	19.53	0.00
6	Mixed (full)	22.10	0.00
7	Uncompetitive (full)	34.31	0.00
8	Substrate cooperative	36.62	0.00
9	Cooperative binding	36.66	0.00
10	Uncompetitive (partial)	36.71	0.00
11	Cooperative binding 1	36.89	0.00
12	Competitive (full)	39.23	0.00
13	Inhibitor effects cooperativity	50.64	0.00
14	Ligand exclusion	74.83	0.00
15	Substrate non-cooperative	77.40	0.00
16	Competitive (partial)	120.1	0.00

c

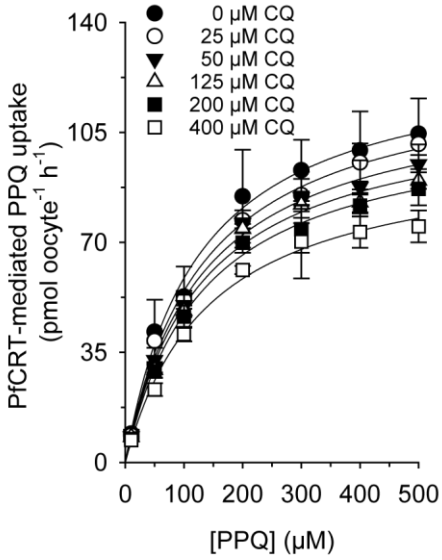

d

	Proposed mechanism	ΔAIC$_c$	Akaike weight
1	Noncompetitive (partial)	0.00	0.76
2	Mixed (partial)	2.57	0.21
3	Noncompetitive (full)	8.72	0.01
4	Cooperative binding 2	8.91	0.01
5	Two-site pure competitive	10.05	0.00
6	Mixed (full)	11.05	0.00
7	Uncompetitive (full)	14.50	0.00
8	Cooperative binding	16.18	0.00
9	Inhibitor effects cooperativity	16.44	0.00
10	Competitive (partial)	16.51	0.00
11	Uncompetitive (partial)	16.70	0.00
12	Competitive (full)	18.16	0.00
13	Substrate cooperative	19.32	0.00
14	Cooperative binding 1	20.35	0.00
15	Ligand exclusion	39.65	0.00
16	Substrate non-cooperative	42.28	0.00

Figure 3.2.6. CQ and PPQ are partial noncompetitive inhibitors of PfCRT^{Dd2}. a, PfCRT^{Dd2}-mediated transport of total CQ (radiolabelled plus unlabelled) in the presence of increasing concentration of unlabelled PPQ. **b**, Sixteen different models of substrate competition were globally fit to the data in (**a**), using the least-squared method. The likelihood of each model was evaluated by calculated the Akaike information criterion difference (ΔAIC_C) and the Akaike weight, with the most plausible model ranking first. **c**, **d**, The same experiment and analysis as in (**a**) and (**b**), but using total PPQ (radiolabelled plus unlabelled) and unlabelled CQ. Per condition, the mean ± SEM of at least 3 biological replicates is shown. Taken from Gomez *et al.* (2023) [223].

To further support these findings, I repeated the substrate competition kinetics experiment, but using radiolabelled PPQ as substrate and unlabelled CQ as inhibitor

(Figure 3.2.6c,d). The experimental and analytical procedures were as described above. Here, partial noncompetitive inhibition and partial mixed-type inhibition best described the data, according to their ΔAIC_C and their Akaike weights. An F-test again favoured the partial noncompetitive inhibition model (p = 0.47, F = 0.524, df = 37). The parameters derived are summarized in Table 3.2.2.

Table 3.2.2. Kinetic parameters of the interaction of PfCRT^{Dd2} with CQ and PPQ. Shown are the parameters from the two best models describing the data from Figure 3.2.6. V_{max}, maximal velocity of drug transport; K_S, dissociation constant for the PfCRT-substrate complex; α, K_S interaction factor; β, partiality factor; SEM, standard error of the mean; CI, confidence interval. Taken from Gomez *et al.* (2023) [223].

Substrate (inhibitor)	Parameter	Noncompetitive (partial)		Mixed (partial)	
		Mean ± SEM	95 % CI	Mean ± SEM	95 % CI
CQ (PPQ)	V_{max} (pmol.oocyte^{-1}.h^{-1})	32 ± 1	30-34	33 ± 1	30-35
	K_S^{CQ} (μM)	250 ± 20	224-284	260 ± 25	207-306
	K_S^{PPQ} (μM)	200 ± 30	133-269	210 ± 50	114-296
	α			1.0 ± 0.2	0.5-1.4
	β^{CQ}	0.38 ± 0.04	0.3-0.5	0.38 ± 0.06	0.3-0.5
PPQ (CQ)	V_{max} (pmol.oocyte^{-1}.h^{-1})	131 ± 2	126-136	130 ± 3	123-136
	K_S^{PPQ} (μM)	130 ± 6	118-142	125 ± 9	107-143
	K_S^{CQ} (μM)	240 ± 80	75-402	210 ± 80	60-369
	α			1.2 ± 0.3	0.7-1.7
	β^{PPQ}	0.60 ± 0.06	0.5-0.7	0.63 ± 0.08	0.5-0.8

Noncompetitive and mixed-type inhibition occur when the inhibitor can bind to an allosteric site whether or not the substrate is bound in the substrate binding site. The difference between the two models lies in how much the affinity for the substrate changes when the inhibitor binds, and vice versa, which is represented by the parameter α. In noncompetitive inhibition, α = 1 (affinity is not affected). Instead, in mixed-type inhibition, α ≠ 1 and α > 0 (affinity increases when 0 < α < 1; affinity decreases when 1 < α). To have an extra means to discriminate between the two models, I re-analysed the data in Figure 3.2.6. First, I fit the Henri-Michaelis-Menten equation to each of the curves that shared the same inhibitor concentration, to derive the apparent K_M ($K_M$app) and apparent V_{max} (V_{max}app) for each curve.

The analysis was done for the dataset obtained using radiolabelled CQ and unlabelled PPQ (Figure 3.2.6a), as well as for the dataset using radiolabelled PPQ and unlabelled CQ (Figure 3.2.6b). Plotting V_{max}app as a function of inhibitor concentration (Figure 3.2.7a) yields a hyperbole whose half-maximum inhibitory concentration equals the dissociation constant between the substrate and the PfCRT^{Dd2}-inhibitor complex (αK_S^{CQ} or αK_S^{PPQ}). Similarly, plotting V_{max}app/$K_M$app as a function of inhibitor concentration (Figure 3.2.7b) yields a hyperbole whose half-maximum inhibitory concentration equals the dissociation constant between the substrate and free PfCRT^{Dd2} (K_S^{CQ} or K_S^{PPQ}). Thus, α can be calculated in each case by dividing αK_S by its respective K_S. The resulting values were α = 1.0 ± 0.3 for pre-bound CQ, and α = 0.9 ± 0.7 for pre-bound PPQ. Altogether, these results were consistent with the model discrimination based on information theory (ΔAIC_C) and on statistics, namely the F-test.

Partial inhibition means that even at an infinitely high concentration of inhibitor, the substrate can still bind and be translocated, i.e., the activity never becomes 0 due to the presence of the inhibitor [246]. The difference between full and partial inhibition lies in the value of the partiality factor β, a parameter that describes how high the activity of the PfCRT-substrate-inhibitor complex is relative to that of the PfCRT-substrate complex [249]. If CQ and PPQ are partial inhibitors of PfCRT^{Dd2}, then plotting the kinetic data in the form of a fractional velocity plot will result in a straight line that intercepts the y-axis at β(1-β). In cases of full inhibition, β = 0 (the PfCRT-substrate-inhibitor complex is inactive), so the straight line passes through the origin. As seen in Figure 3.2.7b, the results obtained confirmed the partial nature of the inhibition, with PPQ slowing down PfCRT^{Dd2}-mediated CQ transport by β^{CQ} = 0.35 ± 0.06.

The kinetics of the interaction between PfCRT^{Dd2}, CQ and PPQ was modelled (Figure 3.2.7c,d) by overlaying the partial noncompetitive model (red lines) with the experimentally derived data (black circles). Lastly, using the partial noncompetitive inhibition equation and comparing it to the experimental data, I obtained and plotted the residuals as a function of substrate or inhibitor concentration (Figure 3.2.7d,f). The residuals were randomly distributed, suggesting that the model is a proper fit to the data [250].

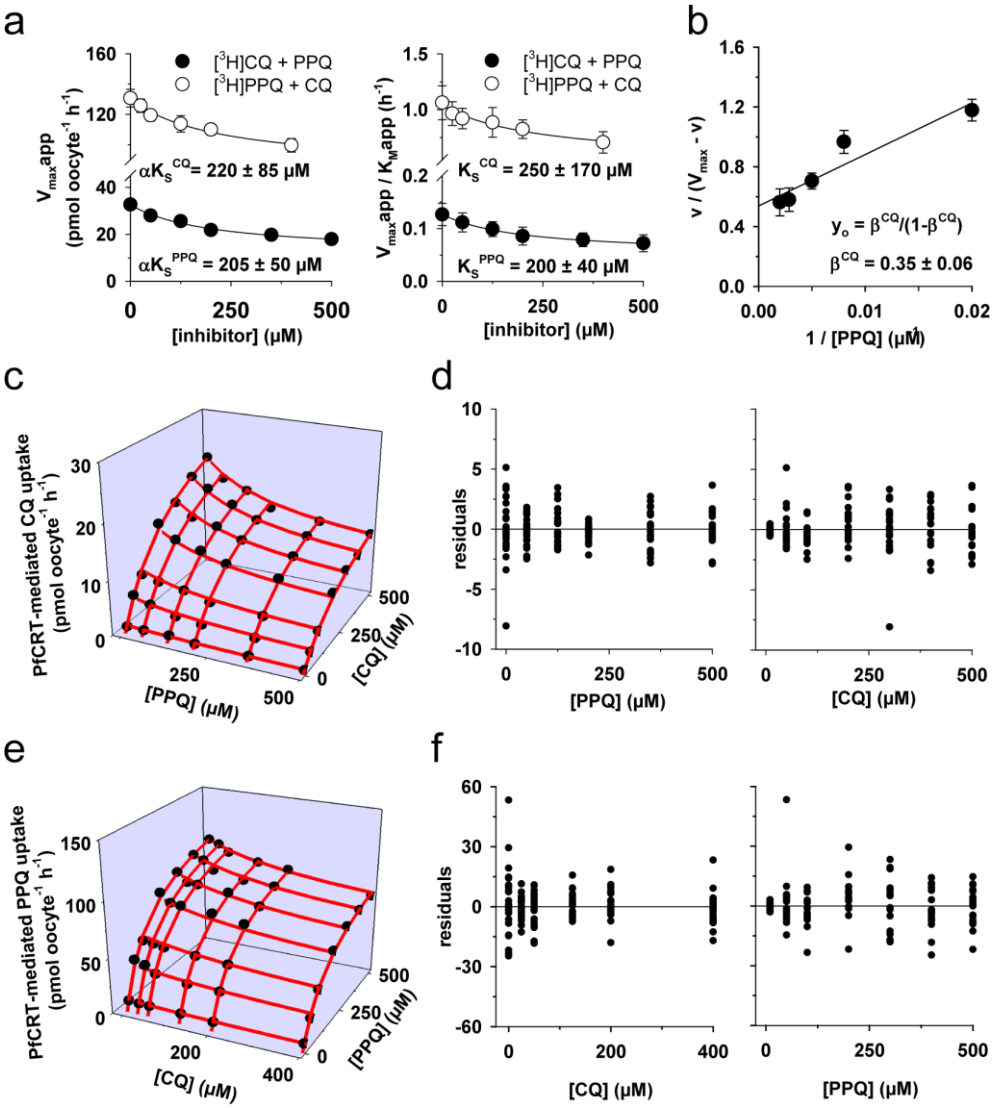

Figure 3.2.7. Modelling the interaction of CQ and PPQ with PfCRT^{Dd2} using the partial noncompetitive mechanism. a, *Left*, The apparent maximal velocity of transport (V_{max}app) shown as a function of the respective inhibitor concentration, yielding a hyperbole whose half-maximal inhibitory concentration equated to αK_S^{CQ} (open circles) or to αK_S^{PPQ} (filled circles). *Right*, The ratios of V_{max}app to the corresponding apparent Michaelis constant ($K_M$app) are shown as a function of the respective inhibitor concentration, yielding hyperboles whose half-maximal inhibitory concentrations equated to K_S^{CQ} (open circles) or K_S^{PPQ} (filled circles). The mean ± SD is shown per condition. **b**, The partiality factor β was derived by plotting the ratio of uptake (v) to V_{max} - v versus the reciprocal of the inhibitor concentration. **c**, The inhibition of CQ transport by PPQ was modelled using the partial noncompetitive equation and displayed as a 3D plot (red lines). The parameters used are those in Table 3.2.2. The experimentally derived data were overlaid for comparison (black circles). **d**, The difference between experimentally derived uptake values and the values predicted by the model was calculated and plotted as a function of the PPQ concentration (*left*) or of the CQ concentration (*right*). **e**, As in (**c**), but inhibition of PPQ transport by CQ. **f**, As in (**d**), but for the inhibition of PPQ transport by CQ. Taken from Gomez *et al.* (2023) [223].

3.2.6 CQ and PPQ are partial noncompetitive inhibitors of PfCRT^{Dd2_F145I}

To test whether the F145I amino acid substitution changes how CQ and PPQ interact with PfCRT, I conducted the same substrate competition kinetics experiments as described above but using PfCRT^{Dd2_F145I}. All assays and analyses favoured the partial noncompetitive inhibition mechanism for the interaction between PfCRT^{Dd2_F145I}, CQ and PPQ, including the global fit of the 16 models of substrate competition to the data using radiolabelled CQ or PPQ (Figure 3.2.8).

a

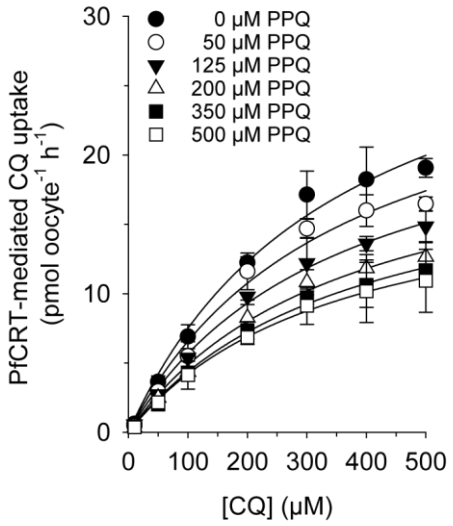

b

	Proposed mechanism	ΔAIC_c	Akaike weight
1	Noncompetitive (partial)	0.00	0.71
2	Mixed (partial)	2.71	0.18
3	Two-site pure competitive	4.10	0.09
4	Cooperative binding 2	8.56	0.01
5	Inhibitor effects cooperativity	12.84	0.00
6	Competitive (partial)	17.77	0.00
7	Cooperative binding	19.99	0.00
8	Substrate cooperative	20.50	0.00
9	Noncompetitive (full)	20.51	0.00
10	Mixed (full)	23.09	0.00
11	Competitive (full)	29.12	0.00
12	Cooperative binding 1	31.63	0.00
13	Uncompetitive (full)	33.37	0.00
14	Uncompetitive (partial)	35.94	0.00
15	Ligand exclusion	52.01	0.00
16	Substrate non-cooperative	105.7	0.00

c

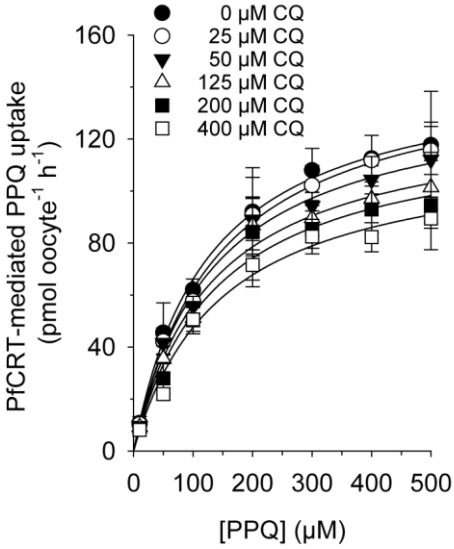

d

	Proposed mechanism	ΔAIC_c	Akaike weight
1	Noncompetitive (partial)	0.00	0.76
2	Mixed (partial)	2.57	0.21
3	Two-site pure competitive	8.72	0.01
4	Cooperative binding 2	8.91	0.01
5	Noncompetitive (full)	10.05	0.00
6	Competitive (partial)	11.05	0.00
7	Mixed (full)	14.50	0.00
8	Uncompetitive (full)	16.18	0.00
9	Substrate cooperative	16.44	0.00
10	Cooperative binding 1	16.51	0.00
11	Uncompetitive (partial)	16.70	0.00
12	Inhibitor effects cooperativity	18.16	0.00
13	Competitive (full)	19.32	0.00
14	Cooperative binding	20.35	0.00
15	Ligand exclusion	39.65	0.00
16	Substrate non-cooperative	42.28	0.00

Figure 3.2.8. CQ and PPQ are partial noncompetitive inhibitors of PfCRT^{Dd2_F145I}. **a**, PfCRT^{Dd2_F145I}-mediated transport of total CQ (radiolabelled plus unlabelled) in the presence of increasing concentration of unlabelled PPQ. **b**, Sixteen different models of substrate competition were globally fit to the data in (**a**), using the least-squared method. The likelihood of each model was evaluated by calculated the Akaike information criterion difference (ΔAIC_C) and the Akaike weight, with the most plausible

model ranking first. **c**, **d**, The same experiment and analysis as in (**a**) and (**b**), but using total PPQ (radiolabelled plus unlabelled) and unlabelled CQ. Per condition, the mean ± SEM of at least 3 biological replicates is shown. Parameters are summarized in Table 3.2.3. Taken from Gomez *et al.* (2023) [223].

Table 3.2.3. Kinetic parameters of the interaction of PfCRT^{Dd2_F145I} with CQ and PPQ. Shown are the parameters from the two best models describing the data from Figure 3.2.8. V_{max}, maximal velocity of drug transport; K_S, dissociation constant for the PfCRT-substrate complex; α, K_S interaction factor; β, partiality factor; SEM, standard error of the mean; CI, confidence interval. Taken from Gomez *et al.* (2023) [223].

Substrate (inhibitor)	Parameter	Noncompetitive (partial)		Mixed (partial)	
		Mean ± SEM	95 % CI	Mean ± SEM	95 % CI
CQ (PPQ)	V_{max} (pmol.oocyte^{-1}.h^{-1})	34 ± 2	31-38	34 ± 2	29-39
	K_S^{CQ} (µM)	360 ± 30	299-416	350 ± 50	260-445
	K_S^{PPQ} (µM)	170 ± 30	103-231	160 ± 40	83-244
	α			1.0 ± 0.3	0.4-1.7
	β^{CQ}	0.40 ± 0.04	0.3-0.5	0.41 ± 0.08	0.3-0.6
PPQ (CQ)	V_{max} (pmol.oocyte^{-1}.h^{-1})	152 ± 4	145-160	150 ± 5	141-160
	K_S^{PPQ} (µM)	134 ± 8	119-150	128 ± 11	105-151
	K_S^{CQ} (µM)	230 ± 90	39-411	200 ± 90	27-374
	α			1.2 ± 0.3	0.6-1.8
	β^{PPQ}	0.61 ± 0.07	0.5-0.7	0.64 ± 0.09	0.5-0.8

The graphical analyses (Vmaxapp and Vmaxapp/KMapp as functions of the inhibitor concentration) used to confirm the noncompetitive nature of the mechanism of inhibition, the fractional velocity plot to confirm the partiality of the inhibition, and the analysis of the residuals as a function of substrate or inhibitor concentration also supported the partial noncompetitive inhibition model (Figure 3.2.9). The kinetic parameters of the two best models are summarized in Table 3.2.3.

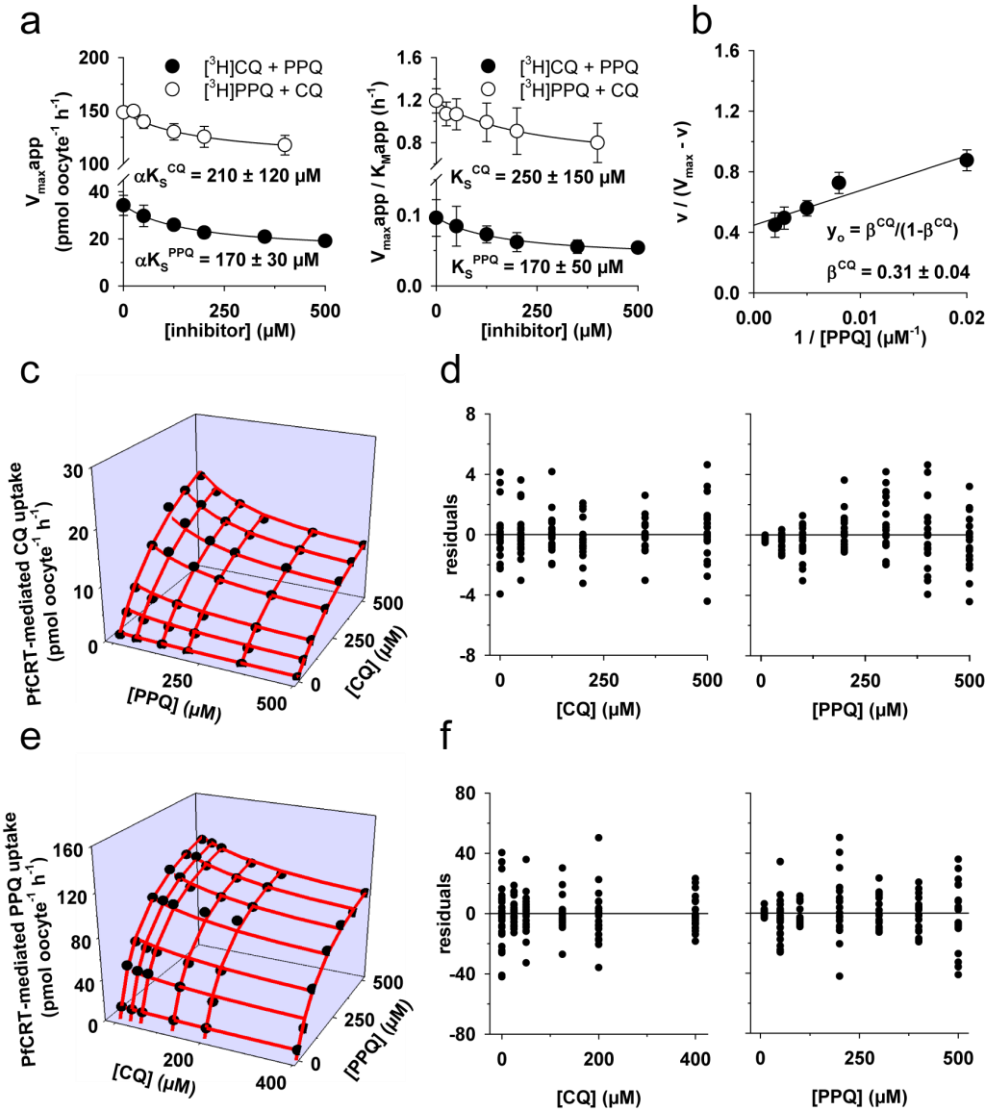

Figure 3.2.9. Modelling the interaction of CQ and PPQ with PfCRT^{Dd2_F145I} using the partial noncompetitive mechanism. a, *Left*, The apparent maximal velocity of transport (V_{max}app) shown as a function of the respective inhibitor concentration, yielding a hyperbole whose half-maximal inhibitory concentration equated to αK_S^{CQ} (open circles) or to αK_S^{PPQ} (filled circles). *Right*, The ratios of V_{max}app to the corresponding apparent Michaelis constant ($K_M$app) are shown as a function of the respective inhibitor concentration, yielding hyperboles whose half-maximal inhibitory concentrations equated to K_S^{CQ} (open circles) or K_S^{PPQ} (filled circles). The mean ± SD is shown per condition. **b**, The partiality factor β was derived by plotting the ratio of uptake (v) to V_{max} - v versus the reciprocal of the inhibitor concentration. **c**, The inhibition of CQ transport by PPQ was modelled using the partial noncompetitive equation and displayed as a 3D plot (red lines). The parameters used are those in Table 3.2.3. The experimentally derived data were overlaid for comparison (black circles). **d**, The difference between experimentally derived uptake values and the values predicted by the model was calculated and plotted as a function of the PPQ concentration (*left*) or of the CQ concentration (*right*). **e**, As in (**c**), but inhibition of PPQ transport by CQ. **f**, As in (**d**), but for the inhibition of PPQ transport by CQ. Taken from Gomez *et al.* (2023) [223].

3.2.7 Docking and molecular dynamics simulations support the allosteric binding model

As mentioned above, as I inspected the kinetic parameters of the mutants summarised in Table 3.2.1, I wondered whether H97 and F145 are involved in binding CQ. If they were, then that would explain why mutating those residues affects the K_M^{CQ}. More generally, knowledge on where CQ and PPQ might bind in the cavity of PfCRT is lacking. To find evidence that CQ binds to H97 and F145, docking simulations were performed by Dr. Giulia D'Arrigo and Dr. Rebecca Wade from the Heidelberg Institute for Theoretical Studies (HITS), in Heidelberg, Germany. The $PfCRT^{7G8}$ cryo-EM structure [156] was used as a template to model the tertiary structure of $PfCRT^{Dd2}$. The structure was solved with a Fab fragment inserted into the cavity, so the template is forced in the open-to-vacuole conformation. For the modelling of $PfCRT^{Dd2}$, the Fab fragment was disregarded, and the obtained modelled structure was still in the open-to-vacuole conformation. A high-quality model was obtained, according to the MolProbity utility from SWISS-MODEL (Annex III) [225], thanks to the high-sequence identity of the two PfCRT isoforms of 98 %.

The binding of CQ and PPQ to $PfCRT^{Dd2}$ was investigated first by molecular docking. The two drugs were tested in their fully protonated states (CQ^{2+} and PPQ^{4+}), given the slightly acidic pH of the digestive vacuole of parasites of 5.2. To overcome a potential influence of the absence of the Fab fragment on the docking results, induced-fit docking was performed considering the whole cavity as the docking space [229]. Up to 10 poses were generated for each drug. CQ bound to two preferred regions: the first one involved the top central part of the cavity (poses 1 and 2; see Annex IV). The second one was occupied by the majority of the poses (poses 3 to 10) and lied in a small pocket in the bottom left side of the cavity, and agreed with my hypothesis that H97 and F145 bind CQ. In the highest-ranking of these poses (Figure 3.2.10a), CQ established polar interactions via its two positively charged nitrogen atoms: the one in the diethylamino tail formed a salt bridge with E75 on TM1, while the nitrogen of the 4-aminoquinoline ring made a hydrogen bond with S257 on TM7. Hydrophobic interactions were formed by the quinoline ring with V141, F145, and I260. Replacing each of V141, S257 and I260 for Ala significantly reduced PfCRT-mediated CQ transport in *X. laevis* oocytes, relative to parental $PfCRT^{Dd2}$ (Figure 3.2.10b).

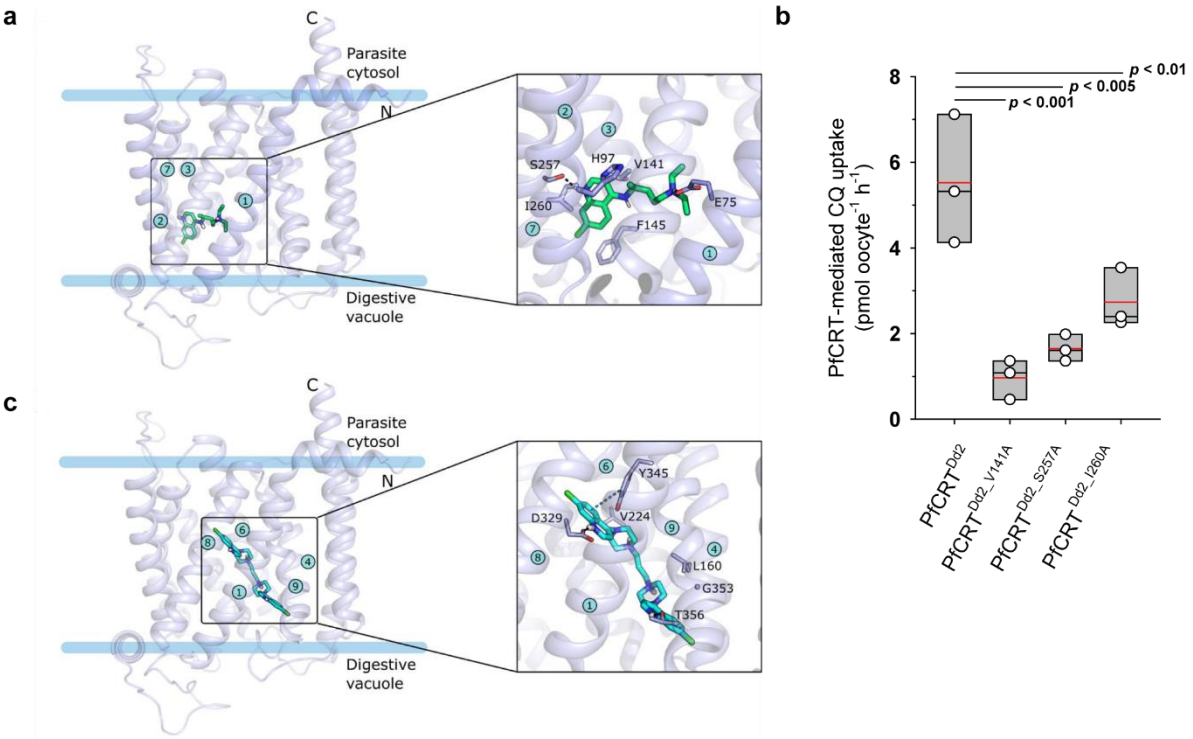

Figure 3.2.10. CQ and PPQ dock in different pockets in the cavity of PfCRT^{Dd2}. a, The docking pose of CQ within the whole protein structure is shown with a close-up of the binding pocket and the established interactions in the inset. The protein is shown in transparent light blue cartoon representation, and the substrates and interacting residues are shown as sticks. The N- and C-termini, the transmembrane helices and the residues involved in ligand binding are labelled. Interactions between drugs and protein are shown by dashed lines: hydrogen bonds and salt-bridges in black; π-π interactions in grey. **b**, The PfCRT-mediated CQ transport was measured in oocytes expressing PfCRT^{Dd2}, PfCRT^{Dd2_V141A}, PfCRT^{Dd2_S257A}, or PfCRT^{Dd2_I260A}. A box plot analysis is overlaid over the individual data points (independent biological replicates), with the median (black lines), mean (red lines), and 25 and 75 % quartile ranges shown. Multiple comparisons versus the PfCRT^{Dd2} control were performed (Holm-Sidak ANOVA). **c**, Same as in (**a**), but for PPQ. The docking simulations were performed by Dr. Giulia D'Arrigo and Prof. Dr. Rebecca Wade. Taken from Gomez *et al.* (2023) [223].

PPQ showed more variability in the generated poses: the two best-ranking poses located to the right side of the cavity in a relatively vertical fashion, while the rest (poses 3 to 9) tended to occupy the full cavity horizontally. In the top-ranked pose (Figure 3.2.10c), the protonated nitrogen atoms of the two piperazine moieties formed hydrogen bonds with D329 on TM8 and T356 on TM9. The piperazine moieties also established hydrophobic contacts with L160 and V224, and one quinoline ring formed a π-π interaction with Y345 on TM9. Notably, the docking scores for CQ and PPQ reflected the differences in the experimentally measured affinities for PfCRT^{Dd2}, with CQ having less favourable docking scores compared to PPQ (see Annex IV).

Molecular dynamics (MD) simulations were then used to simulate the co-existence of both drugs in the cavity of PfCRT^{Dd2} (Figure 3.2.11). The initial state was pose 3 of CQ and pose 1 of PPQ. CQ moved only on the left side of the channel, where it eventually found a stable arrangement forming a hydrogen bond with D137 and N98, and hydrophobic contacts with F101, V141, and F322. PPQ underwent a large conformational change in which it was pulled down to the digestive vacuole even further than when it was simulated alone. This arrangement was stabilised by a methionine-aromatic contact between M305, in the vacuolar loop, and the quinoline ring, and by a polar contact between the protonated piperazine moiety and E207. Additional hydrophobic interactions were established by the piperazine moiety with T205 and V369, and by the other quinoline ring with L160 and T356.

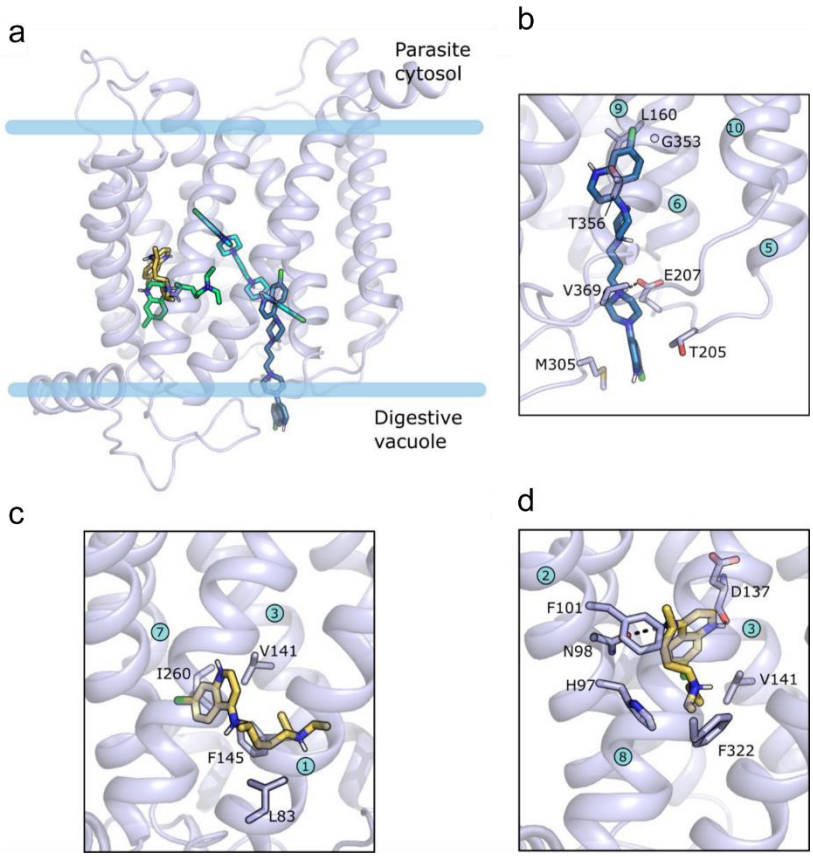

Figure 3.2.11. MD simulation of PfCRT^{Dd2} in complex with both CQ and PPQ. a, The last frame of the simulation is shown superimposed to the original docking poses of CQ and PPQ. **b**, Interactions established by PPQ during the last hundred ns of simulation. **c**, Pose and interactions of CQ in the central part of the simulation (400-600 ns). **d**, Final pose and interactions established by CQ in the last hundred ns. The docking and the MD final poses are shown in green and yellow, respectively, for CQ, and in cyan and blue, respectively, for PPQ. The protein and interacting amino acid residues are shown in light blue. The simulations were performed by Dr. Giulia D'Arrigo and Prof. Dr. Rebecca Wade. Taken from Gomez *et al.* (2023) [223].

3.2.8 Docking simulations provide evidence for isoform-specific binding of CQ and PPQ

As mentioned above, Kim and colleagues found that CQ and PPQ act as competitive inhibitors of PfCRT^{7G8} [156]. Given the discrepancy between their findings and mine, CQ and PPQ were docked into the cryo-EM structure of said isoform. While the docking of CQ to PfCRT^{7G8} agreed with that of CQ to PfCRT^{Dd2}, PPQ mainly occupied the centre-left side of the cavity, without entirely occupying its right-side (Figure 3.2.12). The differences in the amino acid sequence on the right side of the channel (I356 and R371 in PfCRT^{7G8}, and T356 and I371 in PfCRT^{Dd2}) may prevent binding of PPQ in the 7G8 isoform, resulting in overlapping binding sites for the 2 drugs in that isoform. These results supported the suggested competitive binding of drugs to PfCRT^{7G8} and pointed at an isoform-specific pattern of drug binding.

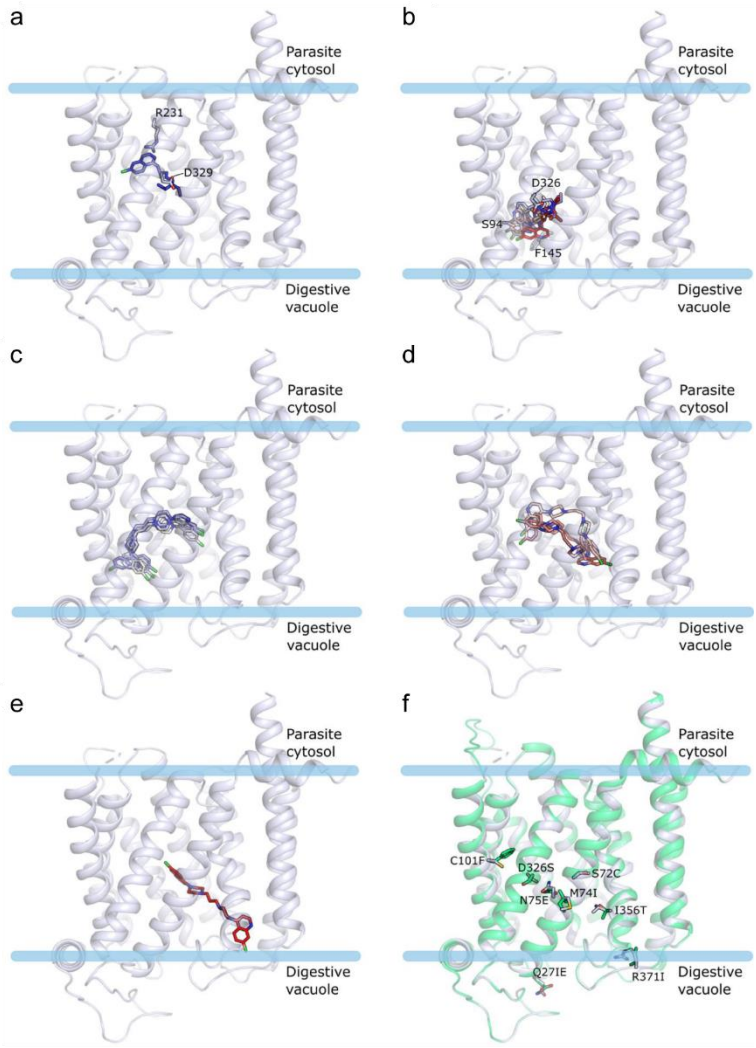

Figure 3.2.12. Docking of CQ and PPQ in the cavity of PfCRT^{7G8}. A blue-to-red colour scale shows the generated docking poses for CQ (**a**-**b**) and for PPQ (**c**-**e**),

ranked from the best (blue) to the worst (red) docking score. **f**, Superposition of the Dd2 (green) and the 7G8 (white) isoforms with the residues which are different shown as sticks and labelled. The simulations were performed by Dr. Giulia D'Arrigo and Prof. Dr. Rebecca Wade. Taken from Gomez *et al.* (2023) [223].

4 Discussion

4.1. The phosphorylation of PfCRT

Four phosphorylation sites have been found in PfCRT: Ser33, Ser411, Thr416, and Ser420, all of them localized in cytoplasmic loops [156, 186, 187]. The roles of two of them, namely Ser33 and Thr416, have already been investigated and proved to play critical roles in the functioning and sorting of the protein within the malaria parasite, respectively [187, 188]. Given the importance of these phosphorylation events, it is evident that chemically interfering with them could lead to a poor functioning of PfCRT *in vivo*, as has been observed *in vitro* [187, 188], resulting in antimalarial re-sensitization. However, the identity of the protein kinases responsible for PfCRT's modifications has remained largely obscure. There are numerous methods to determine which proteins from an organism are the target of a specific protein kinase [251-253]. However, the inverse process, e.g. determine which protein kinase targets a specific protein, is far more complicated. As a starting point, one could use predictive bioinformatic tools to at least gain an idea on what proteins could be the ones targeting a desired phosphosite, like Ser33 in PfCRT. However, most of these tools are based on databases built from knowledge on human, bacterial, or yeast kinomes [254, 255], all of which differ greatly from malarial ones [189, 190, 192]. Thus, such approaches often lead to ambiguous results in which different bioinformatic tools rarely provide overlapping or reliable hits.

For the first method employed to uncover the identity of the protein kinase phosphorylating Ser33 of PfCRT, the kinase inhibitors ML-7 and H-89 were used in competition pulldown assays (Figure 3.1.1). The capacity of each of these drugs to deplete kinobeads of protein kinases served to uncover which proteins from the *P. falciparum* Dd2 extracts could bind ML-7 or H-89. A total of 717 proteins were enriched with the kinobeads after pre-incubation with ML-7, and a total of 837 proteins when H-89 was used for the pre-incubation step. Of them, 31 proteins were protein kinases. Considering that *P. falciparum* expresses approximately 50 protein kinases during the trophozoite stage (the actual number depends nowadays on the stringency with which bioinformatic tools assign a putative protein kinase function to a gene), the kinobead approach led to a 62 % coverage of the expected kinome [189-191]. Since both ML-7 and H-89 were shown to increase the sensitivity of Dd2 parasites to CQ and QN [187],

potentially by preventing phosphorylation of PfCRT, they were expected to provide at least one overlapping hit, namely the kinase that acts on PfCRT Ser33. In fact, and somewhat luckily, the only protein found to confidently bind ML-7 and H-89 in a dose-dependent manner was the cAMP-dependent protein kinase, PfPKA. This applies to both the catalytic subunit (PfPKAc; PF3D7_0934800) and the regulatory subunit (PfPKAr; PF3D7_1223100). In each case, the affinity of the drug for the catalytic subunit was twice as high as the affinity for the regulatory subunit, indicating that both drugs mimic ATP better than cyclic AMP (cAMP). Interestingly, ML-7 is known to inhibit human PKA (hPKA), binding to the latter with a Ki = 21 µM [256], similar to the apparent dissociation constant found in the competition assay for PfPKAc of K_d^{app} = 22.6 µM. Similarly, H-89 is a known hPKA inhibitor, though the selectivity for the human homologue is clear, with a Ki = 0.048 µM for hPKA [257] and K_d^{app} = 0.9 µM for PfPKAc. Thus, even though I could profit from using these two kinase inhibitors, their use in treating malaria would be discouraged due to potential side effects and health risks for the patient [258].

The second method used in this work supported the suggestion that PfPKA phosphorylates PfCRT on Ser33. K-CLASP is *a priori* a more direct method because it depends on the direct interaction of a given protein kinase with a user-designed phosphosite-containing peptide (Figure 3.1.2). Even then, PfPKAc could not be considered a hit, given the stringency established for the decision-making process. However, as shown previously, proteins freely diffuse during K-CLASP, which can lead to the crosslinking of the peptide with a protein different from the target protein kinase, but that is associated with it [219, 220]. Considering that, having PfPKAr as a hit was a reasonable result, given the natural interaction of PfPKAc with PfPKAr. Another candidate that arose from this experiment was casein kinase I (CK1; PF3D7_1136500). The protein was observed in the 4 trials run, though only met the criteria in 1, exactly like for PfPKAr. The *P. falciparum* kinome contains only 1 member of the CK1 family [189-191]. The protein is implicated in mRNA splicing, invasion, and in chromatin dynamics [259]. Interestingly, the δ human isoform is phosphorylated by human PKA [260]. If the same were true in *P. falciparum*, it would be reasonable to say that CK1 was a hit in my K-CLASP experiments because it interacts with PKA. Naturally, the same could be expressed about any other protein that is a target of PKA. However, in the analysis done in this work, protein kinases were the query and focus, among which only CK1 and PKA were observed as hits.

In most studied organisms, PKAr and PKAc form a heterotetrameric complex. Upon binding of some ligand to a G-protein-coupled receptor in the plasma membrane, adenylyl cyclase is activated, leading to a rise in the concentration of cellular cAMP. This second messenger binds to PKAr, inducing a conformational change that results in the release of PKAc. Then, PKAc is active, and can use ATP to phosphorylate a range of proteins, from enzymes and transporters to transcription factors. A single PKAc and a single PKAr gene have been found in *P. falciparum*, whose products form a dimer [261, 262]. PfPKAc has been implicated in several key processes in the intraerythrocytic parasite, highlighting the potential that confirming it as a mediator of PfCRT phosphorylation has. For example, PfPKAc is known to phosphorylate the malaria vaccine candidate apical membrane antigen 1 (AMA1), a merozoite surface protein which is essential for the invasion of the red blood cell [263-265]. In fact, depletion of cAMP levels by conditional knock-down of adenylyl cyclase, or conditional null mutation of the phosphodiesterase β gene, both result in invasion defects [264, 266]. In addition, cAMP/PfPKAc-dependent signalling is implicated in the regulation of ion channel conductance and of the new permeation pathways both in asexual blood-stage parasites and in gametocytes [267, 268]. Thus, it would seem unsurprising if the protein was also responsible for altering the activity of a transporter involved in nutrient transport from the DV to the cytoplasm of the parasite [163].

Direct proof of the phosphorylation of Ser33 in PfCRT by PfPKAc is still lacking, despite efforts done in this doctoral work. Different experiments could be done to confirm that PKAc phosphorylates PfCRT. One of them would be to use a recombinantly expressed PfPKAc and test its activity *in vitro* with a peptide that mimics the phosphosite containing Ser33, as intended originally in this thesis (see Annex I). Expression could be aided by co-expression of PfPKAr, to prevent the possibility of PfPKAc-driven cellular toxicity in the recombinant organism of choice. Another pathway would be to induce the overexpression of PfPKAc to an insoluble form, and later re-solubilize it and re-fold it. Alternatively, the protein could be tagged and purified from the parasite itself, though these strategies are usually the most time and resource-consuming. If unsuccessful, PKA homologues from other organisms could be used in the *in vitro* assay. In particular, human PKAc shares 50 % sequence homology with malarial PKAc and, according to computational models, great structural resemblance [269]. Malarial PKAc has strong conservation of the 11 specific kinase subdomains (I-XI), and several residues required for catalytic activity are also highly conserved [270]. Nonetheless,

these facts are often true for protein kinase homologues, but this does not prevent them from having different substrate specificities. Thus, direct proof will remain a need as long as these difficulties are not overcome.

Of note, in the work by Patel *et al.* (2019) [264], the role of adenylyl cyclase and PfPKA were studied. They used genetically edited *P. falciparum* 3D7 lines, in which they conditionally disrupted either gene. When disrupting *pfpka*, they found that PfCRT was significantly less phosphorylated in Ser33. This result led me to suspect that phosphorylation of that residue is not only important for enhancing the drug-transport activity of PfCRT [187], since the 3D7 line is CQ sensitive. Instead, PfCRT may be phosphorylated at Ser33 to serve a purpose in its natural function: the translocation of peptides from the DV to the cytoplasm. To prove such role, I would suggest to use the Ser33-mutant parasite lines from the work of Sanchez *et al.* (2019) [187] in an experiment similar to the one performed in Sanchez *et al.* (2022) [160]. In the latter, parasites were cultured with fluorescently labelled dipeptides and, the next day, the presence of fluorescent signal in the DV was assessed. The parasites used were genetically edited so that the knock-down of PfCRT could be induced, allowing the authors to confirm that the protein mediated the transport of those peptides from the DV to the cytoplasm.

In the experiment I suggest, an edited Dd2 parasite line carrying the mutation S33A (no phosphorylation possible) and a control Dd2 line (phosphorylation possible) would be fed with the fluorescently labelled peptides, and the presence of fluorescent signal studied (Figure 4.1.1). If the phosphorylation of Ser33 is important for the natural function of PfCRT, then signal would be expected to be concentrated in the DV of the S33A parasites but distributed between DV and cytoplasm of control Dd2 parasites. Understanding the role of the phosphorylation of PfCRT in its natural function will only increase the attractiveness of finding drugs that can interfere with these processes. The knowledge gained thus hopefully helps design and develop new antimalarial drugs.

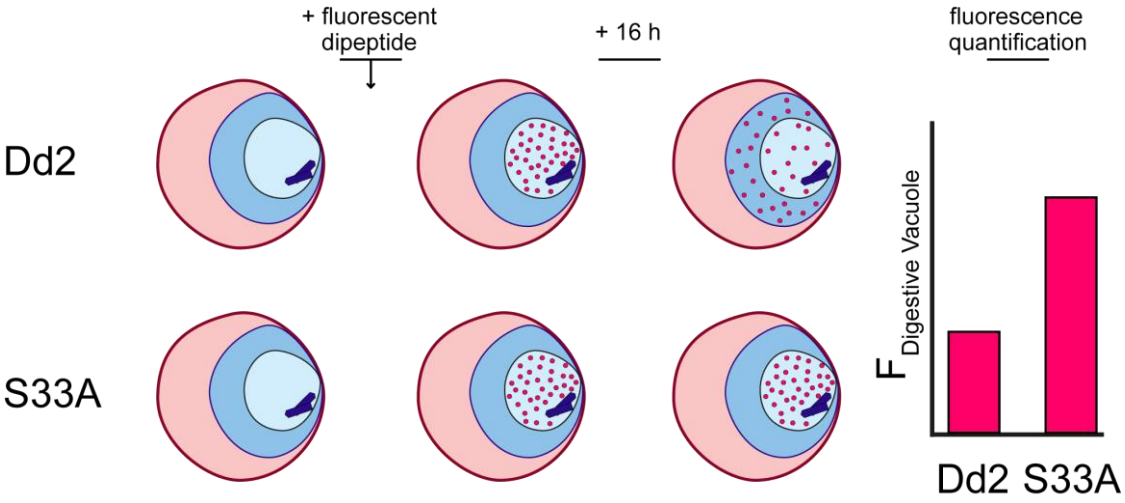

Figure 4.1.1. Proposed experiment for determining the involvement of phosphorylation at Ser33 in PfCRT-mediated oligopeptide transport. When *P. falciparum* Dd2 parasites (blue) are fed with fluorescently labelled dipeptides, these are eventually transported from the digestive vacuole (light blue) to the parasite's cytosol, leading to a distribution of the fluorescent signal from the peptides between both compartments. If phosphorylation of the residue Ser33 in PfCRT is key for its natural function, then genetically edited *P. falciparum* Dd2 parasites carrying the S33A mutation will accumulate peptides in the digestive vacuole, leading to a higher fluorescent signal from the peptides in this compartment, relative to parental Dd2 parasites.

4.2. The mechanisms of drug transport by PfCRT

The *P. falciparum* chloroquine resistance transporter (PfCRT) from the Southeast Asian Dd2 malaria parasite can handle numerous quinoline and quinoline-like antimalarial drugs [150, 156, 172, 196]. To delay and overcome drug resistance emergence, artemisinin-based combination therapies (ACTs) are the chemotherapies of choice. In an ACT, a fast-acting artemisinin drug is given in combination with a slower acting antimalarial. A massively distributed and used ACT in Cambodia was dihydroartemisinin-piperaquine (DHA-PPQ), which proved highly efficacious and tolerable [271-273]. The Thai-Cambodia border, where there is high flow of seasonal workers, has been a niche for the emergence and spread of antimalarial drug resistance since the first reports of chloroquine (CQ) resistance in Thailand in 1961 [125]. More recently, reports of artemisinin tolerance and partner drug resistance have become the norm in that region [3, 4, 134]. Resistance to artemisinins depends on mutations in PfKelch13, which modulate the endocytosis of hemoglobin by the intraerythrocytic parasite, reducing activation and action of that family of drugs. Instead, resistance to the partner drug piperaquine (PPQ) is mediated by mutations in PfCRT [242, 243]. However, upon gaining the PPQ resistance phenotype, parasites become re-sensitized to CQ, an observation that led to the suggestion of using both CQ and PPQ in a combination regime [179, 244].

In this work, I showed that the CQ resistance-conferring Dd2 isoform of PfCRT ($PfCRT^{Dd2}$) can readily transport PPQ (Figure 3.2.1 and Figure 3.2.2). Surprisingly, the amount of drug transported per unit of time is around 1 order of magnitude higher than that measured for other drugs like CQ (this work and others), quinine or quinidine [150, 172, 175]. However, that shows that PPQ transport activity is in itself not sufficient to confer resistance to the drug. To do so, PfCRT must acquire an additional mutation, which can happen in different parts of the protein, usually lining up in its cavity [156, 179]. This study revealed that any of the PPQ resistance-conferring mutations H97Y, F145I, M343L or G353V result in subtle changes in the apparent K_M^{PPQ} and/or V_{max}^{PPQ} (Table 3.2.1). These changes range from 8 to 35 % and combined allow the carrier to surpass a certain resistance threshold. Minimal kinetic requirements for an improved PPQ transporter would involve a 10 % or higher increase in V_{max}^{PPQ} and/or a 20 % or higher decrease in K_M^{PPQ}, relative to $PfCRT^{Dd2}$. The improvement in PPQ transport came at the expense of a reduced CQ transport efficiency, consistent with parasites

having any of these mutations become re-sensitized to CQ. The mutations either reduced the V_{max}^{CQ} in 27 to 30 % or increased the K_M^{CQ} in 42 to 104 %. In fact, I found a negative correlation between V_{max}^{PPQ} and K_M^{CQ} for the tested isoforms. In what would seem to be an evolutionary limit for PfCRT, the protein does not seem yet capable of efficiently handling both CQ and PPQ with a single set of mutations. Thus, this study offered an explanation to why a single amino acid substitution, namely the H97Y, F145I, M343L or G353V, are enough for conferring PPQ resistance and re-sensitizing the parasite to CQ simultaneously. Docking CQ or PPQ to the modelled structure of each of $PfCRT^{Dd2\_H97Y}$, $PfCRT^{Dd2\_F145I}$, $PfCRT^{Dd2\_M343L}$ and $PfCRT^{Dd2\_G353V}$ revealed different patterns of substrate binding (see Annex IV and Annex V), though in general CQ docked within the same region. However, from the docking scores differences between $PfCRT^{Dd2}$ and the related mutants in the binding energies were not observed, likely reflecting the slight changes in the kinetic parameters that the mutations cause.

While the effect of mutations H97Y, F145I and G353V were readily interpretable in terms of the change in the physicochemical properties of the binding pockets and, in general, of the binding cavity of PfCRT, that of the M343L mutation escaped a clear explanation at first. The residue M343 does not face the cavity of the transporter, and even more, it lies on its cytoplasmic side. Thus, its replacement having an impact on the K_M^{CQ} was not an obvious, expectable observation. One has to consider that conventional Michaelis-Menten kinetics was thought for enzyme-substrate to enzyme-product systems, and not for a transporter like PfCRT. However, potential explanations arise when applying Michaelis-Menten concepts to a transport process that within its cycle involves substrate binding, conformational change coupled to substrate movement across the protein, substrate release, and conformational change that recycles the transporter to the initial conformation (“conformational restart”), ready to start the next cycle of transport [274]. With this in mind, in a transporter system, the K_M for a substrate is influenced not only by the rates of substrate binding, but also by the rate of substrate release after transport, and by the rate of conformational restart. Thus, it is probable that the replacement of M343 for Leu, while it cannot affect CQ binding because the residue is at the cytoplasmic side, affects one or both of the other two processes. For this reason, I hypothesize a putative role of M343 in substrate release and/or conformational restart of PfCRT.

All of the tested isoforms were readily blocked by the CQ resistance-reverser verapamil (VP) (Figure 3.2.3). The drug is a partial mixed type inhibitor of PfCRT-mediated drug transport [150], which was once thought to be usable as a CQ re-sensitizing agent [275]. The isoforms that were most affected were the CQ resistance-conferring $PfCRT^{Dd2}$ in the case of CQ transport, and the highly PPQ resistance-conferring $PfCRT^{Dd2\_F145I}$ in the case of PPQ. In fact, the addition of 100 µM VP reduced the uptake to what seemed to be basal levels (2-2.5 pmol/oocyte/h for CQ; 20-30 pmol/oocyte/h for PPQ). Interestingly, the $PfCRT^{Dd2\_G353V}$ mutant was the least affected by VP, with a reduction of CQ transport of 26 % and a reduction of PPQ transport of 45 %. A docking simulation of VP into the cavity of $PfCRT^{Dd2}$ ran as a preliminary experiment showed that G353 is in close proximity with VP (see Annex VI). Together, these results suggest that VP binds to a pocket involving G353, and that the mutation G353V affects binding of the drug, leading to a reduced blocking effect.

The fact that the H97Y mutation reduced the K_M^{CQ} was at first surprising. In all cases but this, the PPQ resistance-conferring mutations had a detrimental effect on the kinetic parameters for CQ transport. Why the H97Y would increase the affinity that PfCRT has for CQ was puzzling. However, considering that H97 is in the vicinity of F145, that substituting the latter for isoleucine reduced the affinity for the drug, and that both mutations involved aromatic side chains (H97Y introduces an aromatic side chain, while F145I eliminates one), the pieces came together. A possible explanation would be that CQ binds to $PfCRT^{Dd2}$ in a pocket that contains both H97 and F145, and that establishing an interaction with an aromatic side chain was necessary for binding. Indeed, the docking of CQ into the cavity of $PfCRT^{Dd2}$ revealed that the drug binds in a pocket defined by transmembrane domains (TM) 1, 2, 3 and 7, where hydrophobic contacts are established between the quinoline ring and F145, among other residues. The residue H97 bonded with CQ only in some of the docking poses, which could mean that upon mutagenesis the ligand finds more favourable environments in a scenario where there is Y97 and F145 simultaneously. Because the residues H97 and F145 are part of the pocket binding CQ, I evaluated whether the affinity-increasing effect of replacing H97 for Tyr (H97Y) could compensate for the affinity-decreasing effect of replacing F145 for Ile (F145I). To do so, I generated an artificial double mutant to be expressed in the *Xenopus laevis* oocyte system, carrying both the H97Y and the F145I mutations ($PfCRT^{Dd2\_H97Y\_F145I}$) (Figure 3.2.2). The double mutant had identical K_M^{CQ} than parental $PfCRT^{Dd2}$, confirming my hypothesis (Table 3.2.1). The value of the K_M^{CQ}

fell in between those of the single mutant parental isoforms (184 µM for $PfCRT^{Dd2\_H97Y}$, 240 µM for $PfCRT^{Dd2\_H97Y\_F145I}$, 370 µM for $PfCRT^{Dd2\_F145I}$). In contrast, the V_{max}^{CQ} was equal to that of the parental $PfCRT^{Dd2\_F145I}$ isoform (35 pmol/oocyte/h), which was in turn similar to the V_{max}^{CQ} found for $PfCRT^{Dd2}$ (33 pmol/oocyte/h), and much higher than that of the other single mutant $PfCRT^{Dd2\_H97Y}$ (24 pmol/oocyte/h). A possible explanation for this observation could be that, because the $PfCRT^{Dd2\_H97Y}$ isoform binds CQ more tightly (with a higher affinity), the drug does not easily guide the conformational changes necessary in the carrier for substrate translocation.

Surprisingly, the transport activity of the double mutant $PfCRT^{Dd2\_H97Y\_F145I}$ did not follow Michaelis-Menten kinetics, but instead showed a sigmoidal response that gave a reliable fit to the Hill equation, with a Hill coefficient of $H_C = 1.6 \pm 0.2$ for CQ and of $H_C = 2.0 \pm 0.3$ for PPQ transport. In enzyme kinetics, a sigmoidal response and the Hill equation are usually associated with a cooperative binding process, in which the protein can bind multiple substrate molecules at once, and in which binding of one molecule of substrate changes the affinity that the protein has for a second substrate molecule [246]. In those cases, the Hill coefficient indicate the minimum number of binding sites that the protein has for the substrate, where one has to round non-integer numbers up (in the case of $PfCRT^{Dd2\_H97Y\_F145I}$: $H_C = 1.6$ for CQ would mean at least 2 binding sites for CQ; $H_C = 2.0$ for PPQ would mean at least 2 binding sites for PPQ). Cooperativity is often observed in oligomeric protein complexes, such as hemoglobin. However, in the case of monomeric transporters, sigmoidal responses can be found when a single-existing binding site transitions between conformations with different affinities for the substrate [276, 277]. Yet, having found two separate binding sites in the cavity of PfCRT (Figure 3.2.10), substrate cooperativity cannot be immediately ruled out.

In a cellular context, the Michaelis constant value (K_M) of an enzyme/substrate complex is usually in the range of that substrate's physiological concentration [246]. In that way, the enzyme can respond quickly and efficiently to changes in the availability of the substrate, since the activity when the substrate concentration $\approx K_M$ is often in the "linear" part of the hyperbole. According to my results and others, the concentration of CQ in the parasite's DV would be in the order of 200 µM [150, 172, 175], consistent with a previous report measuring the concentration vacuolar bromoquine (an analogue of CQ that has a Br instead of a Cl substituent) at 150 ± 50 µM [127]. That would

explain why PfCRT^{Dd2} can bind and transport CQ to an extent that it confers resistance to the drug, while the highly PPQ resistance-conferring PfCRT^{Dd2_F145I} cannot. If vacuolar CQ concentration is ≈ 200 µM, then PfCRT^{Dd2} works at 43 % V_{max}^{CQ}, while PfCRT^{Dd2_F145I} does so at 35 % V_{max}^{CQ} (Table 3.2.1). When considering that both isoforms have comparable V_{max}^{CQ} values, then it becomes clear that PfCRT^{Dd2} can transport more CQ per unit of time than its mutant counterpart. A recent study has proposed a strategy in which CQ and PPQ are used together in a combination therapy, with the argument that the parasite cannot be resistant to both drugs simultaneously, and thus this would prevent further spread of resistance [244]. However, my findings on the double mutant PfCRT^{Dd2_H97Y_F145I} that it outperforms the CQ resistance-conferring PfCRT^{Dd2} in CQ transport and the PPQ resistance-conferring PfCRT^{Dd2_F145I} in PPQ transport shed light on a different scenario. As stated, if drug concentration in the DV is ≈ 200 µM, then a parasite with these two mutations would count with a transporter that can deal with both drugs at least as efficiently as isoforms associated with resistance to them. In principle, one could hypothesize that such parasite would be resistant to both CQ and PPQ. Whether that is the case, and whether a parasite with both mutations would be viable, are still questions that remain unanswered.

CQ and PPQ share the 4-chloroquinoline moiety (Figure 1.4), with PPQ consisting of two 4-chloroquinoline groups connected to each other via a di-piperazine propane bridge. Based on their structural similarities and the large size of the PPQ molecule, it has been proposed that the two drugs occupy the same or at least overlapping binding pockets in the cavity of PfCRT. Indeed, proximity-based binding assays supported such hypothesis by revealing that CQ and PPQ are competitive inhibitors of the Brazilian CQ resistance-conferring 7G8 isoform (PfCRT^{7G8}) [156]. However, my results are contradictory with those observations. Firstly, I performed the competition plot experiment, in which a protein and two of its substrates are tested to see whether the two small molecules bind at the same or at separate sites. When using either the PfCRT^{Dd2} or the PfCRT^{Dd2_F145I} isoform, the total uptake (V_{total} in Figure 3.2.5) deviated from a horizontal line, indicating that CQ and PPQ do not compete for binding to either protein. Instead, my results suggested an allosteric binding model. To further dissect how the two drugs interact for binding to PfCRT, I counted on substrate competition kinetics experiments, in which the concentration-dependence of the transport of a substrate is tested at different concentrations of a second substrate. This approach has already been used to confirm that CQ has overlapping sites with quinine (QN) and

with VP [150]. In my experiments with PfCRT^{Dd2}, it was clear that from the graphs that inhibition of CQ transport by PPQ (and of PPQ transport by CQ) was not full-type inhibition (Figure 3.2.6). The former is because the separation between consequent curves was lower at higher concentrations of inhibiting substrate, i.e. the rate of reduction of CQ (PPQ) transport activity decreased the higher the concentration of PPQ (CQ). Model discriminating information theory (Figure 3.2.6 and Figure 3.2.8) and graphical analyses (Figure 3.2.7 and Figure 3.2.9) indicated and confirmed that CQ and PPQ are instead partial noncompetitive inhibitors of PfCRT^{Dd2}- and PfCRT^{Dd2_F145I}-mediated drug transport. Partial noncompetitive inhibition occurs when the two drugs can bind to the protein simultaneously with unaltered affinity ($\alpha = 1$), yielding a ternary complex capable of completing the transport cycle, yet with a reduced rate, as indicated by $0 < \beta < 1$ (Figure 4.2.1). Whether one or the two drugs are released per conformational cycle remains unclear and needs to be clarified with further studies. Of note, various cases of noncompetitive inhibition have been described for different systems protein-substrate-inhibitor, including some involving quinoline drugs [278-280].

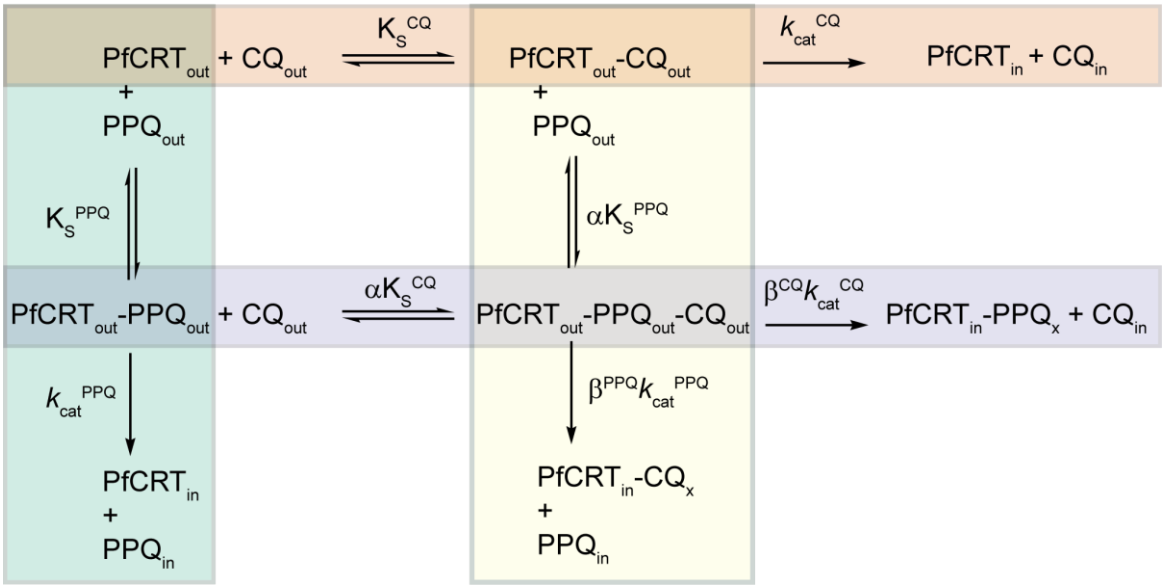

Figure 4.2.1. Proposed transport mechanism of CQ and PPQ mediated by PfCRT. The mechanism from binding of drugs outside of the oocyte (out) until drugs are released into the oocyte (in). PfCRT$_{out}$ can bind CQ$_{out}$ with dissociation constant K_S^{CQ} (red). Once bound, CQ is translocated and released inside the oocyte as CQ$_{in}$ with a rate dependent on k_{cat}^{CQ}. Similarly, PfCRT$_{out}$ can bind PPQ$_{out}$ with dissociation constant K_S^{PPQ} (green), and release it inside the oocyte as PPQ$_{in}$ with a rate constant k_{cat}^{PPQ}. Alternatively, before translocation, PfCRT$_{out}$-CQ$_{out}$ can bind PPQ$_{out}$ with a dissociation constant of αK_S^{PPQ}, forming a ternary complex PfCRT$_{out}$-CQ$_{out}$-PPQ$_{out}$ that can release PPQ inside the oocyte (PPQ$_{in}$) with a rate constant of $\beta^{PPQ} k_{cat}^{PPQ}$ (yellow).

Lastly, $PfCRT_{out}$-PPQ_{out} can bind CQ_{out} with a dissociation constant of αK_S^{CQ}, releasing CQ inside the oocyte (CQ_{in}) with a rate constant of $\beta^{CQ}k_{cat}^{CQ}$ (blue). Notably, from my experiments it is not clear whether the ternary complex transports both drugs simultaneously or if it transports one at a time, therefore the subscript "x" in the complexes $PfCRT_{in}$-PPQ_x and $PfCRT_{in}$-CQ_x.

The second most plausible model describing the interaction of either $PfCRT^{Dd2}$ or $PfCRT^{Dd2\_F145I}$ with CQ and PPQ was partial mixed inhibition (Figure 3.2.6 and Figure 3.2.8). This type is similar to partial noncompetitive inhibition, with the exception that binding of the first molecule of substrate affects the affinity for the binding of the other substrate by a factor of α. However, both in the global fit and in the graphical analyses performed, α was not different from 1 in any of the four studied cases. Likely because of this, the partial mixed inhibition model was overall less likely than the partial noncompetitive model, which is in the end a special case of the former where α =1.

The allosteric binding model was supported by docking and molecular dynamics (MD) simulations, in which either CQ or PPQ was docked into the modelled open-to-vacuole conformation of $PfCRT^{Dd2}$ (Figure 3.2.10). The protein structure was modelled by homology using the cryo-EM structure of the related $PfCRT^{7G8}$ isoform as a template and, owing to the high sequence identity between the two isoforms (98 %), a high quality model was obtained (see Annex III). In the docking simulations, most CQ poses had this drug occupying a pocket surrounded by TM 1, 2, 3 and 7, where the drug formed contacts with F145 and H97, as discussed above. In these binding modes, CQ often established a salt bridge between its diethylamino tail and E75. This highlights the importance that the mutations N75E and K76T have in giving PfCRT the property of transporting CQ [172], with the former introducing a negative charge capable of interacting with the positively charged drug, and the latter eliminating a positive charge that could otherwise cause electrostatic repulsion and exclusion of CQ from the protein's cavity. MD simulations confirmed the preference of CQ for binding to that side of $PfCRT^{Dd2}$. PPQ instead preferably occupied the opposite side of the cavity, a position that was also maintained during the MD simulations. The drug stayed in close vicinity of G353, which would explain why the G353V mutation alters the parasite's responsiveness to PPQ. In particular, G353 localizes around the middle of TM 9, and its replacement by a less flexible residue like Val is expected to translate into a structural change, which was not explored in the simulations run. Notably, the difference in affinity observed for the two drugs and $PfCRT^{Dd2}$ (Table 3.2.1) was

consistent with the different docking scores obtained for them in the docking simulations (see Annex IV).

A remarkable difference between the docking simulations and my substrate competition kinetics studies is that in the former each drug is analysed separately, while in the latter both drugs were present simultaneously in the system. To overcome that distinction, CQ and PPQ were simulated together in the cavity of $PfCRT^{Dd2}$, and MD simulations were run to let the drugs explore the transporter (Figure 3.2.11). After 1000 ns, CQ moved and stably positioned itself around H97 and E75, a path potentially explored in nature when transitioning through the transport cycle. Instead, PPQ moved to a position slightly outside of the cavity, where it formed a stable interaction with loop residues T205, E207, M305 and V369, which was key to anchoring the drug there. Simulations with both drugs together provided a molecular insight into their coexistence within the transporter and gave further support to the noncompetitive nature of the two antimalarials.

Lastly, a question remained as to why my competition plot, substrate competition kinetics, and the docking and MD simulations were not in agreement with the data by Kim *et al.* (2019) [156]. Docking CQ or PPQ to the published cryo-EM structure of $PfCRT^{7G8}$, the isoform with which Kim and colleagues proved the competitive nature of CQ and PPQ binding, revealed an isoform-specific behaviour (Figure 3.2.12 and Annex IV). While the docking of CQ to $PfCRT^{7G8}$ was mostly in agreement with that to $PfCRT^{Dd2}$, PPQ bound closer to the centre of the cavity, where it shared common space with some poses of CQ. The differences in the amino acid sequence of the transporter (I356 and R371 in $PfCRT^{7G8}$, and T356 and I371 in $PfCRT^{Dd2}$) may favour a different accommodation of PPQ in the 7G8 isoform, resulting in overlapping binding sites for CQ and PPQ. These findings were consistent with those by Kim *et al.* (2019), and lead to a hypothesis in which a noncompetitive binding model is specific to the Dd2 isoform. Thus, it seems that the substrate binding cavity of PfCRT is highly flexible and able to offer alternative solutions to particular drug challenges.

5 Outlook

This doctoral project was undertaken to further our understanding of how PfCRT mediates drug resistance in malaria, in terms of the mutations and of the post-translational modifications the protein carries.

Firstly, the cAMP-dependent protein kinase (PKA) was proposed as the protein responsible for the phosphorylation of the residue Ser33 in the cytoplasmic loop of PfCRT. Direct evidence of the enzymatic activity of PKA on the carrier must however be provided. To do that, successful recombinant expression of the kinase in a soluble, active form needs to be achieved for the *in vitro* testing of its activity in the presence of a peptide mimicking the phosphosite comprising Ser33 in PfCRT. While different strategies have been tried in this study, several possibilities remain and should be explored. Additionally, a putative role of that phosphorylation event on the natural function of PfCRT should be explored by using readily available Ser33 mutant parasite lines and fluorescently labelled dipeptides.

Secondly, this work provided an explanation to why a single amino acid substitution like H97Y, F145I, M343L or G353V changed the susceptibility pattern from CQ resistance and PPQ sensitivity to CQ sensitivity and PPQ resistance, and explored a possible evolutionary pathway that could render the parasites resistant to both drugs simultaneously. By further creating artificial mutants to be studied in the *X. laevis* oocyte system, the properties that favour binding and transport of different antimalarials by PfCRT could be disguised. Additionally, by introducing the mutations H97Y and F145I into the sequence of PfCRT of Dd2 parasites, the fitness cost and drug resistance profile of the genetically edited parasites could be studied, with the results complementing the findings obtained in this study. Furthermore, CQ resistant parasites (e.g. Dd2 strain) could be cultured in the presence of both CQ and PPQ to select for those mutants that can tolerate these antimalarials simultaneously.

Thirdly, this thesis described for the first time the binding pockets of CQ and PPQ within the cavity of $PfCRT^{Dd2}$, both with kinetic analyses and computational tools. By performing different sets of simulations, such as those employing metadynamics, the conformational pathways that start in substrate binding and lead to substrate translocation and release across the membrane could be simulated. The different

amino acids observed to participate could be mutagenized and analysed in the *X. laevis* oocyte system to confirm the findings.

Overall, this work provides strong evidence for a candidate protein kinase that phosphorylates PfCRT and contributes to a better understanding of the functioning of PfCRT. By gaining knowledge on the intricate process of drug resistance in malaria, we set the ground for designing strategies aimed at preventing the emergence and spread of resistance. Be it by designing antimalarials that will compete with CQ or PPQ for binding to PfCRT, that will prevent the conformational transition necessary for drug translocation, or that will prevent PfCRT from being post-translationally modified to a fully functional form, researchers count now with new information to help them meet the worldwide desire of malaria eradication.

6 References

1. World Health Organization. World Malaria Report 2023. Geneva, 2023.
2. Phillips MA, Burrows JN, Manyando C, van Huijsduijnen RH, Van Voorhis WC, Wells TNC. Malaria. Nature Reviews Disease Primers. 2017;3(1):17050. https://doi.org/10.1038/nrdp.2017.50. PMID: 28770814.
3. Noedl H, Se Y, Schaecher K, Smith BL, Socheat D, Fukuda MM. Evidence of Artemisinin-Resistant Malaria in Western Cambodia. New England Journal of Medicine. 2008;359(24):2619-20. https://doi.org/10.1056/NEJMc0805011. PMID: 19064625.
4. Ashley EA, Dhorda M, Fairhurst RM, Amaratunga C, Lim P, Suon S, et al. Spread of Artemisinin Resistance in Plasmodium falciparum Malaria. New England Journal of Medicine. 2014;371(5):411-23. https://doi.org/10.1056/NEJMoa1314981. PMID: 25075834.
5. Balikagala B, Fukuda N, Ikeda M, Katuro OT, Tachibana S-I, Yamauchi M, et al. Evidence of Artemisinin-Resistant Malaria in Africa. New England Journal of Medicine. 2021;385(13):1163-71. https://doi.org/10.1056/NEJMoa2101746. PMID: 34551228.
6. Ranson H, Lissenden N. Insecticide resistance in African Anopheles mosquitoes: a worsening situation that needs urgent action to maintain malaria control. Trends in parasitology. 2016;32(3):187-96. https://doi.org/10.1016/j.pt.2015.11.010. PMID: 26826784.
7. Hemingway J, Ranson H, Magill A, Kolaczinski J, Fornadel C, Gimnig J, et al. Averting a malaria disaster: will insecticide resistance derail malaria control? The Lancet. 2016;387(10029):1785-8. https://doi.org/10.1016/S0140-6736(15)00417-1. PMID: 26880124.
8. Lindsay S, Birley M. Climate change and malaria transmission. Annals of Tropical Medicine & Parasitology. 1996;90(5):573-88. https://doi.org/10.1080/00034983.1996.11813087. PMID: 9039269.
9. Eikenberry SE, Gumel AB. Mathematical modeling of climate change and malaria transmission dynamics: a historical review. Journal of mathematical biology. 2018;77:857-933. https://doi.org/10.1007/s00285-018-1229-7. PMID: 29691632.
10. Samarasekera U. Climate change and malaria: predictions becoming reality. The Lancet. 2023;402(10399):361-2. https://doi.org/10.1016/S0140-6736(23)01569-6. PMID: 37517424.
11. Simon AK, Hollander GA, McMichael A. Evolution of the immune system in humans from infancy to old age. Proc Biol Sci. 2015;282(1821):20143085. https://doi.org/10.1098/rspb.2014.3085. PMID: 26702035.
12. Mor G, Cardenas I. The Immune System in Pregnancy: A Unique Complexity. American Journal of Reproductive Immunology. 2010;63(6):425-33. https://doi.org/10.1111/j.1600-0897.2010.00836.x. PMID: 20367629.
13. Sharma L, Shukla G. Placental Malaria: A New Insight into the Pathophysiology. Front Med. 2017;4:117. https://doi.org/10.3389/fmed.2017.00117. PMID: 28791290.
14. Homer. The Illiad: Translated by Robert Fagles; 1990.

15. Hippocrates. Epidemics. Boston, Massachusetts: Loeb Classical Library; 1923.
16. Koch R. Die aetiologie der tuberkulose. Mittbeilungen aus dem Kaiserlichen Gesundbeisamte. 1884; 2, 1-88.
17. Pasteur L, Chamberland C, Joubert J. Théorie des germes et ses applications à la médecine et à la chirurgie. 1878.
18. Laveran A. The parasites of malaria. Chinese Medical Journals Publishing House Co., Ltd. 42 Dongsi Xidajie; 1895.
19. Sato S. Plasmodium-a brief introduction to the parasites causing human malaria and their basic biology. J Physiol Anthropol. 2021;40(1):1. https://doi.org/10.1186/s40101-020-00251-9. PMID: 33413683.
20. Menkin-Smith L, Winders WT. Plasmodium vivax Malaria. 2023 Jul 17. In: StatPearls [Internet]. Treasure Island (FL): StatPearls Publishing. PMID: 30855917.
21. Huber JH, Elliott M, Koepfli C, Perkins TA. The Impact of Emerging Plasmodium knowlesi on Accurate Diagnosis by Light Microscopy: A Systematic Review and Modeling Analysis. Am J Trop Med Hyg. 2023;108(1):61-8. https://doi.org/10.4269/ajtmh.21-1155. PMID: 36509046.
22. Ross RIMS. Report on a Preliminary Investigation into Malaria in the Sigur Ghat, Ootacamund. Ind Med Gaz. 1898;33(4):133-6. PMID: 29001780.
23. Pinzon-Ortiz C, Friedman J, Esko J, Sinnis P. The Binding of the Circumsporozoite Protein to Cell Surface Heparan Sulfate Proteoglycans Is Required for PlasmodiumSporozoite Attachment to Target Cells. Journal of Biological Chemistry. 2001;276(29):26784-91. https://doi.org/10.1074/jbc.M104038200. PMID: 11352923.
24. Vaughan AM, Kappe SHI. Malaria Parasite Liver Infection and Exoerythrocytic Biology. Cold Spring Harb Perspect Med. 2017;7(6). https://doi.org/10.1101/cshperspect.a025486. PMID: 28242785.
25. Prudêncio M, Rodriguez A, Mota MM. The silent path to thousands of merozoites: the Plasmodium liver stage. Nat Rev Microbiol. 2006;4(11):849-56. https://doi.org/10.1038/nrmicro1529. PMID: 17041632.
26. Aikawa M, Schwartz A, Uni S, Nussenzweig R, Hollingdale M. Ultrastructure of in vitro cultured exoerythrocytic stage of Plasmodium berghei in a hepatoma cell line. Am J Trop Med Hyg. 1984;33(5):792-9. https://doi.org/10.4269/ajtmh.1984.33.792. PMID: 6091467.
27. Meis JF, Verhave JP, Meuwissen JH, Jap PH, Princen HM, Yap SH. Fine structure of Plasmodium berghei exoerythrocytic forms in cultured primary rat hepatocytes. Cell Biol Int Rep. 1984;8(9):755-65. https://doi.org/10.1016/0309-1651(84)90114-0. PMID: 6388852.
28. Cowman AF, Crabb BS. Invasion of Red Blood Cells by Malaria Parasites. Cell. 2006;124(4):755-66. https://doi.org/10.1016/j.cell.2006.02.006. PMID: 16497586.
29. Bannister LH, Hopkins JM, Margos G, Dluzewski AR, Mitchell GH. Three-dimensional ultrastructure of the ring stage of Plasmodium falciparum: evidence for export pathways. Microsc Microanal. 2004;10(5):551-62. https://doi.org/10.1017/s1431927604040917. PMID: 15525429.

30. Maier AG, Matuschewski K, Zhang M, Rug M. Plasmodium falciparum. Trends in Parasitology. 2019;35(6):481-2. https://doi.org/10.1016/j.pt.2018.11.010. PMID: 30595467.
31. Taylor LH, Read AF. Why so few transmission stages? Reproductive restraint by malaria parasites. Parasitology Today. 1997;13(4):135-40. https://doi.org/10.1016/S0169-4758(97)89810-9. PMID: 15275099.
32. Dash M, Sachdeva S, Bansal A, Sinha A. Gametogenesis in Plasmodium: Delving Deeper to Connect the Dots. Frontiers in Cellular and Infection Microbiology. 2022;12. https://doi.org/10.3389/fcimb.2022.877907. PMID: 35782151.
33. Carter R, Nijhout MM. Control of Gamete Formation (Exflagellation) in Malaria Parasites. Science. 1977;195(4276):407-9. https://doi.org/10.1126/science.12566. PMID: 12566.
34. Arneth B, Keller C, Schaefer S. Malaria exflagellation in a human peripheral blood smear. IDCases. 2017;10:51-2. https://doi.org/10.1016/j.idcr.2017.08.010. PMID: 28924557.
35. Ukegbu CV, Christophides GK, Vlachou D. Identification of Three Novel Plasmodium Factors Involved in Ookinete to Oocyst Developmental Transition. Frontiers in Cellular and Infection Microbiology. 2021;11. https://doi.org/10.3389/fcimb.2021.634273. PMID: 33791240.
36. King JG, Hillyer JF. Infection-induced interaction between the mosquito circulatory and immune systems. PLoS Pathog. 2012;8(11):e1003058. https://doi.org/10.1371/journal.ppat.1003058. PMID: 23209421.
37. Milner DA, Jr. Malaria Pathogenesis. Cold Spring Harb Perspect Med. 2018;8(1). https://doi.org/10.1101/cshperspect.a025569. PMID: 28533315.
38. Mohandas N, An X. Malaria and human red blood cells. Med Microbiol Immunol. 2012;201(4):593-8. https://doi.org/10.1007/s00430-012-0272-z. PMID: 22965173.
39. Haldar K, Mohandas N. Malaria, erythrocytic infection, and anemia. Hematology. 2009;2009(1):87-93. https://doi.org/10.1182/asheducation-2009.1.87. PMID: 20008186.
40. Garnham PC. The role of the spleen in protozoal infections with special reference to splenectomy. Acta Trop. 1970;27(1):1-14. PMID: 4393028.
41. Engwerda CR, Beattie L, Amante FH. The importance of the spleen in malaria. Trends in Parasitology. 2005;21(2):75-80. https://doi.org/10.1016/j.pt.2004.11.008. PMID: 15664530.
42. del Portillo HA, Ferrer M, Brugat T, Martin-Jaular L, Langhorne J, Lacerda MVG. The role of the spleen in malaria. Cellular Microbiology. 2012;14(3):343-55. https://doi.org/10.1111/j.1462-5822.2011.01741.x. PMID: 22188297.
43. White NJ, Pukrittayakamee S, Hien TT, Faiz MA, Mokuolu OA, Dondorp AM. Malaria. The Lancet. 2014;383(9918):723-35. https://doi.org/10.1016/S0140-6736(13)60024-0. PMID: 23953767.
44. White NJ. Malaria parasite clearance. Malaria Journal. 2017;16(1):88. https://doi.org/10.1186/s12936-017-1731-1. PMID: 28231817.

45. Henry B, Roussel C, Carucci M, Brousse V, Ndour PA, Buffet P. The Human Spleen in Malaria: Filter or Shelter? Trends in Parasitology. 2020;36(5):435-46. https://doi.org/10.1016/j.pt.2020.03.001. PMID: 32298631.
46. Skorokhod OA, Caione L, Marrocco T, Migliardi G, Barrera V, Arese P, et al. Inhibition of erythropoiesis in malaria anemia: role of hemozoin and hemozoin-generated 4-hydroxynonenal. Blood. 2010;116(20):4328-37. https://doi.org/10.1182/blood-2010-03-272781. PMID: 20686121.
47. Panichakul T, Payuhakrit W, Panburana P, Wongborisuth C, Hongeng S, Udomsangpetch R. Suppression of erythroid development in vitro by Plasmodium vivax. Malaria Journal. 2012;11(1):173. https://doi.org/10.1186/1475-2875-11-173. PMID: 22624872.
48. Thawani N, Tam M, Bellemare M-J, Bohle DS, Olivier M, de Souza JB, et al. Plasmodium Products Contribute to Severe Malarial Anemia by Inhibiting Erythropoietin-Induced Proliferation of Erythroid Precursors. The Journal of Infectious Diseases. 2013;209(1):140-9. https://doi.org/10.1093/infdis/jit417. PMID: 23922378.
49. Luzolo AL, Ngoyi DM. Cerebral malaria. Brain Research Bulletin. 2019;145:53-8. https://doi.org/10.1016/j.brainresbull.2019.01.010. PMID: 30658131.
50. Ilunga-Ilunga F, Levêque A, Dramaix M. Influence de l'âge et du niveau de transmission sur l'expression clinique et biologique du paludisme grave de l'enfant. Archives de Pédiatrie. 2016;23(5):455-60. https://doi.org/10.1016/j.arcped.2016.01.017. PMID: 27067189.
51. Jensen AR, Adams Y, Hviid L. Cerebral Plasmodium falciparum malaria: The role of PfEMP1 in its pathogenesis and immunity, and PfEMP1-based vaccines to prevent it. Immunol Rev. 2020;293(1):230-52. https://doi.org/10.1111/imr.12807. PMID: 31562653.
52. Koshy JM, Koshy J. Clinical profile of cerebral malaria at a secondary care hospital. J Family Med Prim Care. 2014;3(1):54-7. https://doi.org/10.4103/2249-4863.130276. PMID: 24791238.
53. Gillrie MR, Lee K, Gowda DC, Davis SP, Monestier M, Cui L, et al. Plasmodium falciparum Histones Induce Endothelial Proinflammatory Response and Barrier Dysfunction. The American Journal of Pathology. 2012;180(3):1028-39. https://doi.org/10.1016/j.ajpath.2011.11.037. PMID: 22260922.
54. Lennartz F, Smith C, Craig AG, Higgins MK. Structural insights into diverse modes of ICAM-1 binding by Plasmodium falciparum-infected erythrocytes. Proceedings of the National Academy of Sciences. 2019;116(40):20124-34. https://doi.org/10.1073/pnas.1911900116. PMID: 31527263.
55. Lennartz F, Adams Y, Bengtsson A, Olsen RW, Turner L, Ndam NT, et al. Structure-Guided Identification of a Family of Dual Receptor-Binding PfEMP1 that Is Associated with Cerebral Malaria. Cell Host & Microbe. 2017;21(3):403-14. https://doi.org/10.1016/j.chom.2017.02.009. PMID: 28279348.
56. Tuikue Ndam N, Moussiliou A, Lavstsen T, Kamaliddin C, Jensen ATR, Mama A, et al. Parasites Causing Cerebral Falciparum Malaria Bind Multiple Endothelial Receptors and Express EPCR and ICAM-1-Binding PfEMP1. The Journal of Infectious

Diseases. 2017;215(12):1918-25. https://doi.org/10.1093/infdis/jix230. PMID: 28863469.
57. Ponsford MJ, Medana IM, Prapansilp P, Hien TT, Lee SJ, Dondorp AM, et al. Sequestration and Microvascular Congestion Are Associated With Coma in Human Cerebral Malaria. The Journal of Infectious Diseases. 2011;205(4):663-71. https://doi.org/10.1093/infdis/jir812. PMID: 22207648.
58. Newton C, Taylor T, Whitten R. Pathophysiology of fatal falciparum malaria in African children. The American journal of tropical medicine and hygiene. 1998;58(5):673-83. https://doi.org/10.4269/ajtmh.1998.58.673. PMID: 9598460.
59. Wang W, Qian H, Cao J. Stem cell therapy: a novel treatment option for cerebral malaria? Stem Cell Research & Therapy. 2015;6(1):141. https://doi.org/10.1186/s13287-015-0138-6. PMID: 26253514.
60. Idro R, Kakooza-Mwesige A, Asea B, Ssebyala K, Bangirana P, Opoka RO, et al. Cerebral malaria is associated with long-term mental health disorders: a cross sectional survey of a long-term cohort. Malaria Journal. 2016;15(1):184. https://doi.org/10.1186/s12936-016-1233-6. PMID: 27030124.
61. Golgi C. Sulla infezione malarica. Vincenzo Bona; 1886.
62. Chin W, Contacos PG, Coatney GR, Kimball HR. A naturally-acquired quotidian-type malaria in man transferable to monkeys. Science. 1965;149(3686):865. https://doi.org/10.1126/science.149.3686.865. PMID: 14332847.
63. Karunaweera ND, Grau GE, Gamage P, Carter R, Mendis KN. Dynamics of fever and serum levels of tumor necrosis factor are closely associated during clinical paroxysms in Plasmodium vivax malaria. Proc Natl Acad Sci U S A. 1992;89(8):3200-3. https://doi.org/10.1073/pnas.89.8.3200. PMID: 1565611.
64. Chakravorty Srabasti J, Hughes Katie R, Craig Alister G. Host response to cytoadherence in Plasmodium falciparum. Biochemical Society Transactions. 2008;36(2):221-8. https://doi.org/10.1042/bst0360221. PMID: 18363564.
65. Randall LM, Engwerda CR. TNF family members and malaria: Old observations, new insights and future directions. Experimental Parasitology. 2010;126(3):326-31. https://doi.org/10.1016/j.exppara.2010.04.016. PMID: 20433831.
66. Hsia CCW. Respiratory Function of Hemoglobin. New England Journal of Medicine. 1998;338(4):239-48. https://doi.org/10.1056/nejm199801223380407. PMID: 9435331.
67. D'Alessandro A, Dzieciatkowska M, Nemkov T, Hansen KC. Red blood cell proteomics update: is there more to discover? Blood Transfus. 2017;15(2):182-7. https://doi.org/10.2450/2017.0293-16. PMID: 28263177.
68. D'Alessandro A, Kriebardis AG, Rinalducci S, Antonelou MH, Hansen KC, Papassideri IS, et al. An update on red blood cell storage lesions, as gleaned through biochemistry and omics technologies. Transfusion. 2015;55(1):205-19. https://doi.org/10.1111/trf.12804. PMID: 25130459.
69. Counihan NA, Modak JK, de Koning-Ward TF. How Malaria Parasites Acquire Nutrients From Their Host. Frontiers in Cell and Developmental Biology. 2021;9. https://doi.org/10.3389/fcell.2021.649184. PMID: 33842474.

70. Ginsburg H, Krugliak M, Eidelman O, Cabantchik ZI. New permeability pathways induced in membranes of Plasmodium falciparum infected erythrocytes. Mol Biochem Parasitol. 1983;8(2):177-90. https://doi.org/10.1016/0166-6851(83)90008-7. PMID: 6348537.
71. Ginsburg H, Kutner S, Krugliak M, Cabantchik ZI. Characterization of permeation pathways appearing in the host membrane of Plasmodium falciparum infected red blood cells. Mol Biochem Parasitol. 1985;14(3):313-22. https://doi.org/10.1016/0166-6851(85)90059-3. PMID: 3887158.
72. Spielmann T, Gras S, Sabitzki R, Meissner M. Endocytosis in Plasmodium and Toxoplasma Parasites. Trends in Parasitology. 2020;36(6):520-32. https://doi.org/10.1016/j.pt.2020.03.010. PMID: 32340866.
73. Elsworth B, Keroack CD, Duraisingh MT. Elucidating Host Cell Uptake by Malaria Parasites. Trends in Parasitology. 2019;35(5):333-5. https://doi.org/10.1016/j.pt.2019.03.005. PMID: 31003757.
74. Elliott DA, McIntosh MT, Hosgood HD, Chen S, Zhang G, Baevova P, et al. Four distinct pathways of hemoglobin uptake in the malaria parasite Plasmodium falciparum. Proceedings of the National Academy of Sciences. 2008;105(7):2463-8. https://doi.org/10.1073/pnas.0711067105. PMID: 18263733.
75. Bakar NA, Klonis N, Hanssen E, Chan C, Tilley L. Digestive-vacuole genesis and endocytic processes in the early intraerythrocytic stages of Plasmodium falciparum. Journal of Cell Science. 2010;123(3):441-50. https://doi.org/10.1242/jcs.061499. PMID: 20067995.
76. Aikawa M, Hepler PK, Huff CG, Sprinz H. The feeding mechanism of avian malarial parasites. J Cell Biol. 1966;28(2):355-73. https://doi.org/10.1083/jcb.28.2.355. PMID: 5914696.
77. Slomianny C, Prensier G, Charet P. Ingestion of erythrocytic stroma by Plasmodium chabaudi trophozoites: ultrastructural study by serial sectioning and 3-dimensional reconstruction. Parasitology. 1985;90 (Pt 3):579-88. https://doi.org/10.1017/s0031182000055578. PMID: 4011321.
78. Milani KJ, Schneider TG, Taraschi TF. Defining the morphology and mechanism of the hemoglobin transport pathway in Plasmodium falciparum-infected erythrocytes. Eukaryot Cell. 2015;14(4):415-26. https://doi.org/10.1128/ec.00267-14. PMID: 25724884.
79. Marengo-Rowe AJ. Structure-function relations of human hemoglobins. Proc (Bayl Univ Med Cent). 2006;19(3):239-45. https://doi.org/10.1080/08998280.2006.11928171. PMID: 17252042.
80. Hill AV. The Combinations of Haemoglobin with Oxygen and with Carbon Monoxide. I. Biochemical Journal. 1913;7(5):471-80. https://doi.org/10.1042/bj0070471. PMID: 16742267.
81. Sawicki CA, Gibson QH. Quaternary conformational changes in human hemoglobin studied by laser photolysis of carboxyhemoglobin. Journal of Biological Chemistry. 1976;251(6):1533-42. https://doi.org/10.1016/S0021-9258(17)33681-5. PMID: 3499.

82. Alayash AI. βCysteine 93 in human hemoglobin: a gateway to oxidative stability in health and disease. Laboratory Investigation. 2021;101(1):4-11. https://doi.org/10.1038/s41374-020-00492-3. PMID: 32980855.
83. Francis SE, Sullivan Jr. DJ, Goldberg DE. Hemoglobin metabolism in the malaria parasite Plasmodium falciparum. Annual Review of Microbiology. 1997;51(1):97-123. https://doi.org/10.1146/annurev.micro.51.1.97. PMID: 9343345.
84. Banerjee R, Liu J, Beatty W, Pelosof L, Klemba M, Goldberg DE. Four plasmepsins are active in the Plasmodium falciparum food vacuole, including a protease with an active-site histidine. Proceedings of the National Academy of Sciences. 2002;99(2):990-5. https://doi.org/10.1073/pnas.022630099. PMID: 11782538.
85. Francis SE, Banerjee R, Goldberg DE. Biosynthesis and Maturation of the Malaria Aspartic Hemoglobinases Plasmepsins I and II. Journal of Biological Chemistry. 1997;272(23):14961-8. https://doi.org/10.1074/jbc.272.23.14961. PMID: 9169469.
86. Klemba M, Beatty W, Gluzman I, Goldberg DE. Trafficking of plasmepsin II to the food vacuole of the malaria parasite Plasmodium falciparum. Journal of Cell Biology. 2004;164(1):47-56. https://doi.org/10.1083/jcb200307147. PMID: 14709539.
87. Subramanian S, Sijwali PS, Rosenthal PJ. Falcipain Cysteine Proteases Require Bipartite Motifs for Trafficking to the Plasmodium falciparum Food Vacuole. Journal of Biological Chemistry. 2007;282(34):24961-9. https://doi.org/10.1074/jbc.M703316200. PMID: 17565983.
88. Drew ME, Banerjee R, Uffman EW, Gilbertson S, Rosenthal PJ, Goldberg DE. Plasmodium Food Vacuole Plasmepsins Are Activated by Falcipains. Journal of Biological Chemistry. 2008;283(19):12870-6. https://doi.org/10.1074/jbc.M708949200. PMID: 18308731.
89. Kapishnikov S, Weiner A, Shimoni E, Guttmann P, Schneider G, Dahan-Pasternak N, et al. Oriented nucleation of hemozoin at the digestive vacuole membrane in Plasmodium falciparum. Proceedings of the National Academy of Sciences. 2012;109(28):11188-93. https://doi.org/10.1073/pnas.1118120109. PMID: 22745164.
90. Huy NT, Shima Y, Maeda A, Men TT, Hirayama K, Hirase A, et al. Phospholipid membrane-mediated hemozoin formation: the effects of physical properties and evidence of membrane surrounding hemozoin. PLoS One. 2013;8(7):e70025. https://doi.org/10.1371/journal.pone.0070025. PMID: 23894579.
91. Nasamu AS, Polino AJ, Istvan ES, Goldberg DE. Malaria parasite plasmepsins: More than just plain old degradative pepsins. Journal of Biological Chemistry. 2020;295(25):8425-41. https://doi.org/10.1074/jbc.REV120.009309. PMID: 32366462.
92. Goldberg DE, Slater AF, Beavis R, Chait B, Cerami A, Henderson GB. Hemoglobin degradation in the human malaria pathogen Plasmodium falciparum: a catabolic pathway initiated by a specific aspartic protease. Journal of Experimental Medicine. 1991;173(4):961-9. https://doi.org/10.1084/jem.173.4.961. PMID: 2007860.
93. Francis SE, Gluzman IY, Oksman A, Knickerbocker A, Mueller R, Bryant ML, et al. Molecular characterization and inhibition of a Plasmodium falciparum aspartic

hemoglobinase. Embo j. 1994;13(2):306-17. https://doi.org/10.1002/j.1460-2075.1994.tb06263.x. PMID: 8313875.
94. Gluzman IY, Francis SE, Oksman A, Smith CE, Duffin KL, Goldberg DE. Order and specificity of the Plasmodium falciparum hemoglobin degradation pathway. The Journal of clinical investigation. 1994;93(4):1602-8. https://doi.org/10.1172/JCI117140. PMID: 8163662.
95. Francis SE, Gluzman IY, Oksman A, Banerjee D, Goldberg DE. Characterization of native falcipain, an enzyme involved in Plasmodium falciparum hemoglobin degradation. Molecular and Biochemical Parasitology. 1996;83(2):189-200. https://doi.org/10.1016/S0166-6851(96)02772-7. PMID: 9027752.
96. Subramanian S, Hardt M, Choe Y, Niles RK, Johansen EB, Legac J, et al. Hemoglobin Cleavage Site-Specificity of the Plasmodium falciparum Cysteine Proteases Falcipain-2 and Falcipain-3. PLOS ONE. 2009;4(4):e5156. https://doi.org/10.1371/journal.pone.0005156. PMID: 19357776.
97. Krugliak M, Zhang J, Ginsburg H. Intraerythrocytic Plasmodium falciparum utilizes only a fraction of the amino acids derived from the digestion of host cell cytosol for the biosynthesis of its proteins. Molecular and Biochemical Parasitology. 2002;119(2):249-56. https://doi.org/10.1016/S0166-6851(01)00427-3. PMID: 11814576.
98. Lew VL, Tiffert T, Ginsburg H. Excess hemoglobin digestion and the osmotic stability of Plasmodium falciparum-infected red blood cells. Blood. 2003;101(10):4189-94. https://doi.org/10.1182/blood-2002-08-2654. PMID: 12531811.
99. Esposito A, Tiffert T, Mauritz JMA, Schlachter S, Bannister LH, Kaminski CF, et al. FRET Imaging of Hemoglobin Concentration in Plasmodium falciparum-Infected Red Cells. PLOS ONE. 2008;3(11):e3780. https://doi.org/10.1371/journal.pone.0003780. PMID: 19023444.
100. Harteveld CL, Achour A, Arkesteijn SJG, ter Huurne J, Verschuren M, Bhagwandien-Bisoen S, et al. The hemoglobinopathies, molecular disease mechanisms and diagnostics. International Journal of Laboratory Hematology. 2022;44(S1):28-36. https://doi.org/10.1111/ijlh.13885. PMID: 36074711.
101. Taylor SM, Parobek CM, Fairhurst RM. Haemoglobinopathies and the clinical epidemiology of malaria: a systematic review and meta-analysis. The Lancet Infectious Diseases. 2012;12(6):457-68. https://doi.org/10.1016/S1473-3099(12)70055-5. PMID: 22445352.
102. Modiano D, Luoni G, Sirima BS, Simporé J, Verra F, Konaté A, et al. Haemoglobin C protects against clinical Plasmodium falciparum malaria. Nature. 2001;414(6861):305-8. https://doi.org/10.1038/35104556. PMID: 11713529.
103. Aidoo M, Terlouw DJ, Kolczak MS, McElroy PD, Ter Kuile FO, Kariuki S, et al. Protective effects of the sickle cell gene against malaria morbidity and mortality. The Lancet. 2002;359(9314):1311-2. https://doi.org/10.1016/S0140-6736(02)08273-9. PMID: 11965279.
104. Fairhurst RM, Fujioka H, Hayton K, Collins KF, Wellems TE. Aberrant development of Plasmodium falciparum in hemoglobin CC red cells: implications for

the malaria protective effect of the homozygous state. Blood. 2003;101(8):3309-15. https://doi.org/10.1182/blood-2002-10-3105. PMID: 12480691.
105. Williams TN, Mwangi TW, Wambua S, Alexander ND, Kortok M, Snow RW, et al. Sickle Cell Trait and the Risk of Plasmodium falciparum Malaria and Other Childhood Diseases. The Journal of Infectious Diseases. 2005;192(1):178-86. https://doi.org/10.1086/430744. PMID: 15942909.
106. May J, Evans JA, Timmann C, Ehmen C, Busch W, Thye T, et al. Hemoglobin Variants and Disease Manifestations in Severe Falciparum Malaria. JAMA. 2007;297(20):2220-6. https://doi.org/10.1001/jama.297.20.2220. PMID: 17519411.
107. Hedrick PW. Population genetics of malaria resistance in humans. Heredity. 2011;107(4):283-304. https://doi.org/10.1038/hdy.2011.16. PMID: 21427751.
108. Hershko C. Mechanism of Iron Toxicity. Food and Nutrition Bulletin. 2007;28(4_suppl4):S500-S509. https://doi.org/10.1177/15648265070284s403. PMID: 18297888.
109. Cadenas E. Biochemistry of oxygen toxicity. Annu Rev Biochem. 1989;58:79-110. https://doi.org/10.1146/annurev.bi.58.070189.000455. PMID: 2673022.
110. Cox FE. History of the discovery of the malaria parasites and their vectors. Parasit Vectors. 2010;3(1):5. https://doi.org/10.1186/1756-3305-3-5. PMID: 20205846.
111. Kapishnikov S, Hempelmann E, Elbaum M, Als-Nielsen J, Leiserowitz L. Malaria Pigment Crystals: The Achilles′ Heel of the Malaria Parasite. ChemMedChem. 2021;16(10):1515-32. https://doi.org/10.1002/cmdc.202000895. PMID: 33523575.
112. Fitch CD, Kanjananggulpan P. The state of ferriprotoporphyrin IX in malaria pigment. J Biol Chem. 1987;262(32):15552-5. PMID: 3119578.
113. Jani D, Nagarkatti R, Beatty W, Angel R, Slebodnick C, Andersen J, et al. HDP-a novel heme detoxification protein from the malaria parasite. PLoS Pathog. 2008;4(4):e1000053. https://doi.org/10.1371/journal.ppat.1000053. PMID: 18437218.
114. Chugh M, Sundararaman V, Kumar S, Reddy VS, Siddiqui WA, Stuart KD, et al. Protein complex directs hemoglobin-to-hemozoin formation in Plasmodium falciparum. Proc Natl Acad Sci U S A. 2013;110(14):5392-7. https://doi.org/10.1073/pnas.1218412110. PMID: 23471987.
115. Nakatani K, Ishikawa H, Aono S, Mizutani Y. Identification of essential histidine residues involved in heme binding and Hemozoin formation in heme detoxification protein from Plasmodium falciparum. Sci Rep. 2014;4:6137. https://doi.org/10.1038/srep06137. PMID: 25138161.
116. Gupta P, Mehrotra S, Sharma A, Chugh M, Pandey R, Kaushik A, et al. Exploring Heme and Hemoglobin Binding Regions of Plasmodium Heme Detoxification Protein for New Antimalarial Discovery. Journal of Medicinal Chemistry. 2017;60(20):8298-308. https://doi.org/10.1021/acs.jmedchem.7b00089.
117. Achan J, Talisuna AO, Erhart A, Yeka A, Tibenderana JK, Baliraine FN, et al. Quinine, an old anti-malarial drug in a modern world: role in the treatment of malaria. Malar J. 2011;10:144. https://doi.org/10.1186/1475-2875-10-144. PMID: 21609473.
118. Griffing SM, Gamboa D, Udhayakumar V. The history of 20th century malaria control in Peru. Malaria Journal. 2013;12(1):303. https://doi.org/10.1186/1475-2875-12-303. PMID: 24001096.

119. Simonetti O, Contini C, Martini M. The history of Gin and Tonic; the infectious disease specialist long drink. When gin and tonic was not ordered but prescribed. Infez Med. 2022;30(4):619-26. https://doi.org/10.53854/liim-3004-18. PMID: 36482962.
120. National Academies of Sciences, Engineering, and Medicine; Health and Medicine Division; Committee to Review Long-Term Health Effects of Antimalarial Drugs; Board on Population Health and Public Health Practice. Assessment of Long-Term Health Effects of Antimalarial Drugs When Used for Prophylaxis. Styka AN, Savitz DA, editors. Washington (DC): National Academies Press (US); 2020 Feb 25. https://doi.org/10.17226/25688. PMID: 32369311.
121. Maier J. A field trial of chloroquine (SN 7618) as a suppressive against malaria in the Philippines. Am J Trop Med Hyg. 1948;28(3):407-12. https://doi.org/10.4269/ajtmh.1948.s1-28.407. PMID: 18859829.
122. Nájera JA, González-Silva M, Alonso PL. Some Lessons for the Future from the Global Malaria Eradication Programme (1955–1969). PLOS Medicine. 2011;8(1):e1000412. https://doi.org/10.1371/journal.pmed.1000412. PMID: 21311585.
123. D'Alessandro U, Buttiëns H. History and importance of antimalarial drug resistance. Tropical Medicine & International Health. 2001;6(11):845-8. https://doi.org/10.1046/j.1365-3156.2001.00819.x. PMID: 11703837.
124. Sarah-Matio EM, Guillochon E, Nsango SE, Abate L, Ngou CM, Bouopda GA, et al. Genetic Diversity of Plasmodium falciparum and Distribution of Antimalarial Drug Resistance Mutations in Symptomatic and Asymptomatic Infections. Antimicrob Agents Chemother. 2022;66(8):e0018822. https://doi.org/10.1128/aac.00188-22. PMID: 35862750.
125. World Health Organisation. The work of WHO in the South-East Asia Region: Report of the Regional Director 1 August 1961-1 August 1962. WHO Regional Office for South-East Asia, 1962.
126. Chen L, Qu FY, Zhou YC. Field observations on the antimalarial piperaquine. Chin Med J. 1982;95(4):281-6. PMID: 6813038.
127. Kapishnikov S, Staalsø T, Yang Y, Lee J, Pérez-Berná AJ, Pereiro E, et al. Mode of action of quinoline antimalarial drugs in red blood cells infected by Plasmodium falciparum revealed in vivo. Proc Natl Acad Sci U S A. 2019;116(46):22946-52. https://doi.org/10.1073/pnas.1910123116. PMID: 31659055.
128. Taylor WRJ, White NJ. Antimalarial Drug Toxicity: A Review. Drug Safety. 2004;27(1):25-61. https://doi.org/10.2165/00002018-200427010-00003. PMID: 14720085.
129. Pasay CJ, Rockett R, Sekuloski S, Griffin P, Marquart L, Peatey C, et al. Piperaquine Monotherapy of Drug-Susceptible Plasmodium falciparum Infection Results in Rapid Clearance of Parasitemia but Is Followed by the Appearance of Gametocytemia. J Infect Dis. 2016;214(1):105-13. https://doi.org/10.1093/infdis/jiw128. PMID: 27056954.
130. Hanboonkunupakarn B, Pluijm RWvd, Hoglund R, Pukrittayakamee S, Winterberg M, Mukaka M, et al. Sequential Open-Label Study of the Safety, Tolerability, and Pharmacokinetic Interactions between Dihydroartemisinin-

Piperaquine and Mefloquine in Healthy Thai Adults. Antimicrobial Agents and Chemotherapy. 2019;63(8):e00060-19. https://doi.org/10.1128/aac.00060-19. PMID: 31182525.
131. Benjamin JM, Moore BR, Salman S, Page-Sharp M, Tawat S, Yadi G, et al. Population Pharmacokinetics, Tolerability, and Safety of Dihydroartemisinin-Piperaquine and Sulfadoxine-Pyrimethamine-Piperaquine in Pregnant and Nonpregnant Papua New Guinean Women. Antimicrobial Agents and Chemotherapy. 2015;59(7):4260-71. https://doi.org/10.1128/aac.00326-15. PMID: 25963981.
132. Wang J, Xu C, Wong YK, Li Y, Liao F, Jiang T, et al. Artemisinin, the Magic Drug Discovered from Traditional Chinese Medicine. Engineering. 2019;5(1):32-9. https://doi.org/10.1016/j.eng.2018.11.011.
133. Guidelines for the Treatment of Malaria. 2nd ed. Geneva: World Health Organization; 2010. PMID: 25473692.
134. Dondorp AM, Nosten F, Yi P, Das D, Phyo AP, Tarning J, et al. Artemisinin Resistance in Plasmodium falciparum Malaria. New England Journal of Medicine. 2009;361(5):455-67. https://doi.org/10.1056/NEJMoa0808859. PMID: 19641202.
135. Alker A, Lim P, Sem R, Shah N, Yi P, Mey Bouth D, et al. Pfmdr1 and in vivo resistance to artesunate-mefloquine in falciparum malaria on the Cambodian–Thai border. The American journal of tropical medicine and hygiene. 2007;76(4):641-7. PMID: 17426163.
136. Denis MB, Tsuyuoka R, Lim P, Lindegardh N, Yi P, Top SN, et al. Efficacy of artemether–lumefantrine for the treatment of uncomplicated falciparum malaria in northwest Cambodia. Tropical medicine & international health. 2006;11(12):1800-7. https://doi.org/10.1111/j.1365-3156.2006.01739.x. PMID: 17176344.
137. Meshnick SR, Taylor T, Kamchonwongpaisan S. Artemisinin and the antimalarial endoperoxides: from herbal remedy to targeted chemotherapy. Microbiological reviews. 1996;60(2):301-15. https://doi.org/10.1128/mr.60.2.301-315.1996. PMID: 8801435.
138. Posner GH, O'Neill PM. Knowledge of the proposed chemical mechanism of action and cytochrome p450 metabolism of antimalarial trioxanes like artemisinin allows rational design of new antimalarial peroxides. Accounts of chemical research. 2004;37(6):397-404. https://doi.org/10.1021/ar020227u. PMID: 15196049.
139. Kumar N, Ippel H, Weber C, Hackeng T, Mayo KH. Protein lysine-Nζ alkylation and O-phosphorylation mediated by DTT-generated reactive oxygen species. Protein Sci. 2013;22(3):327-46. https://doi.org/10.1002/pro.2214. PMID: 23315912.
140. Ying-Zi Y, Little B, Meshnick SR. Alkylation of proteins by artemisinin: effects of heme, pH, and drug structure. Biochemical pharmacology. 1994;48(3):569-73. https://doi.org/10.1016/0006-2952(94)90287-9. PMID: 8068044.
141. Meshnick SR. Artemisinin: mechanisms of action, resistance and toxicity. International journal for parasitology. 2002;32(13):1655-60. https://doi.org/10.1016/s0020-7519(02)00194-7. PMID: 12435450.
142. Denis MB, Tsuyuoka R, Poravuth Y, Narann TS, Seila S, Lim C, et al. Surveillance of the efficacy of artesunate and mefloquine combination for the treatment of uncomplicated falciparum malaria in Cambodia. Tropical Medicine & International

Health. 2006;11(9):1360-6. https://doi.org/10.1111/j.1365-3156.2006.01690.x. PMID: 16930257.
143. Efferth T, Kaina B. Toxicity of the antimalarial artemisinin and its dervatives. Critical Reviews in Toxicology. 2010;40(5):405-21. https://doi.org/10.3109/10408441003610571. PMID: 20158370.
144. Luo XD, Shen CC. The chemistry, pharmacology, and clinical applications of qinghaosu (artemisinin) and its derivatives. Med Res Rev. 1987;7(1):29-52. https://doi.org/10.1002/med.2610070103. PMID: 3550324.
145. Price R, van Vugt M, Phaipun L, Luxemburger C, Simpson J, McGready R, et al. Adverse effects in patients with acute falciparum malaria treated with artemisinin derivatives. Am J Trop Med Hyg. 1999;60(4):547-55. https://doi.org/10.4269/ajtmh.1999.60.547. PMID: 10348227.
146. Wellems TE, Walker-Jonah A, Panton LJ. Genetic mapping of the chloroquine-resistance locus on Plasmodium falciparum chromosome 7. Proceedings of the National Academy of Sciences. 1991;88(8):3382-6. https://doi.org/10.1073/pnas.88.8.3382. PMID: 1673031.
147. Fidock DA, Nomura T, Talley AK, Cooper RA, Dzekunov SM, Ferdig MT, et al. Mutations in the P. falciparum Digestive Vacuole Transmembrane Protein PfCRT and Evidence for Their Role in Chloroquine Resistance. Molecular Cell. 2000;6(4):861-71. https://doi.org/10.1016/S1097-2765(05)00077-8. PMID: 11090624.
148. Bray PG, Martin RE, Tilley L, Ward SA, Kirk K, Fidock DA. Defining the role of PfCRT in Plasmodium falciparum chloroquine resistance. Mol Microbiol. 2005;56(2):323-33. https://doi.org/10.1111/j.1365-2958.2005.04556.x. PMID: 15813727.
149. Valderramos SG, Valderramos J-C, Musset L, Purcell LA, Mercereau-Puijalon O, Legrand E, et al. Identification of a Mutant PfCRT-Mediated Chloroquine Tolerance Phenotype in Plasmodium falciparum. PLOS Pathogens. 2010;6(5):e1000887. https://doi.org/10.1371/journal.ppat.1000887. PMID: 20485514.
150. Bellanca S, Summers RL, Meyrath M, Dave A, Nash MN, Dittmer M, et al. Multiple drugs compete for transport via the Plasmodium falciparum chloroquine resistance transporter at distinct but interdependent sites. J Biol Chem. 2014;289(52):36336-51. https://doi.org/10.1074/jbc.M114.614206. PMID: 25378409.
151. Martin RE, Kirk K. The malaria parasite's chloroquine resistance transporter is a member of the drug/metabolite transporter superfamily. Mol Biol Evol. 2004;21(10):1938-49. https://doi.org/10.1093/molbev/msh205. PMID: 15240840.
152. Tran CV, Saier MH. The principal chloroquine resistance protein of Plasmodium falciparum is a member of the drug/metabolite transporter superfamily. Microbiology. 2004;150(Pt 1):1-3. https://doi.org/10.1099/mic.0.26818-0. PMID: 14702390.
153. Jack DL, Yang NM, Saier MH, Jr. The drug/metabolite transporter superfamily. Eur J Biochem. 2001;268(13):3620-39. https://doi.org/10.1046/j.1432-1327.2001.02265.x. PMID: 11432728.
154. van Klompenburg W, Nilsson I, von Heijne G, de Kruijff B. Anionic phospholipids are determinants of membrane protein topology. Embo j. 1997;16(14):4261-6. https://doi.org/10.1093/emboj/16.14.4261. PMID: 9250669.

155. Heijne G. The distribution of positively charged residues in bacterial inner membrane proteins correlates with the trans-membrane topology. Embo j. 1986;5(11):3021-7. https://doi.org/10.1002/j.1460-2075.1986.tb04601.x. PMID: 16453726.
156. Kim J, Tan YZ, Wicht KJ, Erramilli SK, Dhingra SK, Okombo J, et al. Structure and drug resistance of the Plasmodium falciparum transporter PfCRT. Nature. 2019;576(7786):315-20. https://doi.org/10.1038/s41586-019-1795-x. PMID: 31776516.
157. Coppée R, Sabbagh A, Clain J. Structural and evolutionary analyses of the Plasmodium falciparum chloroquine resistance transporter. Scientific Reports. 2020;10(1):4842. https://doi.org/10.1038/s41598-020-61181-1. PMID: 32179795.
158. Berger F, Gomez GM, Sanchez CP, Posch B, Planelles G, Sohraby F, et al. pH-dependence of the Plasmodium falciparum chloroquine resistance transporter is linked to the transport cycle. Nature Communications. 2023;14(1):4234. https://doi.org/10.1038/s41467-023-39969-2. PMID: 37454114.
159. Zhang M, Wang C, Otto TD, Oberstaller J, Liao X, Adapa SR, et al. Uncovering the essential genes of the human malaria parasite Plasmodium falciparum by saturation mutagenesis. Science. 2018;360(6388). https://doi.org/10.1126/science.aap7847. PMID: 29724925.
160. Sanchez CP, Manson EDT, Cubel SM, Mandel L, Weidt SK, Barrett MP, et al. The Knock-Down of the Chloroquine Resistance Transporter PfCRT Is Linked to Oligopeptide Handling in Plasmodium falciparum. Microbiology Spectrum. 2022;10(4):e01101-22. https://doi.org/10.1128/spectrum.01101-22. PMID: 35867395.
161. Ecker A, Lehane AM, Clain J, Fidock DA. PfCRT and its role in antimalarial drug resistance. Trends Parasitol. 2012;28(11):504-14. https://doi.org/10.1016/j.pt.2012.08.002. PMID: 23020971.
162. Sanchez CP, Dave A, Stein WD, Lanzer M. Transporters as mediators of drug resistance in Plasmodium falciparum. Int J Parasitol. 2010;40(10):1109-18. https://doi.org/10.1016/j.ijpara.2010.04.001. PMID: 20399785.
163. Shafik SH, Cobbold SA, Barkat K, Richards SN, Lancaster NS, Llinás M, et al. The natural function of the malaria parasite's chloroquine resistance transporter. Nat Commun. 2020;11(1):3922. https://doi.org/10.1038/s41467-020-17781-6. PMID: 32764664.
164. Maughan SC, Pasternak M, Cairns N, Kiddle G, Brach T, Jarvis R, et al. Plant homologs of the Plasmodium falciparum chloroquine-resistance transporter, PfCRT, are required for glutathione homeostasis and stress responses. Proceedings of the National Academy of Sciences. 2010;107(5):2331-6. https://doi.org/10.1073/pnas.0913689107. PMID: 20080670.
165. Juge N, Moriyama S, Miyaji T, Kawakami M, Iwai H, Fukui T, et al. Plasmodium falciparum chloroquine resistance transporter is a H+-coupled polyspecific nutrient and drug exporter. Proceedings of the National Academy of Sciences. 2015;112(11):3356-61. https://doi.org/10.1073/pnas.1417102112. PMID: 25733858.
166. Bakouh N, Bellanca S, Nyboer B, Moliner Cubel S, Karim Z, Sanchez CP, et al. Iron is a substrate of the Plasmodium falciparum chloroquine resistance transporter

PfCRT in Xenopus oocytes. Journal of Biological Chemistry. 2017;292(39):16109-21. https://doi.org/10.1074/jbc.M117.805200. PMID: 28768767.
167. Lehane AM, Kirk K. Chloroquine resistance-conferring mutations in pfcrt give rise to a chloroquine-associated H+ leak from the malaria parasite's digestive vacuole. Antimicrob Agents Chemother. 2008;52(12):4374-80. https://doi.org/10.1128/aac.00666-08. PMID: 18852275.
168. Walliker D, Quakyi IA, Wellems TE, McCutchan TF, Szarfman A, London WT, et al. Genetic analysis of the human malaria parasite Plasmodium falciparum. Science. 1987;236(4809):1661-6. https://doi.org/10.1126/science.3299700. PMID: 3299700.
169. Bhasin VK, Trager W. Gametocyte-forming and non-gametocyte-forming clones of Plasmodium falciparum. Am J Trop Med Hyg. 1984;33(4):534-7. https://doi.org/10.4269/ajtmh.1984.33.534. PMID: 6383092.
170. Wellems TE, Oduola AM, Fenton B, Desjardins R, Panton LJ, Rosario VEd. Chromosome size variation occurs in cloned Plasmodium falciparum on in vitro cultivation. Rev bras genét. 1988:813-25.
171. Burkot TR, Williams JL, Schneider I. Infectivity to mosquitoes of Plasmodium falciparum clones grown in vitro from the same isolate. Trans R Soc Trop Med Hyg. 1984;78(3):339-41. https://doi.org/10.1016/0035-9203(84)90114-7. PMID: 6380022.
172. Summers RL, Dave A, Dolstra TJ, Bellanca S, Marchetti RV, Nash MN, et al. Diverse mutational pathways converge on saturable chloroquine transport via the malaria parasite's chloroquine resistance transporter. Proc Natl Acad Sci U S A. 2014;111(17):E1759-67. https://doi.org/10.1073/pnas.1322965111. PMID: 24728833.
173. Wootton JC, Feng X, Ferdig MT, Cooper RA, Mu J, Baruch DI, et al. Genetic diversity and chloroquine selective sweeps in Plasmodium falciparum. Nature. 2002;418(6895):320-3. https://doi.org/10.1038/nature00813. PMID: 12124623.
174. Wellems TE, Plowe CV. Chloroquine-resistant malaria. J Infect Dis. 2001;184(6):770-6. https://doi.org/10.1086/322858. PMID: 11517439.
175. Martin RE, Marchetti RV, Cowan AI, Howitt SM, Bröer S, Kirk K. Chloroquine Transport via the Malaria Parasite's Chloroquine Resistance Transporter. Science. 2009;325(5948):1680-2. https://doi.org/10.1126/science.1175667. PMID: 19779197.
176. Lakshmanan V, Bray PG, Verdier-Pinard D, Johnson DJ, Horrocks P, Muhle RA, et al. A critical role for PfCRT K76T in Plasmodium falciparum verapamil-reversible chloroquine resistance. Embo j. 2005;24(13):2294-305. https://doi.org/10.1038/sj.emboj.7600681. PMID: 15944738.
177. Callaghan PS, Hassett MR, Roepe PD. Functional Comparison of 45 Naturally Occurring Isoforms of the Plasmodium falciparum Chloroquine Resistance Transporter (PfCRT). Biochemistry. 2015;54(32):5083-94. https://doi.org/10.1021/acs.biochem.5b00412. PMID: 26208441.
178. Okombo J, Mok S, Qahash T, Yeo T, Bath J, Orchard LM, et al. Piperaquine-resistant PfCRT mutations differentially impact drug transport, hemoglobin catabolism and parasite physiology in Plasmodium falciparum asexual blood stages. PLOS Pathogens. 2022;18(10):e1010926. https://doi.org/10.1371/journal.ppat.1010926. PMID: 36306287.

179. Ross LS, Dhingra SK, Mok S, Yeo T, Wicht KJ, Kümpornsin K, et al. Emerging Southeast Asian PfCRT mutations confer Plasmodium falciparum resistance to the first-line antimalarial piperaquine. Nat Commun. 2018;9(1):3314. https://doi.org/10.1038/s41467-018-05652-0. PMID: 30115924.
180. Dhingra SK, Small-Saunders JL, Ménard D, Fidock DA. Plasmodium falciparum resistance to piperaquine driven by PfCRT. The Lancet Infectious Diseases. 2019;19(11):1168-9. https://doi.org/10.1016/S1473-3099(19)30543-2. PMID: 31657776.
181. Dhingra SK, Redhi D, Combrinck JM, Yeo T, Okombo J, Henrich PP, et al. A Variant PfCRT Isoform Can Contribute to Plasmodium falciparum Resistance to the First-Line Partner Drug Piperaquine. mBio. 2017;8(3):10.1128/mbio.00303-17. https://doi.org/10.1128/mbio.00303-17. PMID: 28487425.
182. Wicht KJ, Small-Saunders JL, Hagenah LM, Mok S, Fidock DA. Mutant PfCRT Can Mediate Piperaquine Resistance in African Plasmodium falciparum With Reduced Fitness and Increased Susceptibility to Other Antimalarials. The Journal of Infectious Diseases. 2022;226(11):2021-9. https://doi.org/10.1093/infdis/jiac365. PMID: 36082431.
183. Reyes G, Nivillac NM, Karim MZ, Desouza L, Siu KW, Coe IR. The Equilibrative Nucleoside Transporter (ENT1) can be phosphorylated at multiple sites by PKC and PKA. Mol Membr Biol. 2011;28(6):412-26. https://doi.org/10.3109/09687688.2011.604861. PMID: 21809900.
184. Moritz AE, Foster JD, Gorentla BK, Mazei-Robison MS, Yang JW, Sitte HH, et al. Phosphorylation of dopamine transporter serine 7 modulates cocaine analog binding. J Biol Chem. 2013;288(1):20-32. https://doi.org/10.1074/jbc.M112.407874. PMID: 23161550.
185. Zhang L, Yu Z, Xu Y, Yu M, Ren Y, Zhang S, et al. Regulation of the stability and ABA import activity of NRT1.2/NPF4.6 by CEPR2-mediated phosphorylation in Arabidopsis. Mol Plant. 2021;14(4):633-46. https://doi.org/10.1016/j.molp.2021.01.009. PMID: 33453414.
186. Solyakov L, Halbert J, Alam MM, Semblat J-P, Dorin-Semblat D, Reininger L, et al. Global kinomic and phospho-proteomic analyses of the human malaria parasite Plasmodium falciparum. Nature Communications. 2011;2(1):565. https://doi.org/10.1038/ncomms1558. PMID: 22127061.
187. Sanchez CP, Moliner Cubel S, Nyboer B, Jankowska-Döllken M, Schaeffer-Reiss C, Ayoub D, et al. Phosphomimetic substitution at Ser-33 of the chloroquine resistance transporter PfCRT reconstitutes drug responses in Plasmodium falciparum. J Biol Chem. 2019;294(34):12766-78. https://doi.org/10.1074/jbc.RA119.009464. PMID: 31285265.
188. Kuhn Y, Sanchez CP, Ayoub D, Saridaki T, Van Dorsselaer A, Lanzer M. Trafficking of the Phosphoprotein PfCRT to the Digestive Vacuolar Membrane in Plasmodium falciparum. Traffic. 2010;11(2):236-49. https://doi.org/10.1111/j.1600-0854.2009.01018.x. PMID: 20015114.

189. Ward P, Equinet L, Packer J, Doerig C. Protein kinases of the human malaria parasite Plasmodium falciparum: the kinome of a divergent eukaryote. BMC Genomics. 2004;5(1):79. https://doi.org/10.1186/1471-2164-5-79. PMID: 15479470.
190. Talevich E, Tobin AB, Kannan N, Doerig C. An evolutionary perspective on the kinome of malaria parasites. Philos Trans R Soc Lond B Biol Sci. 2012;367(1602):2607-18. https://doi.org/10.1098/rstb.2012.0014. PMID: 22889911.
191. Doerig C, Billker O, Haystead T, Sharma P, Tobin AB, Waters NC. Protein kinases of malaria parasites: an update. Trends in Parasitology. 2008;24(12):570-7. https://doi.org/10.1016/j.pt.2008.08.007. PMID: 18845480.
192. Adderley J, Doerig C. Comparative analysis of the kinomes of Plasmodium falciparum, Plasmodium vivax and their host Homo sapiens. BMC Genomics. 2022;23(1):237. https://doi.org/10.1186/s12864-022-08457-0. PMID: 35346035.
193. Duraisingh MT, Cowman AF. Contribution of the pfmdr1 gene to antimalarial drug-resistance. Acta Trop. 2005;94(3):181-90. https://doi.org/10.1016/j.actatropica.2005.04.008. PMID: 15876420.
194. Rohrbach, P., Sanchez, C. P., Hayton, K., Friedrich, O., Patel, J., Sidhu, A. B. S., Fergid, M. T., Fidock, D. A., Lanzer, M. (2006). Genetic linkage of pfmdr1 with food vacuolar solute import in Plasmodium falciparum. The EMBO journal, 25(13), 3000-3011. https://doi.org/10.1038/sj.emboj.7601203. PMID: 16794577.
195. Sanchez CP, Rotmann A, Stein WD, Lanzer M. Polymorphisms within PfMDR1 alter the substrate specificity for anti-malarial drugs in Plasmodium falciparum. Mol Microbiol. 2008 Nov;70(4):786-98. https://doi.org/10.1111/j.1365-2958.2008.06413.x. PMID: 18713316.
196. Shafik SH, Richards SN, Corry B, Martin RE. Mechanistic basis for multidrug resistance and collateral drug sensitivity conferred to the malaria parasite by polymorphisms in PfMDR1 and PfCRT. PLoS Biol. 2022;20(5):e3001616. https://doi.org/10.1371/journal.pbio.3001616. PMID: 35507548.
197. Witkowski B, Duru V, Khim N, Ross LS, Saintpierre B, Beghain J, et al. A surrogate marker of piperaquine-resistant Plasmodium falciparum malaria: a phenotype-genotype association study. Lancet Infect Dis. 2017;17(2):174-83. https://doi.org/10.1016/s1473-3099(16)30415-7. PMID: 27818097.
198. Leroy D, Macintyre F, Adoke Y, Ouoba S, Barry A, Mombo-Ngoma G, et al. African isolates show a high proportion of multiple copies of the Plasmodium falciparum plasmepsin-2 gene, a piperaquine resistance marker. Malaria Journal. 2019;18(1):126. https://doi.org/10.1186/s12936-019-2756-4. PMID: 30967148.
199. Kane J, Li X, Kumar S, Button-Simons KA, Brenneman KMV, Dahlhoff H, et al. A Plasmodium falciparum genetic cross reveals the contributions of pfcrt and plasmepsin II/III to piperaquine drug resistance. bioRxiv. 2023:2023.06.06.543862. https://doi.org/10.1101/2023.06.06.543862. PMID: 37745488.
200. Goel N, Dhiman K, Kalidas N, Mukhopadhyay A, Ashish F, Bhattacharjee S. Plasmodium falciparum Kelch13 and its artemisinin-resistant mutants assemble as hexamers in solution: a SAXS data-driven modelling study. Febs j. 2022;289(16):4935-62. https://doi.org/10.1111/febs.16378. PMID: 35092154.

201. Birnbaum J, Scharf S, Schmidt S, Jonscher E, Hoeijmakers WAM, Flemming S, et al. A Kelch13-defined endocytosis pathway mediates artemisinin resistance in malaria parasites. Science. 2020;367(6473):51-9. https://doi.org/10.1126/science.aax4735. PMID: 31896710.
202. Barry AE, Schultz L, Buckee CO, Reeder JC. Contrasting population structures of the genes encoding ten leading vaccine-candidate antigens of the human malaria parasite, Plasmodium falciparum. PLoS One. 2009;4(12):e8497. https://doi.org/10.1371/journal.pone.0008497. PMID: 20041125.
203. Neafsey DE, Juraska M, Bedford T, Benkeser D, Valim C, Griggs A, et al. Genetic Diversity and Protective Efficacy of the RTS,S/AS01 Malaria Vaccine. N Engl J Med. 2015;373(21):2025-37. https://doi.org/10.1056/NEJMoa1505819. PMID: 26488565.
204. Stanisic DI, Good MF. Malaria Vaccines: Progress to Date. BioDrugs. 2023;37(6):737-56. https://doi.org/10.1007/s40259-023-00623-4. PMID: 37728713.
205. Payne RO, Milne KH, Elias SC, Edwards NJ, Douglas AD, Brown RE, et al. Demonstration of the Blood-Stage Plasmodium falciparum Controlled Human Malaria Infection Model to Assess Efficacy of the P. falciparum Apical Membrane Antigen 1 Vaccine, FMP2.1/AS01. J Infect Dis. 2016;213(11):1743-51. https://doi.org/10.1093/infdis/jiw039. PMID: 26908756.
206. Sirima SB, Cousens S, Druilhe P. Protection against malaria by MSP3 candidate vaccine. N Engl J Med. 2011;365(11):1062-4. https://doi.org/10.1056/NEJMc1100670. PMID: 21916656.
207. World Health Organisation. Malaria vaccine: WHO position paper. March 2022 - Monthly report on cases of dracunculiasis, January 2022. Weekly Epidemiological Record. 2022;97(09):60-78. https://www.who.int/publications/i/item/who-wer9709-61%E2%80%9380.
208. Datoo MS, Dicko A, Tinto H, Ouédraogo J-B, Hamaluba M, Olotu A, et al. Safety and efficacy of malaria vaccine candidate R21/Matrix-M in African children: a multicentre, double-blind, randomised, phase 3 trial. The Lancet. 2024;403(10426):533-44. https://doi.org/10.1016/S0140-6736(23)02511-4. PMID: 38310910.
209. Mordmüller B, Sulyok Z, Sulyok M, Molnar Z, Lalremruata A, Calle CL, et al. A PfSPZ vaccine immunization regimen equally protective against homologous and heterologous controlled human malaria infection. NPJ Vaccines. 2022;7(1):100. https://doi.org/10.1038/s41541-022-00510-z. PMID: 35999221.
210. Jongo SA, Church LWP, Nchama V, Hamad A, Chuquiyauri R, Kassim KR, et al. Multi-Dose Priming Regimens of PfSPZ Vaccine: Safety and Efficacy against Controlled Human Malaria Infection in Equatoguinean Adults. Am J Trop Med Hyg. 2022;106(4):1215-26. https://doi.org/10.4269/ajtmh.21-0942. PMID: 35130487.
211. Rosenkranz M, Fürle K, Hibbert J, Ulmer A, Ali A, Giese T, et al. Multifunctional IgG/IgM antibodies and cellular cytotoxicity are elicited by the full-length MSP1 SumayaVac-1 malaria vaccine. NPJ Vaccines. 2023;8(1):112. https://doi.org/10.1038/s41541-023-00701-2. PMID: 37558673.

212. Hooft van Huijsduijnen R, Wells TN. The antimalarial pipeline. Curr Opin Pharmacol. 2018;42:1-6. https://doi.org/10.1016/j.coph.2018.05.006. PMID: 29860174.
213. Doherty JP, Lindeman R, Trent RJ, Graham MW, Woodcock DM. Escherichia coli host strains SURE and SRB fail to preserve a palindrome cloned in lambda phage: improved alternate host strains. Gene. 1993;124(1):29-35. https://doi.org/10.1016/0378-1119(93)90758-u. PMID: 8440479.
214. Scholz J BH, Strasser C, Suppmann S. A new method to customize protein expression vectors for fast, efficient and background free parallel cloning. BMC Biotechnol. 2013;13(12). https://doi.org/10.1186/1472-6750-13-12. PMID: 23410102.
215. Trager W, Jensen JB. Human malaria parasites in continuous culture. Science. 1976;193(4254):673-5. https://doi.org/10.1126/science.781840. PMID: 781840.
216. Lambros C, Vanderberg JP. Synchronization of Plasmodium falciparum erythrocytic stages in culture. J Parasitol. 1979;65(3):418-20. PMID: 383936.
217. Reinecke M, Ruprecht B, Poser S, Wiechmann S, Wilhelm M, Heinzlmeir S, et al. Chemoproteomic Selectivity Profiling of PIKK and PI3K Kinase Inhibitors. ACS Chemical Biology. 2019;14(4):655-64. https://doi.org/10.1021/acschembio.8b01020. PMID: 30901187.
218. Suwal S, Pflum MK. Phosphorylation-dependent kinase-substrate cross-linking. Angew Chem Int Ed Engl. 2010;49(9):1627-30. https://doi.org/10.1002/anie.200905244. PMID: 20108289.
219. Beltman RJ, Pflum MKH. Kinase-Catalyzed Crosslinking and Immunoprecipitation (K-CLIP) to Explore Kinase-Substrate Pairs. Curr Protoc. 2022;2(9):e539. https://doi.org/10.1002/cpz1.539. PMID: 36135312.
220. Dedigama-Arachchige PM, Pflum MK. K-CLASP: A Tool to Identify Phosphosite Specific Kinases and Interacting Proteins. ACS Chem Biol. 2016;11(12):3251-5. https://doi.org/10.1021/acschembio.6b00289. PMID: 27726338.
221. Ho SN, Hunt HD, Horton RM, Pullen JK, Pease LR. Site-directed mutagenesis by overlap extension using the polymerase chain reaction. Gene. 1989;77(1):51-9. https://doi.org/10.1016/0378-1119(89)90358-2. PMID: 2744487.
222. Sanger F, Nicklen S, Coulson AR. DNA sequencing with chain-terminating inhibitors. Proc Natl Acad Sci U S A. 1977;74(12):5463-7. https://doi.org/10.1073/pnas.74.12.5463. PMID: 271968.
223. Gomez GM, D'Arrigo G, Sanchez CP, Berger F, Wade RC, Lanzer M. PfCRT mutations conferring piperaquine resistance in falciparum malaria shape the kinetics of quinoline drug binding and transport. PLoS Pathog. 2023;19(6):e1011436. https://doi.org/10.1371/journal.ppat.1011436. PMID: 37285379.
224. Bradford MM. A rapid and sensitive method for the quantitation of microgram quantities of protein utilizing the principle of protein-dye binding. Anal Biochem. 1976;72:248-54. https://doi.org/10.1006/abio.1976.9999. PMID: 942051.
225. Waterhouse A, Bertoni M, Bienert S, Studer G, Tauriello G, Gumienny R, et al. SWISS-MODEL: homology modelling of protein structures and complexes. Nucleic Acids Research. 2018;46(W1):W296-W303. https://doi.org/10.1093/nar/gky427. PMID: 29788355.

226. Madhavi Sastry G, Adzhigirey M, Day T, Annabhimoju R, Sherman W. Protein and ligand preparation: parameters, protocols, and influence on virtual screening enrichments. Journal of Computer-Aided Molecular Design. 2013;27(3):221-34. https://doi.org/10.1007/s10822-013-9644-8. PMID: 23579614.
227. Søndergaard CR, Olsson MHM, Rostkowski M, Jensen JH. Improved Treatment of Ligands and Coupling Effects in Empirical Calculation and Rationalization of pKa Values. Journal of Chemical Theory and Computation. 2011;7(7):2284-95. https://doi.org/10.1021/ct200133y. PMID: 26606496.
228. Shelley JC, Cholleti A, Frye LL, Greenwood JR, Timlin MR, Uchimaya M. Epik: a software program for pKaprediction and protonation state generation for drug-like molecules. Journal of Computer-Aided Molecular Design. 2007;21(12):681-91. https://doi.org/10.1007/s10822-007-9133-z. PMID: 17899391.
229. Sherman W, Beard HS, Farid R. Use of an Induced Fit Receptor Structure in Virtual Screening. Chemical Biology & Drug Design. 2006;67(1):83-4. https://doi.org/10.1111/j.1747-0285.2005.00327.x. PMID: 16492153.
230. Jo S, Kim T, Iyer VG, Im W. CHARMM-GUI: a web-based graphical user interface for CHARMM. J Comput Chem. 2008;29(11):1859-65. https://doi.org/10.1002/jcc.20945. PMID: 18351591.
231. Dickson CJ, Madej BD, Skjevik AA, Betz RM, Teigen K, Gould IR, et al. Lipid14: The Amber Lipid Force Field. J Chem Theory Comput. 2014;10(2):865-79. https://doi.org/10.1021/ct4010307. PMID: 24803855.
232. Jorgensen WL, Chandrasekhar J, Madura JD, Impey RW, Klein ML. Comparison of simple potential functions for simulating liquid water. The Journal of Chemical Physics. 1983;79(2):926-35. https://doi.org/10.1063/1.445869.
233. Wang J, Wolf RM, Caldwell JW, Kollman PA, Case DA. Development and testing of a general amber force field. Journal of Computational Chemistry. 2004;25(9):1157-74. https://doi.org/10.1002/jcc.20035. PMID: 15116359.
234. Jakalian A, Jack DB, Bayly CI. Fast, efficient generation of high-quality atomic charges. AM1-BCC model: II. Parameterization and validation. J Comput Chem. 2002;23(16):1623-41. https://doi.org/10.1002/jcc.10128. PMID: 12395429.
235. Amber Case D, Babin V, Berryman J, Betz R, Cai Q, Cerutti D, et al. AMBER 14. University of California, San Francisco, CA. 2014.
236. Davies H, Belda H, Broncel M, Ye X, Bisson C, Introini V, et al. An exported kinase family mediates species-specific erythrocyte remodelling and virulence in human malaria. Nat Microbiol. 2020;5(6):848-63. https://doi.org/10.1038/s41564-020-0702-4. PMID: 32284562.
237. Wurtz N, Pastorino B, Almeras L, Briolant S, Villard C, Parzy D. Expression and biochemical characterization of the Plasmodium falciparum protein kinase A catalytic subunit. Parasitol Res. 2009;104(6):1299-305. https://doi.org/10.1007/s00436-008-1327-3. PMID: 19159956.
238. Gatton ML, Martin LB, Cheng Q. Evolution of resistance to sulfadoxine-pyrimethamine in Plasmodium falciparum. Antimicrob Agents Chemother. 2004;48(6):2116-23. https://doi.org/10.1128/aac.48.6.2116-2123.2004. PMID: 15155209.

239. Kalra SP, Naithani N, Mehta SR, Kumar R. Resistant Malaria : Current Concepts and Therapeutic Strategies. Med J Armed Forces India. 2002;58(3):228-33. https://doi.org/10.1016/s0377-1237(02)80136-8. PMID: 27407388.
240. Davis TM, Karunajeewa HA, Ilett KF. Artemisinin-based combination therapies for uncomplicated malaria. Medical Journal of Australia. 2005;182(4):181-5. https://doi.org/10.5694/j.1326-5377.2005.tb06650.x. PMID: 15720175.
241. Vries PJd, Bich NN, Thien HV, Hung LN, Anh TK, Kager PA, et al. Combinations of Artemisinin and Quinine for Uncomplicated Falciparum Malaria: Efficacy and Pharmacodynamics. Antimicrobial Agents and Chemotherapy. 2000;44(5):1302-8. https://doi.org/10.1128/aac.44.5.1302-1308.2000. PMID: 10770766.
242. Duru V, Khim N, Leang R, Kim S, Domergue A, Kloeung N, et al. Plasmodium falciparum dihydroartemisinin-piperaquine failures in Cambodia are associated with mutant K13 parasites presenting high survival rates in novel piperaquine in vitro assays: retrospective and prospective investigations. BMC Med. 2015;13:305. https://doi.org/10.1186/s12916-015-0539-5. PMID: 26695060.
243. Agrawal S, Moser KA, Morton L, Cummings MP, Parihar A, Dwivedi A, et al. Association of a Novel Mutation in the Plasmodium falciparum Chloroquine Resistance Transporter With Decreased Piperaquine Sensitivity. The Journal of Infectious Diseases. 2017;216(4):468-76. https://doi.org/10.1093/infdis/jix334. PMID: 28931241.
244. Small-Saunders JL, Hagenah LM, Wicht KJ, Dhingra SK, Deni I, Kim J, et al. Evidence for the early emergence of piperaquine-resistant Plasmodium falciparum malaria and modeling strategies to mitigate resistance. PLOS Pathogens. 2022;18(2):e1010278. https://doi.org/10.1371/journal.ppat.1010278. PMID: 35130315.
245. Martin SK, Ayo MJO, Milhous WK. Reversal of Chloroquine Resistance in Plasmodium falciparum by Verapamil. Science. 1987;235(4791):899-901. https://doi.org/10.1126/science.3544220. PMID: 3544220.
246. Segel I. Enzyme Kinetics - Behavior and analysis of rapid equilibrium and steady-state enyme systems: Wiley; 1993.
247. Chevillard C, Cárdenas ML, Cornish-Bowden A. The competition plot: a simple test of whether two reactions occur at the same active site. Biochem J. 1993;289 (Pt 2)(Pt 2):599-604. https://doi.org/10.1042/bj2890599. PMID: 8424801.
248. Bozdogan H. Model selection and Akaike's Information Criterion (AIC): The general theory and its analytical extensions. Psychometrika. 1987;52(3):345-70. https://doi.org/10.1007/BF02294361.
249. Whiteley CG. Enzyme kinetics: partial and complete non-competitive inhibition. Biochemical Education. 1999;27(1):15-8. https://doi.org/10.1016/S0307-4412(98)00265-9. PMID: 10878310.
250. Cornish-Bowden A. Detection of Errors of Interpretation in Experiments in Enzyme Kinetics. Methods. 2001;24(2):181-90. https://doi.org/10.1006/meth.2001.1179. PMID: 11384193.
251. Xue L, Wang WH, Iliuk A, Hu L, Galan JA, Yu S, et al. Sensitive kinase assay linked with phosphoproteomics for identifying direct kinase substrates. Proc Natl Acad

Sci U S A. 2012;109(15):5615-20. https://doi.org/10.1073/pnas.1119418109. PMID: 22451900.
252. Cohen P, Knebel A. KESTREL: a powerful method for identifying the physiological substrates of protein kinases. Biochem J. 2006;393(Pt 1):1-6. https://doi.org/10.1042/bj20051545. PMID: 16336195.
253. Khati M, Pillay TS. Phosphotyrosine phosphoepitopes can be rapidly analyzed by coexpression of a tyrosine kinase in bacteria with a T7 bacteriophage display library. Anal Biochem. 2004;325(1):164-7. https://doi.org/10.1016/j.ab.2003.09.042. PMID: 14715298.
254. Ma H, Li G, Su Z. KSP: an integrated method for predicting catalyzing kinases of phosphorylation sites in proteins. BMC Genomics. 2020;21(1):537. https://doi.org/10.1186/s12864-020-06895-2. PMID: 32753030.
255. Chen M, Zhang W, Gou Y, Xu D, Wei Y, Liu D, et al. GPS 6.0: an updated server for prediction of kinase-specific phosphorylation sites in proteins. Nucleic Acids Research. 2023;51(W1):W243-W50. https://doi.org/10.1093/nar/gkad383. PMID: 37158278.
256. Saitoh M, Ishikawa T, Matsushima S, Naka M, Hidaka H. Selective inhibition of catalytic activity of smooth muscle myosin light chain kinase. Journal of Biological Chemistry. 1987;262(16):7796-801. https://doi.org/10.1016/S0021-9258(18)47638-7. PMID: 3108259.
257. Bennett V. H-89. In: Enna S.J., Bylund D.B., editors. xPharm: The Comprehensive Pharmacology Reference. Elsevier; New York: 2007. p. 1-2.
258. Mogwera KSP, Chibale K, Arendse LB. Developing kinase inhibitors for malaria: an opportunity or liability? Trends in Parasitology. 2023;39(9):720-31. https://doi.org/10.1016/j.pt.2023.06.001. PMID: 37385921.
259. Dorin-Semblat D, Demarta-Gatsi C, Hamelin R, Armand F, Carvalho TG, Moniatte M, et al. Malaria Parasite-Infected Erythrocytes Secrete PfCK1, the Plasmodium Homologue of the Pleiotropic Protein Kinase Casein Kinase 1. PLOS ONE. 2015;10(12):e0139591. https://doi.org/10.1371/journal.pone.0139591. PMID: 26629826.
260. Giamas G, Hirner H, Shoshiashvili L, Grothey A, Gessert S, Kühl M, et al. Phosphorylation of CK1delta: identification of Ser370 as the major phosphorylation site targeted by PKA in vitro and in vivo. Biochem J. 2007;406(3):389-98. https://doi.org/10.1042/bj20070091. PMID: 17594292.
261. Li J, Cox LS. Isolation and characterisation of a cAMP-dependent protein kinase catalytic subunit gene from Plasmodium falciparum. Mol Biochem Parasitol. 2000;109(2):157-63. https://doi.org/10.1016/s0166-6851(00)00242-5. PMID: 10960174.
262. Baker DA, Drought LG, Flueck C, Nofal SD, Patel A, Penzo M, et al. Cyclic nucleotide signalling in malaria parasites. Open Biol. 2017;7(12). https://doi.org/10.1098/rsob.170213. PMID: 29263246.
263. Leykauf K, Treeck M, Gilson PR, Nebl T, Braulke T, Cowman AF, et al. Protein kinase a dependent phosphorylation of apical membrane antigen 1 plays an important

role in erythrocyte invasion by the malaria parasite. PLoS Pathog. 2010;6(6):e1000941. https://doi.org/10.1371/journal.ppat.1000941. PMID: 20532217.
264. Patel A, Perrin AJ, Flynn HR, Bisson C, Withers-Martinez C, Treeck M, et al. Cyclic AMP signalling controls key components of malaria parasite host cell invasion machinery. PLOS Biology. 2019;17(5):e3000264. https://doi.org/10.1371/journal.pbio.3000264. PMID: 31075098.
265. Wilde ML, Triglia T, Marapana D, Thompson JK, Kouzmitchev AA, Bullen HE, et al. Protein Kinase A Is Essential for Invasion of Plasmodium falciparum into Human Erythrocytes. mBio. 2019;10(5). https://doi.org/10.1128/mBio.01972-19. PMID: 31594816.
266. Flueck C, Drought LG, Jones A, Patel A, Perrin AJ, Walker EM, et al. Phosphodiesterase beta is the master regulator of cAMP signalling during malaria parasite invasion. PLoS Biol. 2019;17(2):e3000154. https://doi.org/10.1371/journal.pbio.3000154. PMID: 30794532.
267. Merckx A, Nivez MP, Bouyer G, Alano P, Langsley G, Deitsch K, et al. Plasmodium falciparum regulatory subunit of cAMP-dependent PKA and anion channel conductance. PLoS Pathog. 2008;4(2):e19. https://doi.org/10.1371/journal.ppat.0040019. PMID: 18248092.
268. Bouyer G, Barbieri D, Dupuy F, Marteau A, Sissoko A, N'Dri ME, et al. Plasmodium falciparum sexual parasites regulate infected erythrocyte permeability. Commun Biol. 2020;3(1):726. https://doi.org/10.1038/s42003-020-01454-7. PMID: 33262483.
269. Wurtz N, Chapus C, Desplans J, Parzy D. cAMP-dependent protein kinase from Plasmodium falciparum: an update. Parasitology. 2011;138(1):1-25. https://doi.org/10.1017/s003118201000096x. PMID: 20663247.
270. Hanks SK, Quinn AM, Hunter T. The Protein Kinase Family: Conserved Features and Deduced Phylogeny of the Catalytic Domains. Science. 1988;241(4861):42-52. https://doi.org/10.1126/science.3291115. PMID: 3291115.
271. Asih PBS, Rozi IE, Dewayanti FK, Wangsamuda S, Zulfah S, Robaha M, et al. Efficacy and safety of dihydroartemisinin-piperaquine for the treatment of uncomplicated Plasmodium falciparum and Plasmodium vivax malaria in Papua and Sumatra, Indonesia. Malar J. 2022;21(1):95. https://doi.org/10.1186/s12936-022-04101-0. PMID: 35305658.
272. Kabanywanyi AM, Baiden R, Ali AM, Mahende MK, Ogutu BR, Oduro A, et al. Multi-Country Evaluation of Safety of Dihydroartemisinin/Piperaquine Post-Licensure in African Public Hospitals with Electrocardiograms. PLoS One. 2016;11(10):e0164851. https://doi.org/10.1371/journal.pone.0164851. PMID: 27764178.
273. Nambozi M, Van Geertruyden J-P, Hachizovu S, Chaponda M, Mukwamataba D, Mulenga M, et al. Safety and efficacy of dihydroartemisinin-piperaquine versus artemether-lumefantrine in the treatment of uncomplicated Plasmodium falciparum malaria in Zambian children. Malaria Journal. 2011;10(1):50. https://doi.org/10.1186/1475-2875-10-50. PMID: 21352609.

274. Vivian D, Polli JE. Mechanistic interpretation of conventional Michaelis-Menten parameters in a transporter system. Eur J Pharm Sci. 2014;64:44-52. https://doi.org/10.1016/j.ejps.2014.08.007. PMID: 25169756.
275. Adovelande J, Delèze J, Schrével J. Synergy between two calcium channel blockers, verapamil and fantofarone (SR33557), in reversing chloroquine resistance in Plasmodium falciparum. Biochem Pharmacol. 1998;55(4):433-40. https://doi.org/10.1016/s0006-2952(97)00482-6. PMID: 9514077.
276. Cárdenas ML. Understanding mechanisms of enzyme co-operativity: The importance of not being at equilibrium. Perspectives in Science. 2015;4:10-6. https://doi.org/10.1016/j.pisc.2014.12.003. PMID: 23468286.
277. Porter CM, Miller BG. Cooperativity in monomeric enzymes with single ligand-binding sites. Bioorganic Chemistry. 2012;43:44-50. https://doi.org/10.1016/j.bioorg.2011.11.001. PMID: 22137502.
278. Capodagli GC, Sedhom WG, Jackson M, Ahrendt KA, Pegan SD. A Noncompetitive Inhibitor for Mycobacterium tuberculosis's Class IIa Fructose 1,6-Bisphosphate Aldolase. Biochemistry. 2014;53(1):202-13. https://doi.org/10.1021/bi401022b. PMID: 24325645.
279. Santos RdLA, Bai L, Singh PK, Murakami N, Fan H, Zhan W, et al. Structure of human immunoproteasome with a reversible and noncompetitive inhibitor that selectively inhibits activated lymphocytes. Nature Communications. 2017;8(1):1692. https://doi.org/10.1038/s41467-017-01760-5. PMID: 29167449.
280. Yelshanskaya Maria V, Singh Appu K, Sampson Jared M, Narangoda C, Kurnikova M, Sobolevsky Alexander I. Structural Bases of Noncompetitive Inhibition of AMPA-Subtype Ionotropic Glutamate Receptors by Antiepileptic Drugs. Neuron. 2016;91(6):1305-15. https://doi.org/10.1016/j.neuron.2016.08.012. PMID: 27618672.

Annex I

Small-scale expression trials of PfPKA in insect cell lines Sf21 and Sf9 (data by Yexin Xie and Dr. Kim Remans from the European Molecular Biology Laboratory (EMBL) in Heidelberg).

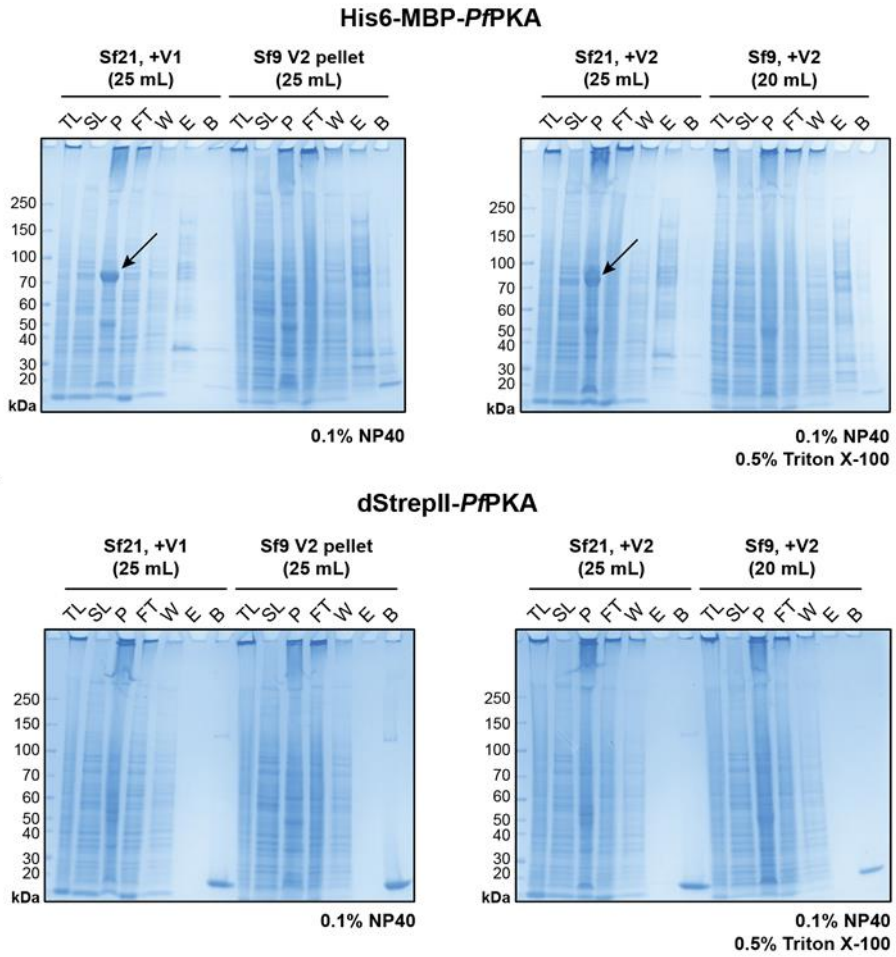

Figure A1. SDS-PAGE of cellular lysates prepared from insect cells. The expression of PfPKAc was tried in small cultures (20-25 mL) of Sf21 or Sf9 cells, transfected with viruses (V1 or V2) prepared with the pCoofy29-PfPKA (His6-MBP-PfPKA) or the pCoofy51-PfPKA (dStrepII-PfPKA) plasmids. Cells were harvested and lysed using either 0.1 % NP40 (*left gels*) or 0.1 % NP40 + 0.5 % Triton X-100 (*right gels*). Different fractions of the purification process are analysed in parallel: TL, total lysate; SL, soluble lysate fraction; P, pellet (insoluble fraction); FT, flow-through; W, washing; E, elution; B, beads. The protein band, indicated with an arrow, shows that PKA was only expressed in Sf21 cells, but in an insoluble form. The data was produced by Yexin Xie and Dr. Kim Remans.

Small-scale expression trials of PfPKA in *E. coli* BL21 (DE3) pLysS cells (data by Yexin Xie from the European Molecular Biology Laboratory (EMBL) in Heidelberg).

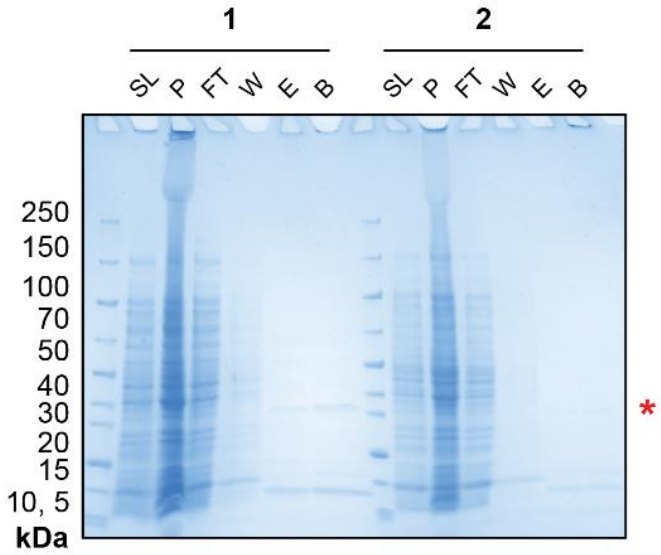

Figure A2. SDS-PAGE of cellular lysates prepared from *E. coli* cells. The expression of PfPKAc was tried in small cultures (50 mL) of *E. coli* BL21 (DE3) or Rosetta (DE3) pLysS cells, transformed with the pET-TOPO-PfPKAc-Dd2 plasmid. Protein expression was induced by addition of 0.5 mM IPTG. Cells were harvested and lysed using freeze-thaw cycles. Different fractions of the purification process are analysed in parallel: SL, soluble lysate fraction; P, pellet (insoluble fraction); FT, flow-through; W, washing; E, elution; B, beads. The protein band highlighted with a red asterisk was sequenced, revealing it was the 50S ribosomal protein L2 from *E. coli*, and not PKA. The data was produced by Yexin Xie and Dr. Kim Remans.

Annex II

Part of the sequence of pSP64T-PfCRT^{Dd2}. The globin regions are highlighted in green, the restriction sites used in this thesis are shown in blue, and the start and end codons of *pfcrt*^{Dd2} are marked in red. The sequence of *pfcrt*^{Dd2} is modified for expression in the oocyte system.

```
1     TACAAGCTTG  CTTGTTCTTT  TTGCAGAAGC  TCAGAATAAA  CGCTCAACTT
51    TGGCAGATCC  TCGAGGGTAC  AAAATTGAAG  ATGAAGTTCG  CCTCTAAGAA
101   GAACAATCAA  AAGAACTCCT  CCAAGAATGC  TGAAAGAGCT  AGAGCTGCTG
151   ATAATGCTGC  TCAAGAAGGT  AACGGTTCTA  GATTGGGTGG  TGGTTCTTGT
201   TTGGGTAAAT  GTGCTCATGC  TGCTAAAGCT  GCCTTCAAAG  AAATCAAGGA
251   CAACATCTTC  ATCTACATCT  TGTCCATCAT  CTACTTGTCC  GTTTGCGTTA
301   TTGAAACCAT  CTTCGCCAAG  AGAACCTTGA  ACAAGATTGG  TAACTACTCT
351   TTCGTTACCT  CTGAAACCCA  TAACTTCATC  TGCATGATCA  TGTTCTTCAT
401   CGTCTATTCC  TTGTTCGGTA  ACAAGAAGGG  TAACTCCAAA  GAAAGACACA
451   GATCCTTCAA  CTTGCAATTC  TTCGCCATTT  CTATGTTGGA  TGCCTGCTCT
501   GTTATTTTGG  CTTTCATCGG  TTTGACTAGA  ACTACCGGTA  ACATCCAATC
551   TTTCGTCTTG  CAATTGTCCA  TTCCAATCAA  TATGTTCTTC  TGCTTCTTGA
601   TCTTGAGATA  CAGATACCAC  TTGTACAATT  ACTTGGGTGC  CGTTATTATT
651   GTCGTTACCA  TTGCCTTGGT  TGAAATGAAG  TTGTCCTTCG  AAACCCAAGA
701   AGAAAACTCC  ACTTGGTTTT  ATCATCTTCA  GATCTCCTCA  TTGATCCCAG
751   TTTGTTTCTC  TAACATGACC  AGAGAAATCG  TTTTCAAGAA  GTACAAGATC
801   GACATCTTGA  GATTGAACGC  TATGGTTTCC  TTCTTCCAAT  TATTCACCTC
851   CTGCTTGATT  TTGCCAGTTT  ACACCTTGCC  ATTCTTGAAA  GAATTGCACT
901   TGCCATACAA  CGAAATTTGG  ACCAACATCA  AGAATGGTTT  CGCTTGTTTG
951   TTCTTGGGTA  GAAACACCGT  TGTTGAAAAC  TGTGGTTTGG  GTATGGCTAA
1001  GTTGTGTGAT  GATTGTGATG  GTGCTTGGAA  AACTTTCGCT  TTGTTCTCCT
1051  TCTTCTCCAT  TTGCGATAAC  TTGATCACCT  CCTACATTAT  CGATAAGTTC
1101  TCCACTATGA  CCTACACTAT  CGTATCTTGC  ATTCAAGGTC  CAGCTACTGC
1151  TATTGCTTAC  TACTTCAAGT  TCTTGGCTGG  TGATGTTGTT  ATTGAACCTA
1201  GATTATTGGA  CTTCGTCACC  TTGTTTGGTT  ACTTGTTCGG  TTCCATTATC
1251  TACAGAGTCG  GTAACATCAT  CTTGGAAAGA  AAGAAGATGA  GAAACGAAGA
1301  AAACGCTGAT  TCTGCTGGTG  CTTTGACTAA  TGTTGATTCT  GCTGCTACTC
1351  AACCTAGGTA  ATCCATGGGA  TCTGGTTACC  ACTAAACCAG  CCTCAAGAAC
1401  ACCCGAATGG  AGTCTCTAAG  CTACATAATA  CCAACTTACA  CTTTACAAAA
1451  TGTTGTCCCC  CAAAATGTAG  CCATTCGTAT  CT
```

Sequence alignments of PfCRT^{Dd2} vs PfCRT^{Dd2_X}. For visualization purposes, only the section of interest of the alignments is shown, in which the introduced mutant codon is centred and surrounded by 12 nucleotides to each side (4 amino acid residues).

```
                    V  I  L  A  F  I  G  L  T
Dd2                 GTTATTTTGGCTTTCATCGGTTTGACT
                    ||||||||||||#|||||||||||||
Dd2_F145I           GTTATTTTGGCTATCATCGGTTTGACT
                    V  I  L  A  I  I  G  L  T


                    T  S  E  T  H  N  F  I  C
Dd2                 ACCTCTGAAACCCATAACTTCATCTGC
                    ||||||||||||#|||||||||||||
Dd2_H97Y            ACCTCTGAAACCTATAACTTCATCTGC
                    T  S  E  T  Y  N  F  I  C


                    K  F  S  T  M  T  Y  T  I
Dd2                 AAGTTCTCCACTATGACCTACACTATC
                    ||||||||||||#|||||||||||||
Dd2_M343L           AAGTTCTCCACTCTGACCTACACTATC
                    K  F  S  T  L  T  Y  T  I


                    S  C  I  Q  G  P  A  T  A
Dd2                 TCTTGCATTCAAGGTCCAGCTACTGCT
                    ||||||||||||#|||||||||||||
Dd2_G353V           TCTTGCATTCAAGTTCCAGCTACTGCT
                    S  C  I  Q  V  P  A  T  A


                    T  S  E  T  H  N  F  I  C        V  I  L  A  F  I  G  L  T
Dd2                 ACCTCTGAAACCCATAACTTCATCTGC      GTTATTTTGGCTTTCATCGGTTTGACT
                    ||||||||||||#|||||||||||||      ||||||||||||#|||||||||||||
Dd2_H97Y_F145I      ACCTCTGAAACCTATAACTTCATCTGC      GTTATTTTGGCTATCATCGGTTTGACT
                    T  S  E  T  Y  N  F  I  C        V  I  L  A  I  I  G  L  T


                    D  A  C  S  V  I  L  A  F
Dd2                 GATGCCTGCTCTGTTATTTTGGCTTTC
                    ||||||||||||#|||||||||||||
Dd2_V141A           GATGCCTGCTCTGCTATTTTGGCTTTC
                    D  A  C  S  A  I  L  A  F


                    Q  L  F  T  S  C  L  I  L
Dd2                 CAATTATTCACCTCCTGCTTGATTTTG
                    ||||||||||||#|||||||||||||
Dd2_S257A           CAATTATTCACCGCCTGCTTGATTTTG
                    Q  L  F  T  A  C  L  I  L


                    T  S  C  L  I  L  P  V  Y
Dd2                 ACCTCCTGCTTGATTTTGCCAGTTTAC
                    ||||||||||||##|||||||||||||
Dd2_I260A           ACCTCCTGCTTGGCTTTGCCAGTTTAC
                    T  S  C  L  A  L  P  V  Y
```

Annex III

Ramachandran plot of the PfCRT^{Dd2} model (data by Dr. Giulia D'Arrigo from the Heidelberg Institute for Theoretical Studies (HITS) in Heidelberg).

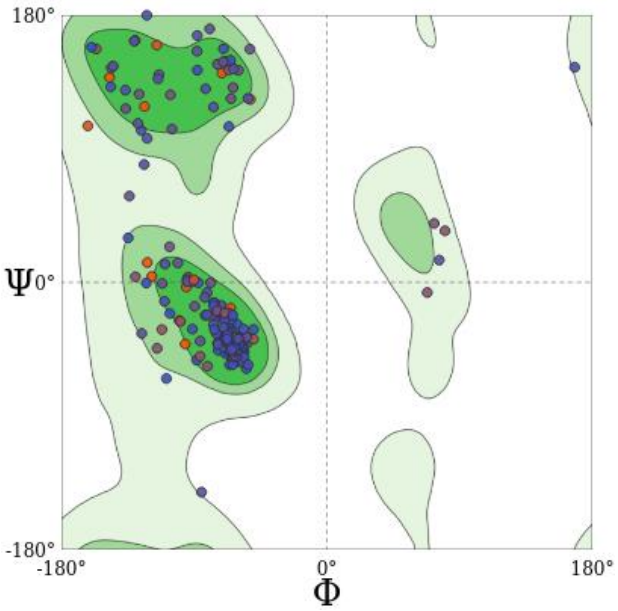

Figure A3. Quality of the PfCRT^{Dd2} model via Ramachandran plot. The structure validation was performed with MolProbity, implemented in the SWISS-MODEL server. 96.64 % of the residues are positioned in favoured regions, and only 0.28 % are in outlier regions. The residues (circles) are coloured according to the QMEAN parameter, an indicator of residue quality, with red colour assigned to bad quality residues, and blue colour to good quality residue. The simulations were performed by Dr. Giulia D'Arrigo and Prof. Dr. Rebecca Wade. Taken from Gomez *et al.* (2023) [223].

Annex IV

Docking scores for the docking of CQ and of PPQ to $PfCRT^{Dd2}$, $PfCRT^{7G8}$, $PfCRT^{Dd2\_F145I}$, $PfCRT^{Dd2\_H97Y}$, $PfCRT^{Dd2\_G353V}$, $PfCRT^{Dd2\_M343L}$, and $PfCRT^{Dd2\_H97Y\_F145I}$ (data by Dr. Giulia D'Arrigo from the Heidelberg Institute for Theoretical Studies (HITS) in Heidelberg).

Figure A4. Glide SP docking scores (kcal/mol) of the 10 poses generated with the induced-fit docking protocol for the binding of CQ or PPQ in the cavity of different PfCRT isoforms. Taken from Gomez *et al.* (2023) [223].

$PfCRT^{Dd2}$

#CQ	Docking score	#PPQ	Docking score
1	-6.743	**1**	-9.329
2	-6.562	**2**	-8.647
3	-5.734	**3**	-8.550
4	-5.729	**4**	-7.941
5	-5.684	**5**	-7.888
6	-5.640	**6**	-6.924
7	-5.428	**7**	-6.895
8	-5.168	**8**	-6.697
9	-4.713	**9**	-6.496
10	-4.324	**10**	n.a.

$PfCRT^{7G8}$

#CQ	Docking score	#PPQ	Docking score
1	-6.287	**1**	-9.606
2	-5.874	**2**	-9.077
3	-5.874	**3**	-8.631
4	-5.785	**4**	-8.469
5	-5.566	**5**	-8.298
6	-5.540	**6**	-7.927
7	-5.472	**7**	-7.504
8	-5.095	**8**	-7.366
9	n.a	**9**	-7.043
10	n.a	**10**	-6.750

$PfCRT^{Dd2\_F145I}$

#CQ	Docking score	#PPQ	Docking score
1	-6.884	**1**	-8.990
2	-6.884	**2**	-8.400
3	-6.663	**3**	-8.107
4	-5.764	**4**	-7.969
5	-5.575	**5**	-7.796
6	-5.383	**6**	-7.683
7	-5.193	**7**	-7.456
8	-5.086	**8**	-7.200
9	-5.075	**9**	-7.146
10	-3.846	**10**	-6.758

$PfCRT^{Dd2\_H97Y}$

#CQ	Docking score	#PPQ	Docking score
1	-6.663	**1**	-9.151
2	-6.289	**2**	-8.838
3	-5.715	**3**	-8.230
4	-5.543	**4**	-7.944
5	-5.524	**5**	-7.858
6	-5.091	**6**	-7.757
7	-5.063	**7**	-7.119
8	-4.956	**8**	-6.677
9	-4.651	**9**	n.a
10	n.a	**10**	n.a

$PfCRT^{Dd2\_G353V}$

#CQ	Docking score	#PPQ	Docking score
1	-6.670	**1**	-9.086
2	-6.583	**2**	-8.645
3	-5.960	**3**	-8.154
4	-5.587	**4**	-7.732
5	-5.552	**5**	-7.585
6	-5.526	**6**	-7.067
7	-5.501	**7**	-6.497

$PfCRT^{Dd2\_M343L}$

#CQ	Docking score	#PPQ	Docking score
1	-6.169	**1**	-8.350
2	-5.614	**2**	-8.012
3	-5.607	**3**	-7.786
4	-5.577	**4**	-7.741
5	-5.387	**5**	-7.733
6	-5.322	**6**	-7.655
7	-5.210	**7**	-6.940

8	-5.317	**8**	n.a	**8**	-5.201	**8**	-6.885
9	-4.612	**9**	n.a	**9**	-5.192	**9**	-6.800
10	n.a	**10**	n.a	**10**	-4.775	**10**	-6.584

PfCRT^{Dd2_H97Y_F145I}

#CQ	Docking score	#PPQ	Docking score
1	-6.617	**1**	-10.109
2	-6.303	**2**	-9.881
3	-5.590	**3**	-8.941
4	-5.516	**4**	-8.714
5	-5.353	**5**	-7.995
6	-5.316	**6**	-7.699
7	-5.268	**7**	-7.594
8	-5.059	**8**	-7.491
9	-4.858	**9**	n.a
10	-4.513	**10**	n.a

Annex V

Docking simulations of CQ or PPQ to the modelled structures of different PfCRT isoforms associated with PPQ resistance (data by Dr. Giulia D'Arrigo from the Heidelberg Institute for Theoretical Studies (HITS) in Heidelberg).

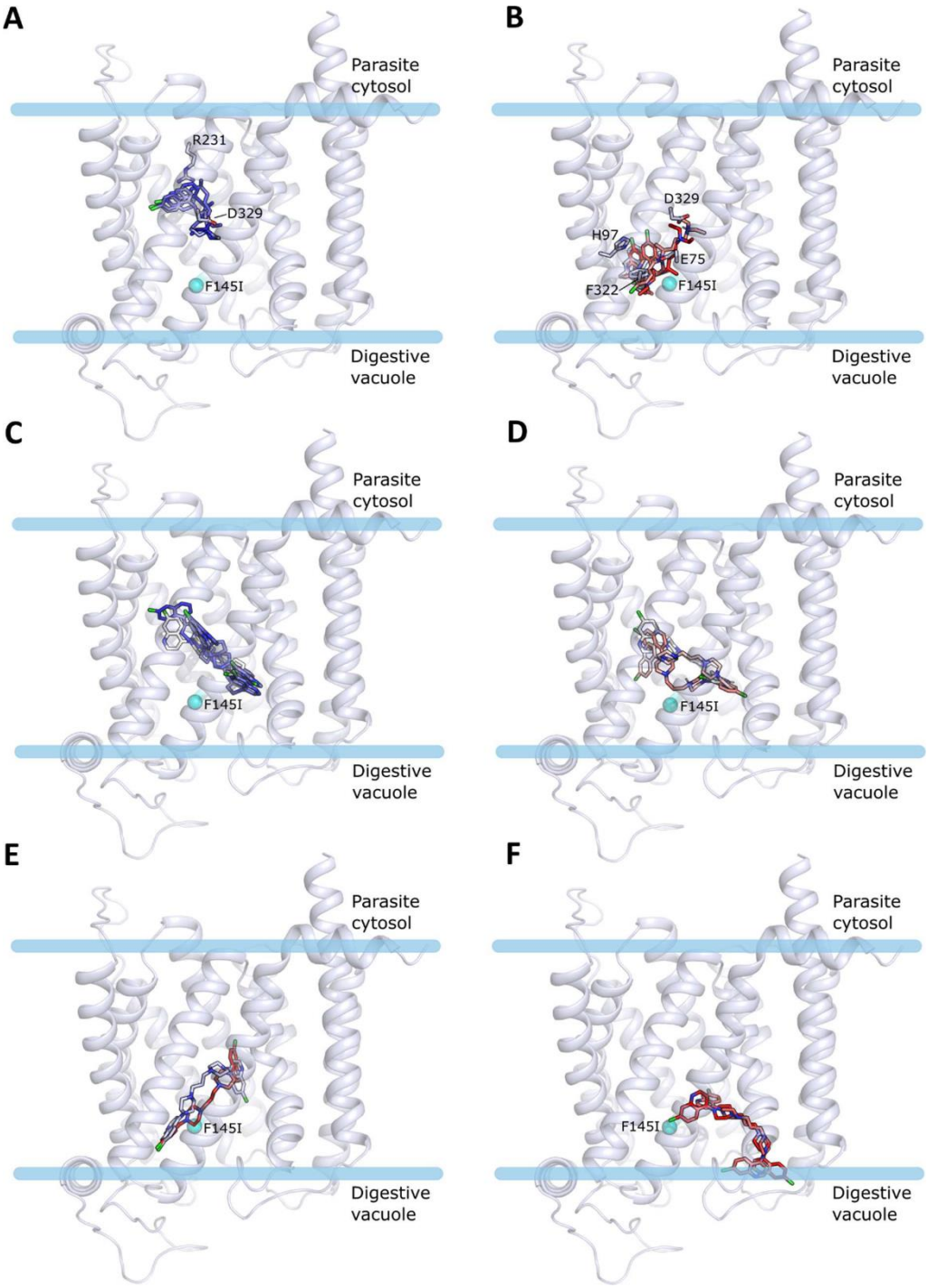

Figure A5.1. Most representative docking results of CQ and PPQ to PfCRT^{Dd2_F145I}. A blue-to-red color scale shows the generated docking poses for CQ (**A-B**) and PPQ (**C-F**), ranked from the best (blue) to the worst (red) docking score. The F145I mutation is indicated as a sphere in cyan. The simulations were performed

by Dr. Giulia D'Arrigo and Prof. Dr. Rebecca Wade. Taken from Gomez *et al.* (2023) [223].

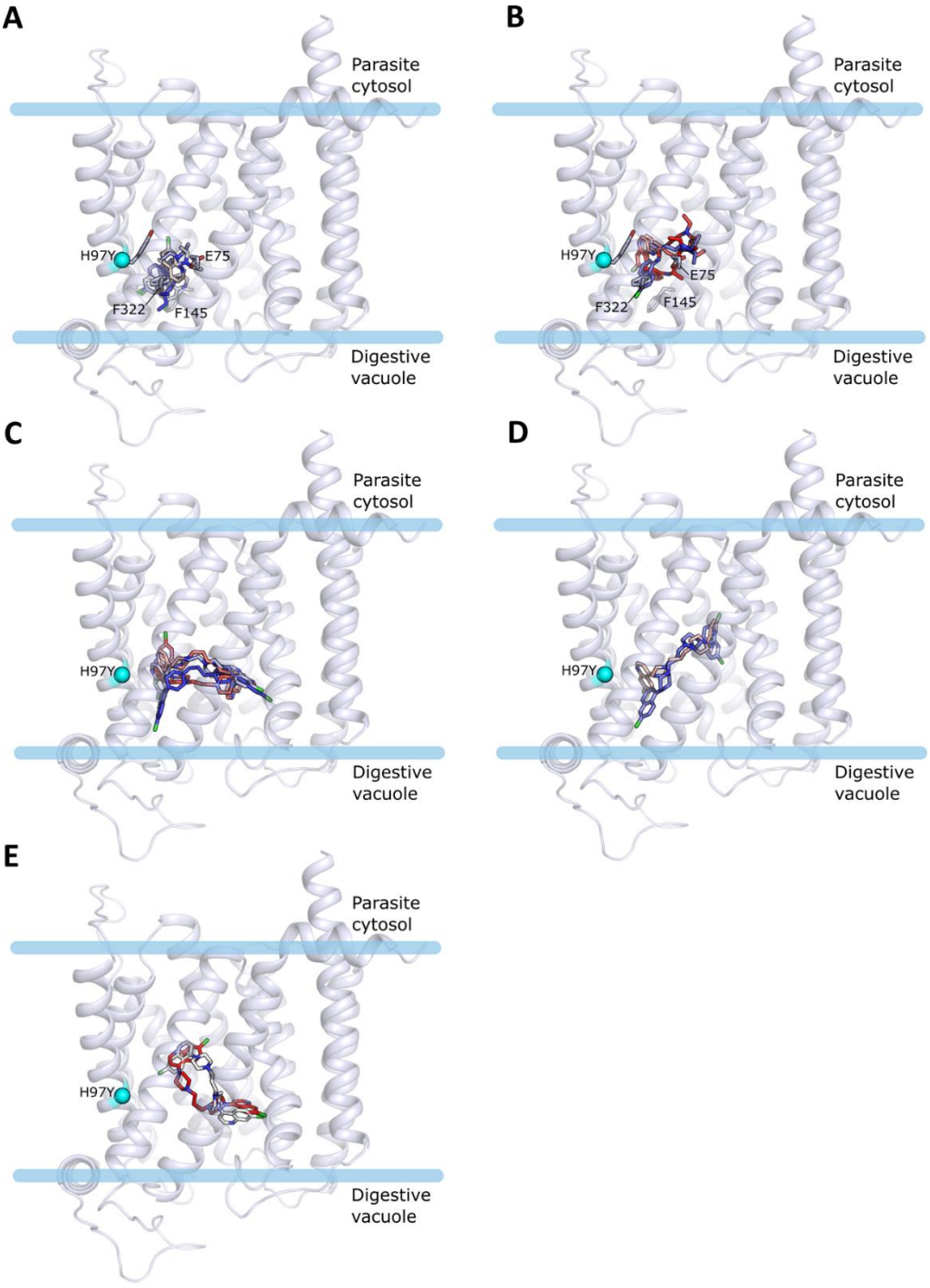

Figure A5.2. Most representative docking results of CQ and PPQ to PfCRT^{Dd2_H97Y}. A blue-to-red color scale shows the generated docking poses for CQ (**A-B**) and PPQ (**C-E**), ranked from the best (blue) to the worst (red) docking score. The H97Y mutation is indicated as a sphere in cyan. The simulations were performed by Dr. Giulia D'Arrigo and Prof. Dr. Rebecca Wade. Taken from Gomez *et al.* (2023) [223].

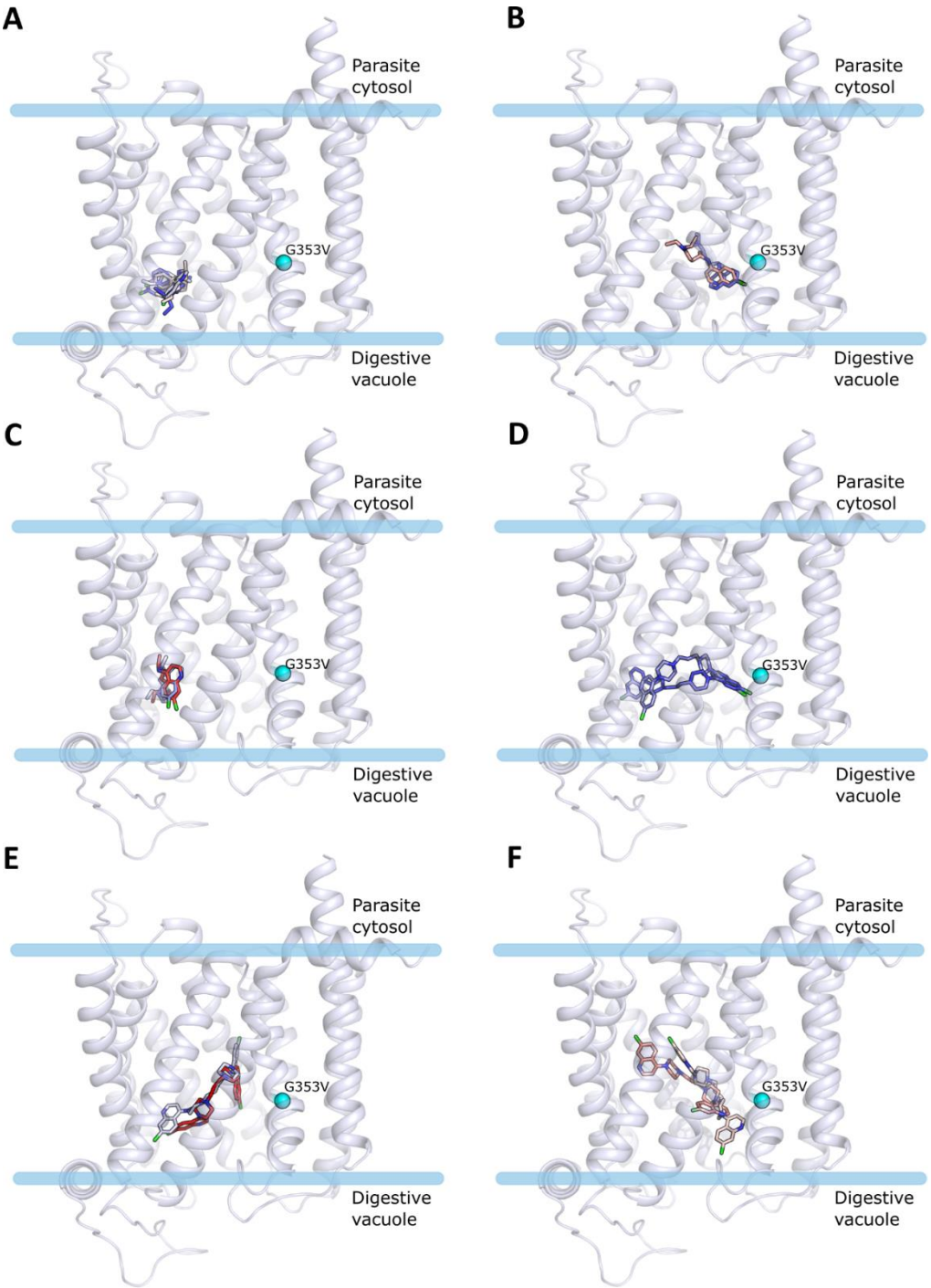

Figure A5.3. Most representative docking results of CQ and PPQ to PfCRT^{Dd2_G353V}. A blue-to-red color scale shows the generated docking poses for CQ (**A-C**) and PPQ (**D-F**), ranked from the best (blue) to the worst (red) docking score. The G353V mutation is shown as a sphere in cyan. The simulations were performed by Dr. Giulia D'Arrigo and Prof. Dr. Rebecca Wade. Taken from Gomez *et al.* (2023) [223].

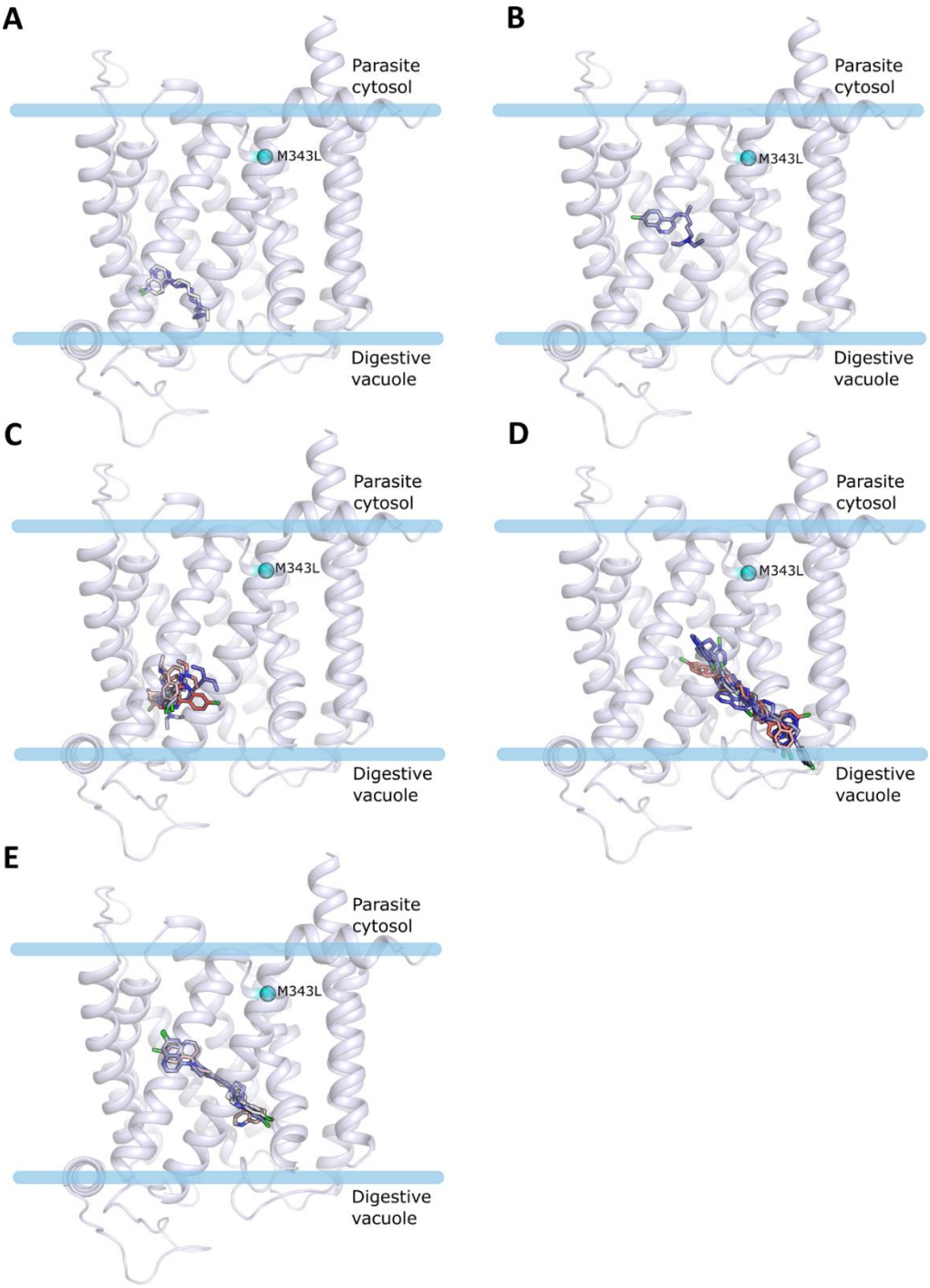

Figure A5.4. Most representative docking results of CQ and PPQ to PfCRT^{Dd2_M343L}. A blue-to-red color scale shows the generated docking poses for CQ (**A-C**) and PPQ (D-E), ranked from the best (blue) to the worst (red) docking score. The M343L mutation is shown as a sphere in cyan. The simulations were performed by Dr. Giulia D'Arrigo and Prof. Dr. Rebecca Wade. Taken from Gomez *et al.* (2023) [223].

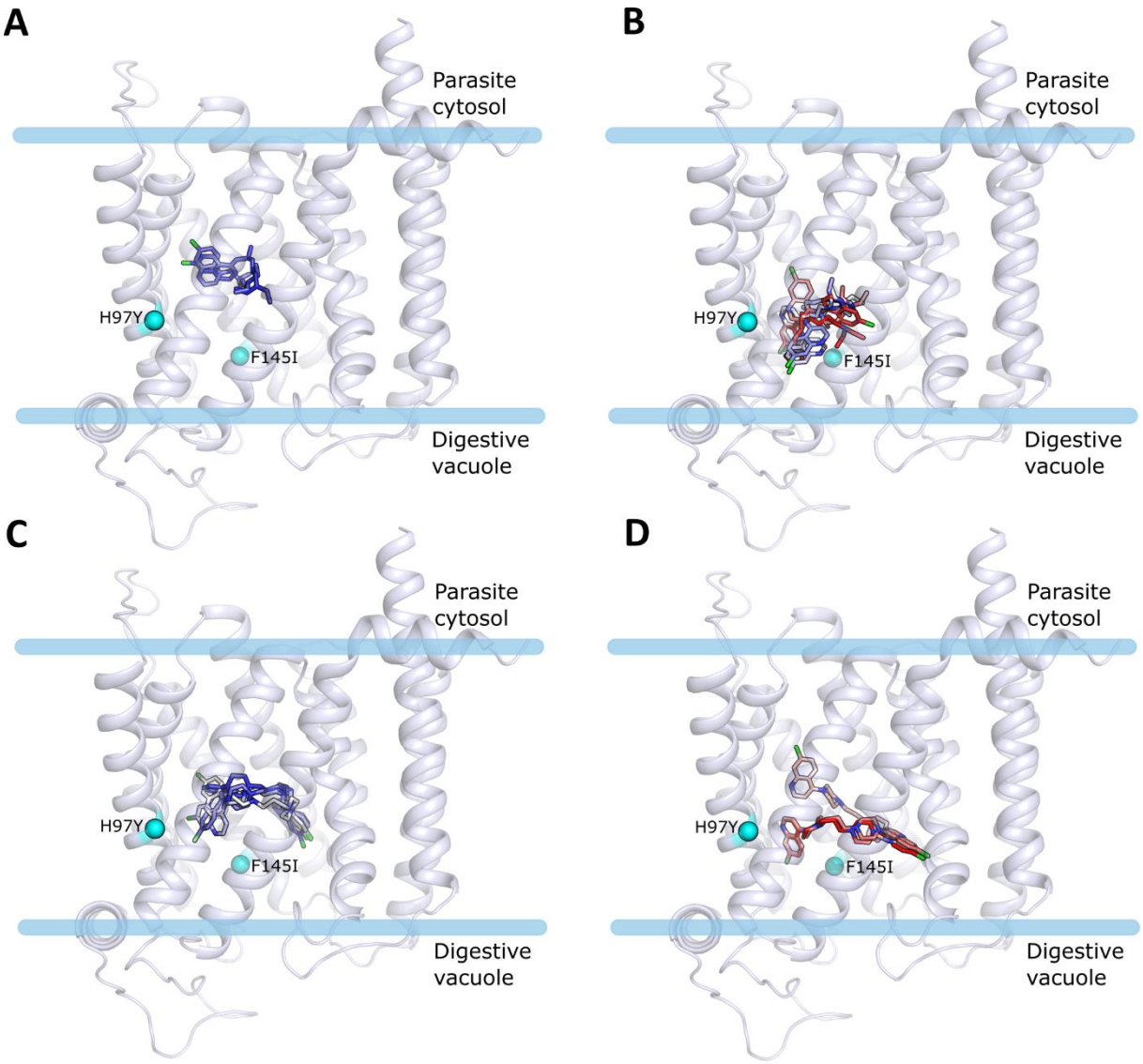

Figure A5.5. Most representative docking results of CQ and PPQ to PfCRT^{Dd2_H97Y_F145I}. A blue-to-red color scale shows the generated docking poses for CQ (**A-B**) and PPQ (**C-D**), ranked from the best (blue) to the worst (red) docking score. The H97Y and F145I mutations are shown as a sphere in cyan. The simulations were performed by Dr. Giulia D'Arrigo and Prof. Dr. Rebecca Wade. Taken from Gomez *et al.* (2023) [223].

Annex VI

Molecular docking of verapamil into the modelled structure of PfCRT^{Dd2} using AutoDock Tools 1.5.7.

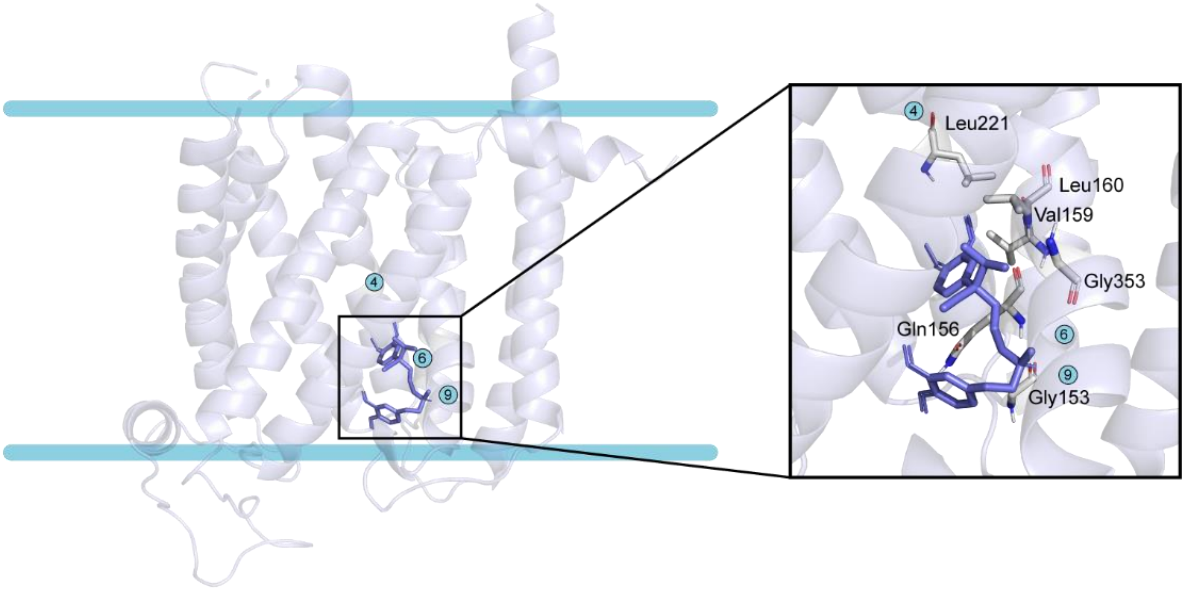

Figure A6. Docking simulation of verapamil into the modelled structure of PfCRT^{Dd2}. The structure of PfCRT^{Dd2} was obtained from the published cryo-EM structure of PfCRT^{7G8} with the Mutagenesis wizard that is integrated in PyMOL. Docking was performed with AutoDock Tools 1.5.7, with a box of 40x40x40 points, centred in the middle of the cavity. The inlet shows the interactions formed by verapamil's highest-ranking pose, with the amino acid residues and the interacting TM domains labelled. The residue Gly353 is shown as well, as it is in the sphere of interaction of verapamil, according to Discovery Studio Visualizer 2021. The protein is shown in a transparent light blue cartoon representation.